

Quantifiable MRI Changes in Cerebral White Matter and Their Importance to Aging, Cognition, and Alzheimer's Disease

by

Emily Rose Lindemer

B.Sc., McGill University (2011)

Submitted to the Harvard Medical-MIT Division of Health Sciences and Technology

in partial fulfillment of the requirements for the degree of

Doctor of Philosophy

at the

MASSACHUSETTS INSTITUTE OF TECHNOLOGY

June 2017

© Massachusetts Institute of Technology 2017. All rights reserved.

Author
Harvard Medical-MIT Division of Health Sciences and Technology
May 17, 2017

Certified by
David H. Salat, PhD
Associate Professor in Radiology, Harvard Medical School
Thesis Supervisor

Accepted by
Emery N. Brown, MD, PhD/Director, Harvard-MIT Program in Health Sciences and Technology/Professor of Computational Neuroscience and Health Sciences and Technology
Chairman, Department Committee on Graduate Theses

Quantifiable MRI Changes in Cerebral White Matter and Their Importance to Aging, Cognition, and Alzheimer's Disease

by

Emily Rose Lindemer

Submitted to the Harvard Medical-MIT Division of Health Sciences and Technology
on May 17, 2017, in partial fulfillment of the
requirements for the degree of
Doctor of Philosophy

Abstract

Alzheimer's disease (AD) is a neurodegenerative disease for which there are no preventative or therapeutic interventions. It is currently understood to be linked to the accumulation of pathologic proteins in the brain. In the past several decades, a strong body of evidence has accumulated that is suggestive of a vascular-related pathway in AD. A deeper understanding of this phenomenon is critical in advancing our understanding of the AD biological process as well and may lead to the discovery of novel therapeutic targets. A common age-related change in the brain is the development of white matter signal abnormalities (WMSA) as seen on magnetic resonance imaging (MRI). These lesions are related to cognitive function and are thought to be due to compromised integrity of the brain's vascular system. Despite evidence that WMSA are known to influence the clinical progression of AD, we do not currently view AD as a vascular disease nor do we use WMSA as a clinical indicator of AD. This is because we still do not know whether or not WMSA are a distinct phenomenon in AD, their relationship to traditional AD biomarkers, and how they independently contribute to clinical status. In this work, we examine if and how WMSA are related to AD conversion, whether they differ in their spatial distribution between typical aging and AD, and how they are linked to classic pathologic markers of AD. This work also includes technical development for WMSA quantification and baseline studies of WMSA in cognitively healthy aging. The main findings of this work suggest that WMSA are distinctly different in AD than in typical aging and have a unique role in AD progression. This not only motivates the utility of WMSA in our clinical treatment of AD, but also provides insight into the biological underpinnings of the disease process that may lead to novel therapeutic targets.

Thesis Supervisor: David H. Salat, PhD
Title: Associate Professor in Radiology, Harvard Medical School

Acknowledgments

"Well, how did I get here?"

-David Byrne (Talking Heads), "Once In A Lifetime," 1980

On my first day at MIT I asked myself, "*How did I get here?*" It became more and more clear to me throughout graduate school that my path was built by those who believed in me, especially before it made any sense to do so. I could fill an entire book with the names of everyone who fall into this category, but I would like to acknowledge a select few who have made major contributions to my development below.

The first person I have to thank is David Salat. You have been there from the very beginning of my journey into the neuroimaging world and gave me the freedom to explore it that many others would not have. Without your encouragement, I might never have gone to graduate school and for that I can never thank you enough.

I learned (almost) everything I know about statistics from Doug Greve. Thank you so much for the patience and attention that you gave to me, particularly in the earliest days of graduate school when I was floundering around trying to figure out what you meant when you told me to perform simulations.

To Bruce Fischl, working in your lab was an incredibly unique and positive experience. I am sure that you have two brains in your head, because I don't know anyone else who is as simultaneously productive, successful, and compassionate towards his people as you are and I thank you for setting this example for me.

To Teresa Gomez-Isla, you were a pivotal component of my thesis committee and without your clinical expertise and guidance this body of work would not have the translational reach that it does. I admire you immensely in your career and am extremely grateful to have had you as a mentor and role model.

To Elfar Adalsteinsson, everyone should be so lucky as to have someone like you as a mentor in life. Never before have I met someone who so genuinely cares about the individual goals and personalities of his students, and I truly believe that I would have been lost at MIT without your tremendous guidance that started on day one. I hope to know you for a very long time.

To the HST community, particularly the entering class of 2013 and the administrative staff: the world that you created and let me live in with you is unparalleled. Almost no one gets the chance to go to graduate school with such a brilliant and diverse group of individuals and it is you who have motivated me to always think outside of the box and challenge my own understanding of the world around me. I want to especially thank those who were there through the most challenging times: Julie Greenberg for your intense caring, Sam Osseiran for being my first friend and Charlie's Kitchen frequent-flyer, Nil Gural for your steadfast friendship and emotional support, Chris Lee for always doing your own thing, Giorgia Grisot for being a fantastic labmate and sounding board, Colin Buss for being such a solidly reliable friend, and David Miranda-Nieves for being an amazing partner through the crazy experience that was ICM 2.

To the Martinos Center community, particularly LCN and the BaND Lab. I always felt supported here, and always in awe of the brilliance around me. A particular thanks to Bruce Rosen and to Randy Gollub for their dedication to graduate students and personal investment in my academic career. In terms of my emotional well-being, I must personally thank Allison Stevens, Jean Augustinack, Andre van der Kouwe, Martin Reuter, Caroline Magnain, Paul Wighton, Zeke Kaufman, and Emma Boyd.

To the Graduate Women at MIT Executive Board: you gave me a greater purpose in this community. Thank you for teaching me how to be a better leader, and empowering me as a woman in STEM. We are the future.

To my wonderful friends who have been there since before graduate school: Alexandra Skerry, Katelyn Saaristo, Monica Rosenberg, Elizabeth McNamee, Heather McLaren, Alanna Houston, Kydlan Margulies, Andy Rosenblatt, Rana Cooney, Vinny Valant, Kevin and Rachael McLaughlin, Andrea Levine – you are my foundation.

To my family, especially my parents Kevin and Christine who prioritized my education over almost everything else. Dad, pricking your finger when I was seven so that I could see what blood looked like under a microscope was totally worth it! And Mom, I firmly believe that if you hadn't taken me to the library *every day* as a toddler I would not be where I am today. To my other family – Pete, Mary, and Kate – boy did I get lucky with you guys, thank you from the bottom of my heart for everything you have done for me.

Last and most importantly, thank you to my husband Liam. There are no words that can possibly describe how appreciative I am of your unfailing support. No one forces me to be as true to myself as you do. Thank you for being an undying source of support and love, for being the best friend imaginable, for all of the home-cooked dinners and late-night pep talks, and for creating the happiest of homes with me and Zoom. I would have dropped out of graduate school one hundred times over if it were not for you. Thank you for the adventures and not so much for pushing me outside of my comfort zone, but for skydiving out of it with me while holding my hand. What I am most proud of in life is what we have built together and I am so excited to see where you and I will go. Without you my life would be boring.

Contents

1	Introduction	23
1.1	Motivations for Studying White Matter	25
1.1.1	Relation to Cerebrovascular Integrity	26
1.1.2	Findings in Brain Aging	27
1.2	Alzheimer’s Disease in Context	28
1.2.1	Current Understanding of Alzheimer’s Disease	29
1.2.2	White Matter and Alzheimer’s Disease	30
2	Computational Methods for WMSA Analysis	33
2.1	Automatic Segmentation	34
2.1.1	Technical Development	34
2.1.2	Validation	37
2.2	Novel Metrics for WMSA	40
2.2.1	Technical Development	41
2.2.2	An Application in Disease Populations	44
2.3	Conclusions	48
3	Assessing WMSA in Healthy Aging	51
3.1	A Novel Staging Mechanism: Technical Development	52
3.2	Applications	56
3.2.1	WMSA Staging in Healthy Aging	56
3.2.2	Comparison to MCI and AD	65
3.3	Conclusions	67

4 Assessing WMSA in AD	69
4.1 Total WMSA Burden and Clinical Diagnosis	70
4.2 Regional WMSA Burden and Diagnosis	77
4.3 Longitudinal WM Quality Changes in AD Conversion	84
4.4 Conclusions	89
5 Relating WMSA to Classic AD Biomarkers	93
5.1 Diagnostic Classification	94
5.2 Associations with Cognitive Measures	100
5.2.1 High-level view across all stages of AD	102
5.2.2 A closer look in a ‘healthy’ biomarker subset	104
5.3 Conclusions	111
6 Discussion	115
6.1 Technical Developments	116
6.2 Aging	117
6.3 Alzheimer’s Disease	119
A Supplementary Tables	123
B Supplementary Figures	127
C Complete List of Work	131
D A CV of Failures	141

List of Figures

1-1	Example of gray matter (GM), white matter (WM), and white matter signal abnormality (WMSA) appearance on T1-weighted (left) and T2-weighted (right) MRI.	25
2-1	A) Flowchart of major steps involved in automatic WMSA labeling pipeline. B) Visual representation of Mahalanobis distance, using a single WMSA voxel and 100 randomly selected NAWM voxels from an ADNI data set. Red point indicates a single WMSA voxel's position in T1/T2/PD intensity space, and blue dots indicate positions of NAWM voxels. The WMSA voxel's MD is measured from NAWM using Equation 1. C) Comparison of the automatic WMSA labeling with only the MMGCA step to the manual labels (C.3) and comparison using the automatic labeling using MMGCA + MD refinement (C.4). This single subject is a representation of the general trend seen in the ADNI data, where the MMGCA labeling frequently failed to label connected sections of WMSA voxels that were detected by a manual labeler, and these sections were corrected with the MD refinement step. We additionally note that the “false” positives seen in C.4 are addressed in the Validation section of the Methods, and actually reflect damaged tissue that was undetected by the human rater. Subtle differences in tissue signal intensity in these regions can be seen in the T1-weighted image (C.1).	36

3-4 Surface maps depicting which scaling cluster each region's underlying WM belongs to, with respect to WMSA percent of total ROI WM (WMSA percent), as determined by statistically different WMSA measurements across all four quartiles of WMSA burden. Scaling here refers to the strength of the statistical significance when assessing WMSA burden across the four quartiles for a given region, where "high-scaling" indicates that the increase in regional WMSA with increasing quartile is highly significant	61
3-5 Left column: Individual subject data across all 4 quartiles showing the percent of the total WM occupied by WMSA in the inferior parietal region (top); a scaling curve for percent WMSA created by plotting mean values per quartile (second); individual raw WMSA volumes across the 4 quartiles in inferior parietal WM (third); a scaling curve for raw WMSA volume (bottom) (Individual data points: white=hypertensive, black=non-hypertensive, circle=male, triangle=female; red: mean, pink: 95% confidence interval of the mean; blue: 1 standard deviation). Middle column: Same data shown for fusiform WM, a mid-scaling region. Right column: Same data shown for inferior temporal WM, a non-scaling region.	62
3-6 Flowchart demonstrating cut-off values for inclusion criteria for final staging in OC individuals, based on values derived from quartile-based staging.	65
3-7 Within-group percentages of individuals in each WMSA Stage using secondary staging cut-off values across three diagnostic groups. Significant differences were found between AD and MCI and between AD and OC in Stages I and IV.	66

4-6	Cerebral vascular territories depicted with FreeSurfer parcellations, demonstrating which major cerebral vessels provide the main vascular supply for each ROI. Regions where two supplies meet are known as cerebrovascular boundary zones (or 'watershed' regions) and are most susceptible to hypoperfusion. Inset shows results from manuscript where there is a greater WMSA burden in AD over OC individuals.	83
4-7	Time courses of enduring WMSA MD from enduring NAWM (top) and incident WMSA from enduring NAWM (bottom) in MCI-NC and MCI-C individuals. *Significant interaction ($p < 0.05$), **($p < 0.01$), ***($p < 0.0001$). Error bars are standard error of the mean. Red vertical lines indicate time of AD conversion in MCI-C group.	85
4-8	Time courses of hippocampal volume change in MCI-NC and MCI-C individuals. **Significant interaction in rate of change ($p < 0.01$). Error bars are standard error of the mean. Red vertical line indicates time of AD conversion in MCI-C group.	87
4-9	Hypothetical model of the trajectories of WM damage progression over the course of MCI development in populations that do and do not convert to AD. The width of each bounded region corresponds to the percent of the total WM that is damaged (WMSA to total WM volume). The dashed line in the middle of each region corresponds to the mean MD of all WMSA from NAWM (degree of damage within lesions). At 18 months before AD conversion, the MCI-C group exhibits a faster increase in WMSA development than the MCI- NC group. After AD conversion in the MCI-C group, volume differences start to be seen between the groups, and the MCI-C group exhibits a larger volume increase. Abbreviations: AD, Alzheimer's disease; MCI-C, mild cognitive impairment converters; MCI-NC, mild cognitive impairment nonconverters; MD, Mahalanobis distance; NAWM, normal-appearing white matter; WM, white matter; WMSA, white matter signal abnormality.	90

5-1	CSF biomarker data for all 238 study individuals. Points are weighted by individual total WMSA burden.	98
5-2	Left: Hippocampal volumes in impaired (MCI + AD) individuals in Q1 vs. Q3, showing no significant different ($p=0.50$); Right: WMSA volumes in impaired (MCI + AD) individuals in Q1 vs. Q3, showing significantly higher WMSA in Q3 individuals ($p<0.01$).	106
5-3	Left: Example AD individual from Q1 with hippocampal atrophy; Right: AD individual with similar hippocampal atrophy from Q3. Both individuals are from the bottom quartile of individuals ranked by hippocampal volume in each quadrant.	107
5-4	WMSA volumes in impaired (MCI + AD) vs. OC individuals in Q3, showing significantly higher WMSA in the impaired individuals ($p<0.01$).107	
B-1	Spatial staging of age-associated WMSA into four stages using ROI cut-off values derived from quartile-based staging and described in 3-5. Percent of an ROI's total WM that is occupied by WMSA is used as a metric for comparison across stages (color bar). Surface maps showing the percent of each region's underlying WM that is occupied by WMSA (first and second columns) and an axial slice through the periventricular WM showing these values in a volume view (third column) for WM disease stages I - IV. Demographics for these individuals are reported in Supplementary Table 1.	128

THIS PAGE INTENTIONALLY LEFT BLANK

List of Tables

4.2	Mean and standard error values are reported for continuous measures. ^a Significantly higher than OC group ($p < 0.001$). ^b Significantly higher than all other groups ($p < 0.0001$). ^c Significantly lower than all other groups ($p < 0.0001$).	78
5.1	Demographic information for individuals in the four diagnostic groups. Total WMSA values are the log of the total WMSA volume in mm ³ . Hippocampal volume values are reported as % of total intracranial volume. APOE ε4 values correspond to the percent of each diagnostic group that carries each of the three possible genetic profiles. ^a AD and OC significantly different ($p < 0.05$), ^b AD and MCI significantly different from OC ($p < 0.05$), ^c All three groups significantly different from each other ($p < 0.05$), ^d AD significantly different from MCI and OC ($p < 0.05$).	96
5.2	Results of SVM Classification experiments between AD and OC groups. TPR = true positive rate (correct AD classifications) and TNR = true negative rate (correct OC classifications). Each column is a separate SVM experiment, and X's represent whether or not a given biomarker was used in that classification experiment.	99
5.3	Results of SVM Classification experiments between MCI-C and MCI-NC groups. TPR = true positive rate (correct MCI-C classifications) and TNR = true negative rate (correct MCI-NC classifications). Each column is a separate SVM experiment, and X's represent whether or not a given biomarker was used in that classification experiment.	99
5.4	Results of GLM experiments conducted using baseline memory scores (top) and baseline executive function scores (bottom) as dependent variables across all study subjects, regardless of diagnosis.	102

5.5	Results of GLM experiments conducted using one-year changes in memory scores (top) and one-year changes in executive function scores (bottom) as dependent variables across all study subjects, regardless of diagnosis. Bold values indicate variable coefficients and <i>p</i> -values that attained statistical significance.	103
5.6	Demographic information for individuals in CSF biomarker quadrants Q1 and Q3, delineated in Figure 5-1. MCI and AD individuals in each quadrant are combined in the above table into one "Impaired" group. Hippocampal volume is % of intracranial volume. WMSA are taken as the log-transform of the total volume in mm ³ . APOE ε4 values represent the percent of the within-quadrant diagnostic group that carry each possible allele combination. For example, 25% of the OC individuals in Q1 are APOE ε4-/.	105
5.7	Results of GLM experiments for individuals in Q1 sconducted using one-year changes in memory scores (top) and one-year changes in executive function scores (bottom) as dependent variables across all study subjects, regardless of diagnosis. Bold values indicate variable coefficients and <i>p</i> -values that attain statistical significance.	108
5.8	Results of GLM experiments for individuals in Q3 sconducted using one-year changes in memory scores (top) and one-year changes in executive function scores (bottom) as dependent variables across all study subjects, regardless of diagnosis. Bold values indicate variable coefficients and <i>p</i> -values that attain statistical significance.	109
A.1	Demographics for individuals in secondary staging with mean and standard error of the mean values (above gray row) and mean and variance values for WMSA % in each of the high-scaling ROIs (below gray row). *Significantly different from all other stages (<i>p</i> <0.05)	124

A.2 Demographics for individuals in each of the three demographic groups with mean and standard error of the mean values. AD significantly different from OC ($p<0.05$)* and ($p<0.01$)**. All groups significantly different ($p<0.001$)***	125
C.1 Demographics of individuals from ADNI used in the present study. mean and standard deviations are reported for each group. (ICV = Intracranial Volume, WM = white matter, AD = Alzheimer's disease, MMSE = Mini Mental State Examination).	133

Chapter 1

Introduction

“Begin at the beginning,” the King said, very gravely, “and go on till you come to the end: then stop.”

-Lewis Carroll, “Alice in Wonderland,” 1865

Over the past several decades, tremendous strides have been made in our global community’s understanding of and ability to treat life-threatening illnesses. Less than 30 years ago, diseases such as HIV, Hepatitis C, leukemia, and many other types of cancer were death sentences but are now treatable and have positive long-term prognoses. Despite these advances, the field of neurodegenerative diseases has been relatively stagnant. Currently, 5.3 million Americans suffer from Alzheimer’s disease (AD). This number is expected to rise to 13.1 million by the year 2050 due to the aging population and the lack of any effective therapeutic interventions to slow, stop, or prevent the disease process. If an intervention existed that could slow the disease onset by only five years, however, this 2050 projection would be only 7 million – a reduction of nearly 50% [4]. To date, the only FDA-approved therapies in existence for AD act to slow or reduce disease *symptoms* but do not physically target any of the underlying disease-related pathologies. The most recent of these therapies was approved in 2003 – nearly 15 years ago.

While AD is typically understood as being caused by the accumulation of pathological proteins in the brain, there are other age-related processes that occur in the

brain and are known to influence the clinical progression of AD. As AD is a *disease of aging*, however, it is difficult to disentangle whether or not these processes are a fundamental part of the disease process and what role they play in the presence and in the absence of more classic AD pathologies. The findings in the brains of individuals with more heterogeneous pathological presentations have led to new hypotheses about the underlying disease process that cause the clinical presentation of AD. Among these is the hypothesis that there are vascular contributions to the disease process that either independently cause cognitive decline or are additive to more classically recognized AD pathologies. While the cerebrovascular (CBV) system is difficult to study in humans *in vivo*, the integrity of the cerebral white matter (WM) as seen on magnetic resonance imaging (MRI) can indirectly inform us about CBV pathologies. In particular, lesions known as white matter signal abnormalities (WMSA), sometimes referred to as "hyperintensities" referring to their signal characteristics on a T2-weighted MRI scan, are a common finding on MRI images of aging brains. The histopathological correlates of these lesions are heterogeneous and complex, but more often than not contain vascular pathologies and so are thought to act as a surrogate marker of the CBV system's integrity [5]. WMSA as they relate to aging, cognitive decline, and other biomarkers of AD will be the primary focus of this body of work. I aim to answer four overarching questions in this thesis: 1) *Is there novel information that we can extract from WMSA?*, 2) *What do WMSA look like in "normal" aging?*, 3) *Do WMSA differ from the "normal" aging trajectory in the progression to AD?*, and 4) *Do WMSA matter in the clinical progression of AD?* I develop and describe novel tools that can provide more intricate metrics of WM integrity than previously available, apply these tools to studies of WM brain aging and AD, and draw connections between WM and classic AD pathologies. The goal of this work is to demonstrate the importance of WM in the AD pathological process in order to motivate future work in the study of CBV contributions to AD.

Chapter two describes novel computational methods for the analysis of WM and WMSA as well as a description of their output metrics.

Chapter three describes an assessment of WMSA in the healthy aging brain with

a brief comparison of these findings to individuals with mild cognitive impairment (MCI) and AD.

Chapter four describes an in-depth assessment of WMSA in AD through both cross-sectional and longitudinal analyses, using several of the different output metrics described in chapter two.

Chapter five describes the relationship between WMSA, classic cerebrospinal fluid (CSF) biomarkers of AD, hippocampal volume, and cognitive function.

1.1 Motivations for Studying White Matter

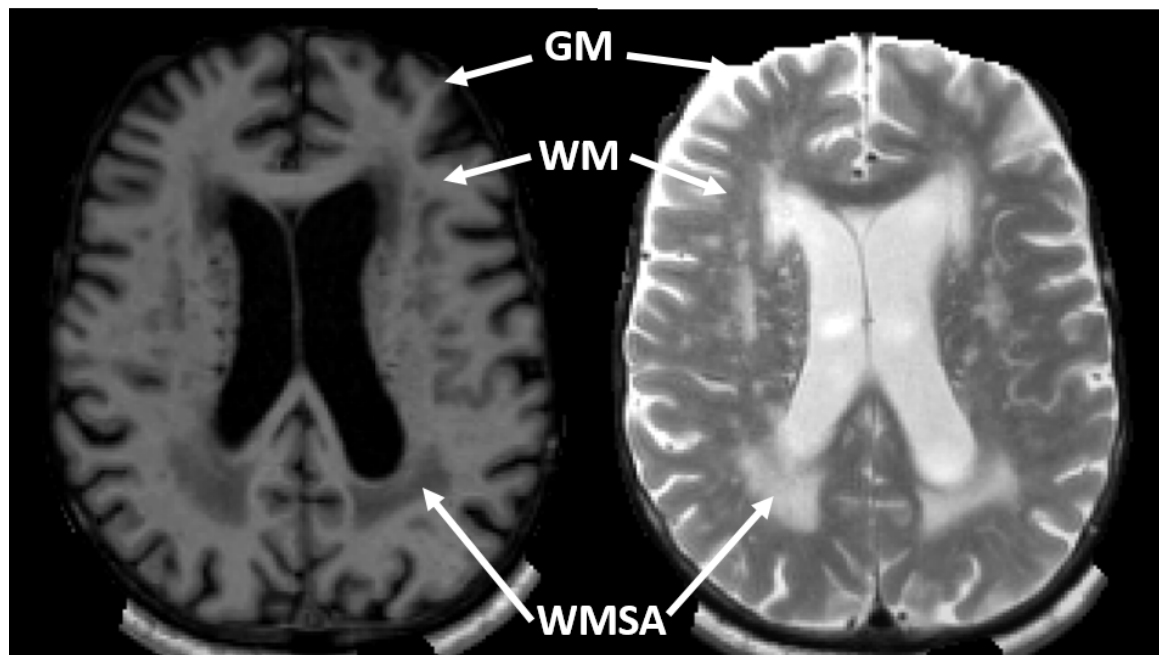


Figure 1-1: Example of gray matter (GM), white matter (WM), and white matter signal abnormality (WMSA) appearance on T1-weighted (left) and T2-weighted (right) MRI.

The human brain is primarily comprised of two tissue types: gray and white matter (Figure 1-1). The gray matter acts as the brain's main processor, full of neurons that compute complex outputs from a series of inputs. The white matter (WM) is the connective tissue of this complex organ, and acts as highways for information processing and communication between different regions of the cerebral cortex and

subcortical structures.

Much of what we know about the cerebral WM comes from neuroimaging studies that employ MRI to study its complex structure *in vivo* in both healthy and disease states. This technology allows us to not only assess its structural integrity at a given snapshot in time, but we can also use MRI to study how WM changes with aging and in neurological and psychiatric diseases. Over the past several decades, technological advances in MRI acquisition as well as post-acquisition analysis have allowed greater insight into the role that WM plays in healthy aging and disease, and with these advances have come an even greater number of new questions.

1.1.1 Relation to Cerebrovascular Integrity

The cerebral WM has long been thought to act as a surrogate by which to study the integrity of the cerebrovascular (CBV) system. To understand this, we must understand the anatomy of the CBV system as well as the metabolic demand of the brain. While the human brain weighs a mere three pounds on average, it consumes nearly 20% of the body's oxygen supply through the circulatory system. The brain is perfused by three major arteries: the anterior cerebral artery (ACA), the middle cerebral artery (MCA), and the posterior cerebral artery (PCA). The gray matter is perfused first before the three major arteries break off into smaller branches and dive into the cerebrum to perfuse the deeper tissue which is mainly comprised of WM. As these vessels become smaller, the pressure and flow within them lessens, causing the deep WM to be more susceptible to hypoperfusion injuries and ischemic damage.

In addition to our understanding of basic anatomy, the relationship between cerebral WM integrity and CBV integrity can be deduced from histopathological-imaging correlation studies. Changes in WM integrity can be evinced on structural MRI. Many studies have attempted to correlate 'pathological' imaging findings with actual histopathological data to determine the underlying mechanisms for their appearance on MRI. Researchers have found that patches of abnormal WM on MRI are associated with a range of pathologies including gliosis, demyelination, reduced fiber density, reduced vessel density, ischemia, and inflammation. While the results of these studies

are heterogeneous, they broadly suggest that there is a cerebrovascular component to many of the WM changes seen on structural MRI.

Several genetic studies have also demonstrated a relationship between WM integrity and CBV. WM pathologies seen on MRI were first found to have a significant genetic component based on their higher prevalence in monozygotic over dizygotic twins [6]. After this establishment, it was later found that MRI-based WM pathologies were associated with variants in the NOTCH3 gene – a gene whose mutations result in a syndrome of cerebral arteriopathy [7]. Finally, others have demonstrated that transcription factor FOXC1 mutations located adjacent to cerebral small vessel disease genetic loci result in the development of MRI-based WM pathologies [8].

A final piece of supporting evidence for the relationship between CBV and WM integrity comes from associations between epidemiological data and neuroimaging findings. With the histopathological discovery of vascular changes in regions of decreased WM integrity on MRI, researchers began to ask questions about the relationship between systemic vascular risk factors and WM integrity. The results of these epidemiological studies demonstrated that WM integrity as seen on MRI is related to hypertension, hypercholesterolemia, diabetes, and a history of smoking [9].

1.1.2 Findings in Brain Aging

For many years we have understood that the cerebral WM changes with aging. These changes take many different forms that can be measured using different types of MRI acquisition and analysis techniques. Changes ranging from subtle histological damage to more substantial lesioned tissue on MRI are often apparent in individuals without any obvious cognitive syndrome and because of this the clinical significance of age-associated changes in WM has been fairly unclear.

One of the simplest metrics of WM that can be assessed is its total volume within the cerebrum. This can be a valuable metric when studying aging and disease state, and it has been demonstrated that total WM volume normally decreases with aging [10, 11]. Deviations from the typical trajectory of WM volume decrease in aging can indicate separate pathological processes. Most regions of the WM decrease in volume

with increasing age in a quadratic fashion, indicating a greater acceleration of loss with increasing age [11].

White matter lesions have been studied extensively in the imaging community, and are more appropriately referred to as white matter signal abnormalities (WMSA) as they can appear darker or brighter than the surrounding healthy WM depending on MRI modality (Figure 1-1). These lesions can be evinced on T1-weighted, T2-weighted, fluid-attenuated inversion recovery (FLAIR), and proton-density (PD) structural MRI. Due to their histological correlations with vascular pathologies, WMSA have recently been termed through consensus as "white matter hyperintensities of presumed vascular origin" [12, 13]. As WMSA are a common imaging finding in aging populations [14], they are typically regarded as benign comorbidities of aging. More recent work, however, has associated their presence with cognitive decline and suggests that they may have a significant contribution to the development of dementia. WMSA will be the primary WM pathology of focus in this body of work, and **Chapter 2** provides an in-depth look at novel metrics for their assessment. Despite our knowledge of the relationship between WMSA and aging, there still exist very little ground-truth descriptions of what make WMSA pathological and what make them a 'normal' component of aging. **Chapter 3** aims to use the tools described in **Chapter 2** to describe a staging mechanism for WMSA in cognitively normal aging. The results in **Chapter 3** provide a basis for comparison for the WMSA findings in AD that are described in **Chapters 4 and 5**.

1.2 Alzheimer's Disease in Context

Dementia refers to a heterogeneous group of neurodegenerative diseases. Of these, Alzheimer's Disease (AD) is the most common. To understand how AD is currently viewed, we must appreciate the historical context of dementia in general. Prior to the distinction of dementia subtypes, the clinical manifestation of dementia as determined by an irreversible loss of cognitive functioning was widely thought of as being vascular in origin [15, 16]. This line of thinking changed, however, when the A β peptide was

discovered to be the main component of the major pathologies seen in the brains of individuals who passed away with a clinical diagnosis of AD [17, 18]. In addition to this, researchers discovered that the genetic underpinnings of early-onset (familial) AD could be linked to mutations in the amyloid precursor protein (APP) gene [19]. Finally, neurofibrillary tangles (NFT) were a second pathology that were discovered to develop in a spatially stereotyped pattern in AD [20–23]. Thus, the clinical community began to think of AD as a separate disease process that involved A β and NFTs as primary pathological culprits, and vascular dementia was deemed a separate diagnosis. More recently, however, another shift in our understanding has occurred with the resurgence of large population-based clinical-pathological studies that demonstrate heterogeneous pathological profiles of individuals with a clinical diagnosis of AD, that more often than not include vascular pathologies [24–27]. The following section aims to introduce how AD is and has been classically thought of over the past several decades, new findings that are emerging from imaging-histopathological studies, and the implications for future thinking about the AD process.

1.2.1 Current Understanding of Alzheimer’s Disease

Although multiple models exist to explain the pathologic processes associated with AD, the dominant model in the field involves age, genetic risk factors, and regional deposition of amyloid β (A β) plaques and neurofibrillary tau tangles into the cerebral cortex [28, 29]. The definitive diagnosis of AD is only made post-mortem using histopathological autopsy samples. These abnormal proteins are thought to reduce interneuronal communication by destroying synaptic connections as well as inhibit intraneuronal axonal transport, contributing to the process of cognitive decline and specifically targeting memory function [22, 30]. These changes have been recognized for decades, yet their origin and development are poorly understood. Furthermore, there are currently no successful therapeutic interventions that target either of these proteins.

In addition to the deposition of A β plaques and tau neurofibrillary tangles, the current model of AD recognizes several other pathological tissue changes that can be

evinced as alterations in brain structure seen on magnetic resonance imaging (MRI). Two of these structural changes that are used to quantify pathology *in vivo* are hippocampal volume decreases in AD brains as well as cortical thinning in regionally-specific patterns [31, 32]. These changes in part reflect degeneration of the cerebral cortex, seen histologically as the degeneration and dropout of neurons as well as gliosis and lipofuscin accumulation in remaining neurons [33]. These pathologies extend to and are exacerbated specifically in the hippocampus and entorhinal cortex, in which layer II neurons appear to be particularly vulnerable [34]. In addition to neuronal degeneration, a regionally-specific reduction in dendritic branching has also been seen in AD brains [35] as well as a significant reduction in the number of regionally-specific synapses [36–39].

1.2.2 White Matter and Alzheimer’s Disease

As described in the previous section, researchers have demonstrated significant changes in the WM as a result of normal aging. Significant reductions in the WM of AD brains that exceed the expectations of normal aging have also been found, but as AD is a *disease of aging* it is difficult to disentangle whether or not these pathological processes are AD-specific. As with ‘normal’ aging, the changes that can be seen with structural imaging include loss of total WM volume and development of WMSA. Due to these similarities, WM pathologies are not typically thought of in AD disease models and are therefore not given significant clinical attention. New findings that point to the clinical significance and potential mechanisms of these changes will be discussed in further chapters.

As with normal aging, the simplest metric of WM change that has been studied in AD is the total volume of cerebral WM. The same study that first demonstrated decreases in cerebral WM volume with aging also demonstrated greater WM loss in individuals with AD than found in normal aging [11]. Other groups have studied the relationship between WM volume and AD with finer granularity by studying the volume of WM in individual gyri and their relationships with surrounding gray matter and sulcal shapes. Widening of sulci has been associated with decreases in

WM volume and cortical thickness in surrounding gyri independent of age. This study found that sulcal changes were most sensitive at discriminating healthy controls from individuals with MCI, potentially suggestive of WM atrophy or cortical thinning [40].

While WMSA are common in normal aging, they are more prevalent in frequency and affect a greater spatial extent of WM in individuals with AD compared to cognitively healthy older individuals [41,42]. Recent evidence also suggests that the spatial pattern of WMSA differs between cognitively healthy older controls and individuals with AD, with specific involvement of parietal WM [43,44]. **Chapter 4** will focus on this idea and demonstrate novel techniques to further discretize the WM leading to novel spatial findings. In addition to volume and spatial distribution, others have suggested that there are other properties of WMSA that may provide useful information in distinguishing between AD-related WMSA and "normal" age-related WMSA [45, 46]. **Chapters 2 and 5** will elaborate on different techniques for using WMSA predictively. A final note about WM and AD relates to the underlying genetics of AD. The primary genetic risk factor for AD is the APOE ϵ 4 allele. The presence of this allele has also been associated with the presence of WMSA [47,48].

Taken together, WM findings in aging and cognitive decline point towards potential pathological pathways in AD that were previously unappreciated. New theories of AD suggest that the disease process is heterogeneous and involves pathologies in addition to amyloid and tau. Whether the upstream cause of this constellation of biological changes is singular or multifaceted is still unknown. Clinicians and researchers have proposed a "multi-hit" hypothesis that attempts to explain the different pathological profiles that manifest in similar cognitive profiles. This work will provide an in-depth assessment of WM in aging and in AD, and will tie these findings together with the more classic AD markers of amyloid and tau in an attempt to explain current gaps in our understanding of the clinical presentation of AD.

THIS PAGE INTENTIONALLY LEFT BLANK

Chapter 2

Computational Methods for WMSA Analysis

“We have so much time and so little do to. Wait a minute. Strike that. Reverse it.”
-Roald Dahl, “Charlie and the Chocolate Factory,” 1964

Over the past decade there have been many attempts to design tools for the computational analysis of white matter signal abnormalities (WMSA), most of which are limited to automatic segmentation of these lesions from normal-appearing white matter (NAWM) [49]. The gold standard for WMSA segmentation is manual segmentation by an expert neuroradiologist which is time-consuming, cumbersome, and prone to inter-rater as well as intra-rater variability. For this reason, semi-quantitative methods for visually assessing WMSA have been developed such as the Fazekas scale which separately rates ‘periventricular’ and ‘deep’ WMSA on a scale of 0-3 based on total volume [50]. These methods, like manual labeling, suffer from subjective variability and do not capture subtle differences in WMSA volume or spatial distribution. In addition to these limitations, more recent work has demonstrated the continuous nature of WM damage suggesting that tools that are capable of labeling WMSA on a continuous scale may be more robust as well as provide more in-depth information regarding the underlying tissue integrity.

2.1 Automatic Segmentation

2.1.1 Technical Development

The initial goal of this body of work was to create a tool that was capable of automatically segmenting WMSA from NAWM intended for use by a broad audience with differing neuroimaging datasets. With a goal of incorporating this tool into the existing FreeSurfer framework for future open source deployment, the development of this tool followed similar methods that are employed in the standard FreeSurfer processing stream for the segmentation of healthy brain structures. In this process, a standard atlas is created from several human brain MRI datasets that have manual labels for all structures created by a trained neuroradiologist, as manual labeling to-date is the "gold standard" of brain segmentation for healthy and pathological structures. This atlas is then used in the automatic segmentation pipeline and is a form of supervised learning.

Data

The data used in the creation of this tool come from the Alzheimer's Disease Neuroimaging Initiative (ADNI) open source dataset.

Methods

MRI Acquisition

All data were acquired on a 1.5-T scanner at rigorously validated sites, which all followed a previously described standardized protocol [51]. The protocol included a high-resolution, T1-weighted sagittal volumetric magnetization prepared rapid gradient echo sequence and axial proton density (PD)/T2-weighted fast spin echo sequence. The ADNI MRI core optimized the acquisition parameters of these sequences for each make and model of scanner included in the study. All scanner sites were required to pass a strict scanner validation test prior to being allowed to scan ADNI participants. Additionally, each scan of ADNI participants included a scan of the phantom, which was required to pass strict validation tests.

MRI Preprocessing

The WMSA segmentation procedure was developed within the FreeSurfer image anal-

ysis suite, which allowed this procedure to be performed in the context of robust whole brain labeling. Cortical reconstruction and volumetric segmentation was performed using FreeSurfer's standard recon-all stream (surfer.nmr.mgh.harvard.edu/, version 5.1). The technical details of these procedures are described in prior publications [1, 52–59].

Atlas Creation

The WMSA atlas was created as an extension of FreeSurfer's unimodal T1-weighted atlas used for standard automatic segmentation of healthy gray and white matter structures [1]. WMSA were manually labeled on 7 subjects by a trained expert (ES) using T1, T2, and PD images as a guide. WMSA were defined based on consensus guidelines for measurement of "WM hyperintensities of presumed vascular origin [60]." Using these new WMSA labels in conjunction with all standard FreeSurfer labels, a multimodal Gaussian classifier array (MMGCA) was created that contained a three-dimensional covariance matrix of intensity values (T1, T2, and PD) with probabilities for each structure at each voxel in addition to spatial and neighborhood prior information. The following results present volumes in terms of number of voxels, where one voxel corresponds to 1mm³ of tissue.

WMSA Segmentation, Classification, and Quantification

Visual guides to supplement the following automatic segmentation methodology are provided in Figure 2-1. A voxel is first classified based on the maximum *a posteriori* probability (MAP) that it is in a given class given the voxel's T1/T2/PD intensity profile and the MMGCA probabilities at that location. We note that this first step extends prior work with T1/T2/PD modalities in WMSA labeling [61, 62]. While this simple atlas approach successfully labels many WMSA, it is not sufficient generally because WMSA can occur anywhere in WM (not just in likely atlas locations) and because the intensities are highly variable (and so not fit well by a Gaussian model; Figure 2-1 C). We therefore follow up the MMGCA procedure with several refinements designed to catch unlabeled WMSA. These refinements rely heavily on the Mahalanobis distance (MD) [63] of a WMSA voxel from NAWM. The MD gives a voxel's distance from a distribution and is defined as:

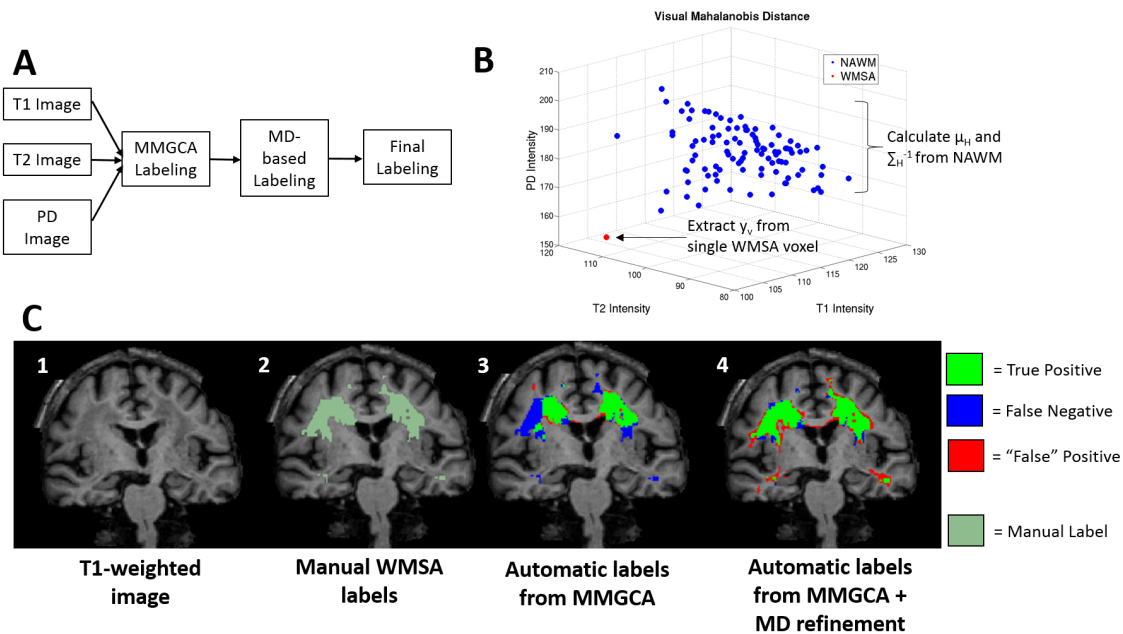


Figure 2-1: A) Flowchart of major steps involved in automatic WMSA labeling pipeline. B) Visual representation of Mahalanobis distance, using a single WMSA voxel and 100 randomly selected NAWM voxels from an ADNI data set. Red point indicates a single WMSA voxel's position in T1/T2/PD intensity space, and blue dots indicate positions of NAWM voxels. The WMSA voxel's MD is measured from NAWM using Equation 1. C) Comparison of the automatic WMSA labeling with only the MMGCA step to the manual labels (C.3) and comparison using the automatic labeling using MMGCA + MD refinement (C.4). This single subject is a representation of the general trend seen in the ADNI data, where the MMGCA labeling frequently failed to label connected sections of WMSA voxels that were detected by a manual labeler, and these sections were corrected with the MD refinement step. We additionally note that the “false” positives seen in C.4 are addressed in the Validation section of the Methods, and actually reflect damaged tissue that was undetected by the human rater. Subtle differences in tissue signal intensity in these regions can be seen in the T1-weighted image (C.1).

$$MD = (y_v - \mu_H)^T \sum_H^{-1} (y_v - \mu_H) \quad (2.1)$$

Where y_v is the vector of multimodal signal intensities at voxel v , μ_H is the vector of mean multimodal intensities in NAWM, and $\sum H$ is the covariance matrix of the multimodal intensities in NAWM (Figure 2-1 B). We interpret the MD as a measure of WM damage.

In the first refinement step, non-WMSA neighbors of voxels initially labeled as WMSA are examined. Using a heuristic that combines information regarding a voxel's:

1. Number of WMSA neighbors
2. Intensity values in relation to the MMGCA intensity values for other tissue types
3. MD from other tissue types defined in the MMGCA

non-WMSA voxels are relabeled as WMSA or left unchanged. In the second refinement step, the MMGCA atlas parameters are abandoned in favor of using statistics from the subject's own NAWM and WMSA as a reference. It follows a similar region-growing procedure as in the first step but uses these individual-based values instead (Figure 2-1 A). This yields a final binary labeling of WMSAs. Although the final labeling retains some "false" positive labeling (Figure 2-1 C.4) compared to the manual label, analyses described in the following validation section suggest that a portion of these voxels are in fact unique and are representative of changing tissue. Difference in signal tissue intensity can be seen in the subject's T1-weighted image in these "false" positive regions (Figure 2-1 C.1).

2.1.2 Validation

Methods

Two methods were used to validate the automatic segmentation procedure. First, a set of manual labels was created from nine of the 459 ADNI subjects by a trained

labeler (KN; example in Figure 2-1 C.2). These data were used as an independent test set for the WMSA segmentation algorithm. For each of these data sets, the overlap between the manual and automatic WMSA labels was quantified using the Dice coefficient:

$$Dice = \frac{(2 \times |AB|)}{(|A| + |B|)} \quad (2.2)$$

where A corresponds to the set of voxels labeled by the manual rater, and B corresponds to the voxels labeled by the automatic procedure.

Low Dice scores (Table 2.1.2) were predominantly due to voxels being labeled as WMSA by the automated procedure that were not labeled by the manual rater (i.e., putative false positives Figure 2-1 C.4). Upon closer visual inspection, these "false" positives (FP) did not appear to be healthy white matter; yet, they were not labeled as WMSA by the manual rater. This motivated a second validation procedure to determine whether the voxels labeled WMSA by the automated procedure, but not by the manual rater, were indeed different from NAWM. The basic idea is that if these voxels are truly healthy then they should appear healthy in future time points and should not progress like WMSA. To test this hypothesis, we identified "false" positive voxels and extracted their T1/T2/PD intensity profiles at baseline (the time of manual labeling) as well as at six and twelve months post-labeling, for a total of nine intensity values for each FP voxel. The mean T1/T2/PD intensities of NAWM at baseline were also calculated. For each FP voxel, the mean baseline NAWM intensity was subtracted from each of the three time points, for a total of nine FP - NAWM difference values. A one-sample t-test was then performed with the nine values for each voxel, with the null hypothesis that these values came from a zero-mean distribution, and were therefore not significantly different from NAWM. All voxels resulting with $p < 0.01$ were used as new 'true positives' (TP) in the recalculation of an updated Dice score. Of note is that the purpose of this longitudinal validation method is to demonstrate the cross-sectional validity of the automatic segmentation tool, and longitudinal data is not necessary for accurate WMSA segmentation.

Subject	Dice coefficient	% FPs with $p < 0.01$	Updated Dice coefficient
1	0.7897	82.4	0.8741
2	0.7008	81.95	0.9260
3	0.7368	81.93	0.9186
4	0.6934	74.32	0.8840
5	0.1613	83.32	0.9086
6	0.7180	65.63	0.8913
7	0.6691	64.16	0.7887
8	0.5916	71.38	0.8891
9	0.7033	78.09	0.9053

Table 2.1: Dice coefficients between all WMSAs labeled by automatic procedure and human rater for 9 data sets with manual labels available (column 2); percent of FPs whose longitudinal NAWM-subtracted intensities resulted in a p -value < 0.01 with a 1-sample t test (column 3); updated Dice coefficients using significant FP voxels as new true positives (column 4). (FPs = false positives; NAWM = normal-appearing white matter; WMSAs = white matter signal abnormalities).

Results

Manual Label Agreements

The Dice coefficients between manual and automated labels are reported in Table 2.1.2. There was variation in the overlap across subjects. A one-sample t-test was used to compare "false positive" (FP) voxels over time to baseline NAWM as described in the Methods section. Under the assumption that these voxels truly were NAWM and were mislabeled by the automatic segmentation, the null hypothesis was that the intensity differences of these voxels from baseline NAWM would resemble values from a zero-mean distribution. Table 2.1.2 also shows the percent of all FP voxels whose intensity difference from NAWM intensities remained significant at $p < 0.01$, indicating a true difference from NAWM. These significant voxels were then relabeled as "true positives" and a new Dice coefficient was calculated, resulting in a substantial improvement for many subjects.

Conclusions

One of the main sources of difficulty in validating any automatic segmentation tool for WMSA lies in the lack of a true gold standard for comparison. Manual labeling of WMSA suffers from low inter-rater and intra-rater reliability. Dice coefficients can vary widely between subjects in the same study, as well as across studies with

different manual raters [64]. Additionally, because the Dice coefficient is defined by true positives, false negatives, negatives, and false positives, two individuals with the same number of erroneous labels may have very different scores, depending on the amount of true lesion as defined by a manual labeler (i.e., subjects with much larger lesion loads will tend to have significantly higher Dice scores). The Dice coefficients calculated for our data indicate high precision for some subjects, but low precision for others as compared with manual labels. This phenomenon is common in the literature [?, ?, 65], and we attempted to investigate the validity of our FPs, which were the major cause of low Dice values, with longitudinal data. Our results suggest that while a manual labeler may not have recognized these voxels as lesions, they contain subtle intensity information that differentiates them from truly NAWM, and can be followed in time to show more profound differences. By following an initial time point's FPs voxels longitudinally, we show compelling evidence that our technique is actually more sensitive to detecting WMSAs than a human rater. We suggest from these findings that future WMSA segmentation procedures be compared with quantitative gold standards derived from signal properties in addition to manual confirmatory procedures.

2.2 Novel Metrics for WMSA

Neuropathology studies demonstrate histopathologic and imaging heterogeneity within and across WMSA [13, 66–70], suggesting that quantifying WMSA on MRI by measuring total volume, as is usually done, may not accurately reflect the total severity of the damage. WMSA are typically reported to have a "penumbra" of abnormal tissue surrounding a damaged core [71]. For example, on a T2-weighted scan some damaged tissue may evince signal intensities as bright as fluid, while other locations exhibit just a slight brightening relative to NAWM intensities. These irregular signal properties contribute to poorly-defined boundaries and create difficulties in automatically segmenting damaged tissue from healthy tissue. The majority of automatic segmentation tools suffer from a lack of validation across multiple datasets and often

have limited utility in that they require a specific set of MRI modalities such as both T1-weighted and FLAIR images, which are not always available. Thus, improvements in the automated segmentation and quantification of WMSAs would contribute to increased reliability, and potentially enhance the clinical utility of this marker of tissue damage [72, 73].

2.2.1 Technical Development

Methods

Data

Several datasets were used in the development of our secondary set of WM tools. The first comes from the Alzheimer’s Disease Neuroimaging Initiative (ADNI) dataset as described in the above section. The second dataset was taken from the 2008 MICCAI MS Lesion Segmentation Challenge. These data are comprised of individuals with multiple sclerosis (MS), a disease in which WMSA are a hallmark neuroimaging finding. Each individual in MICCAI dataset has T1-weighted, T2-weighted, and FLAIR images. For half of the subjects provided by MICCAI, manual WMSA labels are also provided for algorithm training purposes.

Atlas Creation

In the above section, I described an atlas created for the automatic segmentation tool that generates a binary mapping of WMSA through the entire cerebral WM. Here I describe a second type of atlas used for calculating continuous metrics of WM damage.

To make the described tool widely accessible to investigators, I have implemented it such that it can be used on one of the three following combinations of imaging modalities: T1/T2/PD, T1/FLAIR, or T1/T2/FLAIR. For each of these combinations, a regional atlas of image intensity values was created from a set of subjects with low WMSA volumes. For the T1/T2/FLAIR and T1/FLAIR atlases, the MICCAI dataset was used. For the T1/T2/PD atlas the ADNI dataset was used.

For each atlas, the 10 subjects with the lowest levels of WMSA in each respective dataset (ADNI or MICCAI) were selected and processed with FreeSurfer’s recon-all

stream. This process results in automatically-defined WM parcellations for 35 bilateral (70 total) regions of interest (ROI). All subjects were intensity-normalized to a standard atlas using methods previously described and available in FreeSurfer (REF). For each ROI, the distribution of multimodal image intensity values was collected for all 10 atlas individuals in voxels that were definitively NAWM as determined by expert manual labeling. This resulted in a multimodal intensity distribution of NAWM for each of 70 ROIs comprising the entire WM.

Metrics for Continuous Damage

To quantify continuous damage throughout the entire WM, we return to the Mahalanobis distance (MD) metric defined in the above section in Equation 2.1. For a given subject that one wishes to segment for WMSA, the following steps are performed:

1. The T1-weighted image is first processed through FreeSurfer’s recon-all stream to generate parcellations of the 70 WM ROIs.
2. The appropriate WMSA atlas is then chosen depending on the data available (i.e. if a data set only has T1 and FLAIR images, the T1/FLAIR atlas is used).
3. For each ROI, a voxel-by-voxel calculation of the MD from the atlas’s entire ROI distribution is performed for each voxel, and this is the voxel’s continuous damage score.

For example, in a given subject, the MD of each voxel in the middle temporal WM is calculated from the atlas’s entire middle temporal WM distribution of NAWM, and a higher MD indicates more severe damage.

Tool Output

The output of the above tool is a continuous damage map of the entire WM (Figure 2-2). Using the existing FreeSurfer `mri_segstats` tool, mean and standard deviation metrics of these continuous damage values can be generated for each of the 70 WM ROIs and output into a text-based file. Although not yet fully validated, we note that many types of more in-depth metrics and analyses can be extracted from and performed on these continuous damage maps. One such is the creation of subclasses of

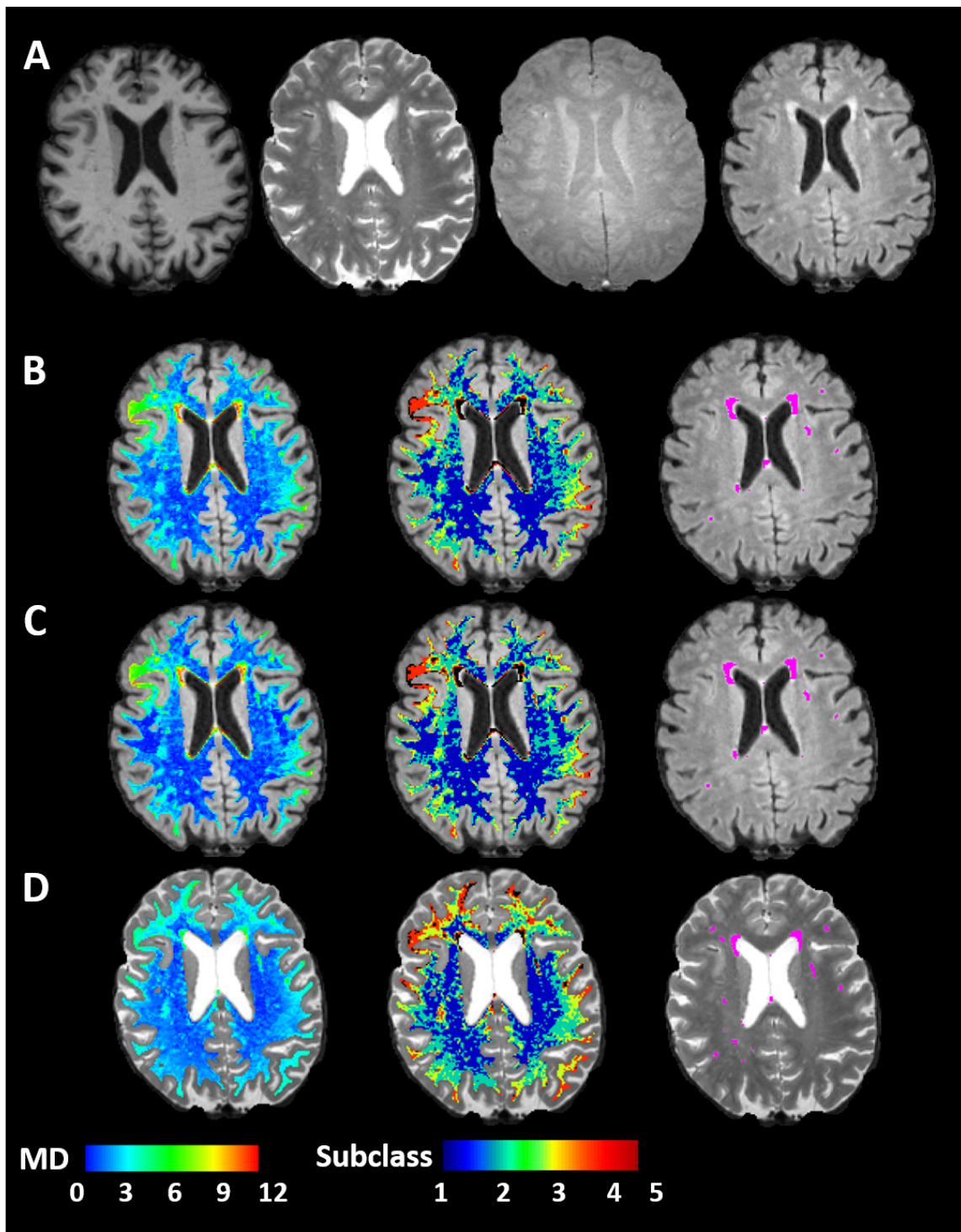


Figure 2-2: A) T1-weighted, T2-weighted, PD-weighted, and FLAIR images for a single subject. B) T1/T2/FLAIR method: continuous (left), subclass (middle), and binary WMSA segmentation (right) using T1/T2/FLAIR method, C) T1/FLAIR method: continuous, subclass, and binary WMSA segmentation using T1/FLAIR method, D) T1/T2/PD method: continuous, subclass, and binary WMSA segmentation using T1/T2/PD method.

WM damage using a k-means clustering algorithm across all voxels. In this scenario, a user can specify how many subclasses they would like to define within the WM, and segment each WM voxel into one of these classes (Figure 2-2 center column demonstrates an example of this using $k=5$). This would result in global volumes of each subclass, as well as within-ROI volumes of each subclass.

We note that the MD values are different between the methods using FLAIR and those that do not (Figure 2-2 B & C vs. Figure 2-2 D). MD, however, is a unitless value and we further note that the spatial pattern of increasing and decreasing MD throughout the WM is the same across all modality combinations, and therefore can be used to demonstrate relative differences across all individuals in a given cohort or study using the same modality combination. Additionally, the subclass demarcation is similar across all modality combinations as is the binary segmentation of WMSA.

We note that binary segmentations can be generated from these continuous damage maps as well by specifying an MD-threshold at which a voxel transitions from NAWM to WMSA. The described tool is equipped with this feature for investigators to experiment with in their own data, as different datasets and different modality combinations may require different MD-thresholds. We refer to **Section 2.1** for a fully validated tool for automated binary segmentation fo WMSA from NAWM.

2.2.2 An Application in Disease Populations

Methods

Data

Data used for the application study in this chapter as an example of the WMSA segmentation tool come from the ADNI database. Subjects used in this application fell into one of four diagnostic categories: older controls (OC), individuals with mild cognitive impairment who did not convert to AD within three years (MCI-NC), individuals with MCI who did convert to AD within three years (MCI-C) and individuals with Alzheimer's disease (AD).

Statistical Analyses

Selected regional quantitative metrics are reported as examples of the application

of the described techniques. I specifically limited analyses to the rostral anterior cingulate WM and the supramarginal WM. The WM metrics of these regions were assessed against age as well as against clinical diagnosis. For continuous assessment with age, general linear models (GLM) were conducted to determine if the given WM measure had a significant association with age. For assessment with clinical diagnosis, a one-way ANOVA was conducted to determine if the WM measure varied significantly between diagnostic groups.

Results

Regional Measures

Figures 2-3 and 2-4 show regional statistics for rostral anterior cingulate (AC) WM and supramarginal WM respectively using the described tool with a T1/T2/PD imaging modality combination. In the top row of each figure, raw WMSA volume is assessed against age, and a GLM shows that this relationship is stronger in rostral AC WM ($p<0.001$) than in supramarginal WM ($p<0.05$). On the other hand, when assessing this measure against clinical diagnosis, supramarginal WM demonstrates a stronger difference between OC and AD individuals ($p<0.001$) than does rostral AC ($p<0.01$). These patterns remain similar in the second row, when assessing WMSA as a percent of the region's entire WM. The third row each figure demonstrates volumes of each damage subclass against age and diagnosis. Rostral AC WM shows no subclass associations with age, but supramarginal WM shows significant increases in high-level damage (subclass 5) and moderate-low-level damage (subclass 2) with age, and decreases in low-level damage (subclass 1) with age. Additionally, the relative volume distributions of these five subclasses differs between the two regions of interest. The highest level of damage (subclass 5) demonstrates a significant relationship with clinical diagnosis, but there are no subclass-diagnosis relationships in rostral AC. The fourth row each figure shows relationships with the average continuous damage level (MD) and age and diagnosis. This measure does not have a significant relationship with age in rostral AC WM, but does in supramarginal WM ($p<0.01$). It shows the same pattern of relationship with clinical diagnosis in both regions in that the OC group has a significantly lower damage value than the other three diagnostic groups,

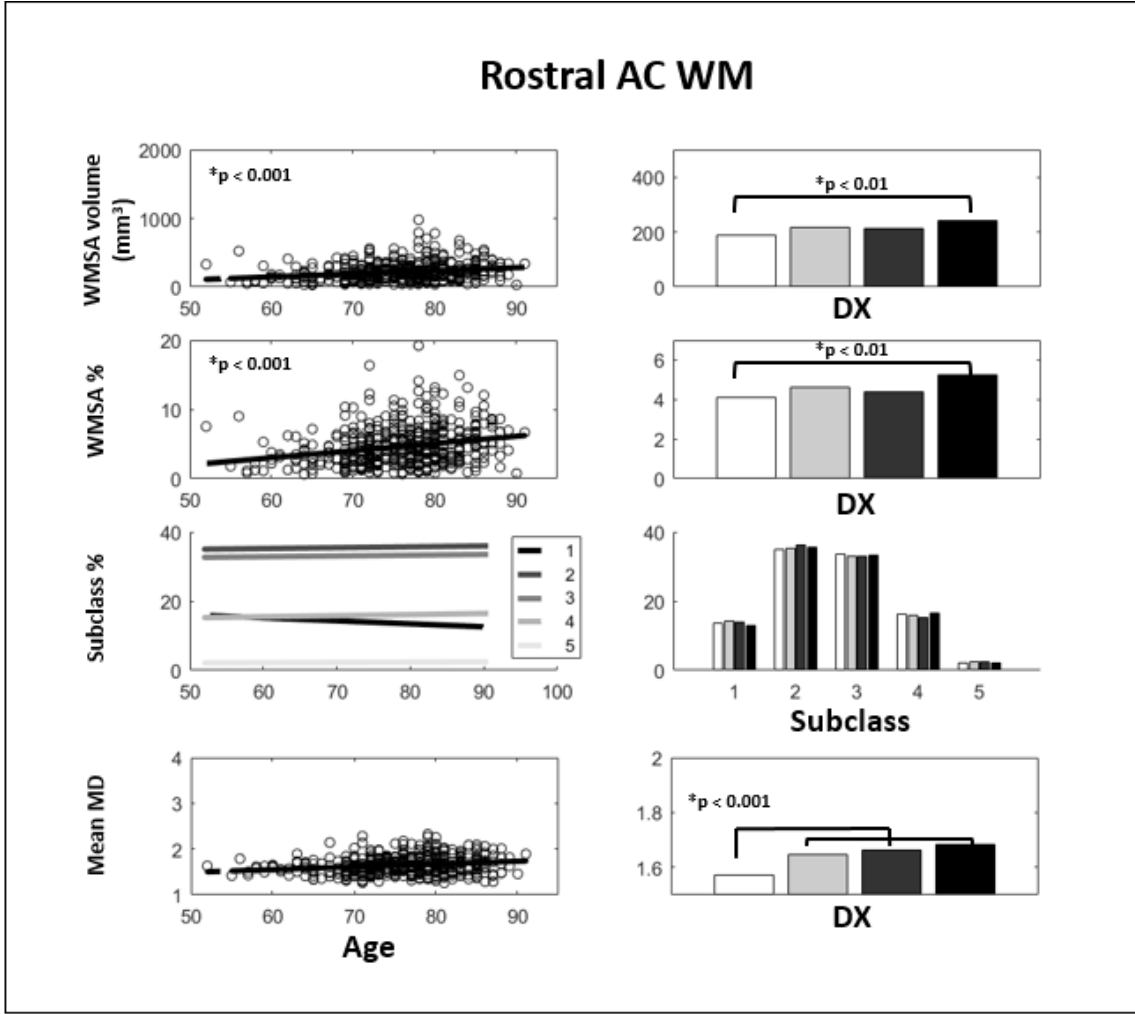


Figure 2-3: Descriptive statistics for rostral anterior cingulate WM (left) and for supramarginal WM (right) with respect to age as well as clinical diagnosis. p -values for analyses with age refer to one-sided t-tests for significance of the slope. p -values for analyses with diagnoses refer to one-way ANOVAs testing for group differences, with brackets indicating specific group differences as determined by follow-up tests. Top row: raw WMSA volume versus age and clinical diagnosis. Second row: WMSA volume as a percent of regional WM volume versus age and clinical diagnosis. Third row: Each subclass's volume as a percent of regional WM versus age and clinical diagnosis. Bottom row: Mean MD of entire WM region versus age and clinical diagnosis.

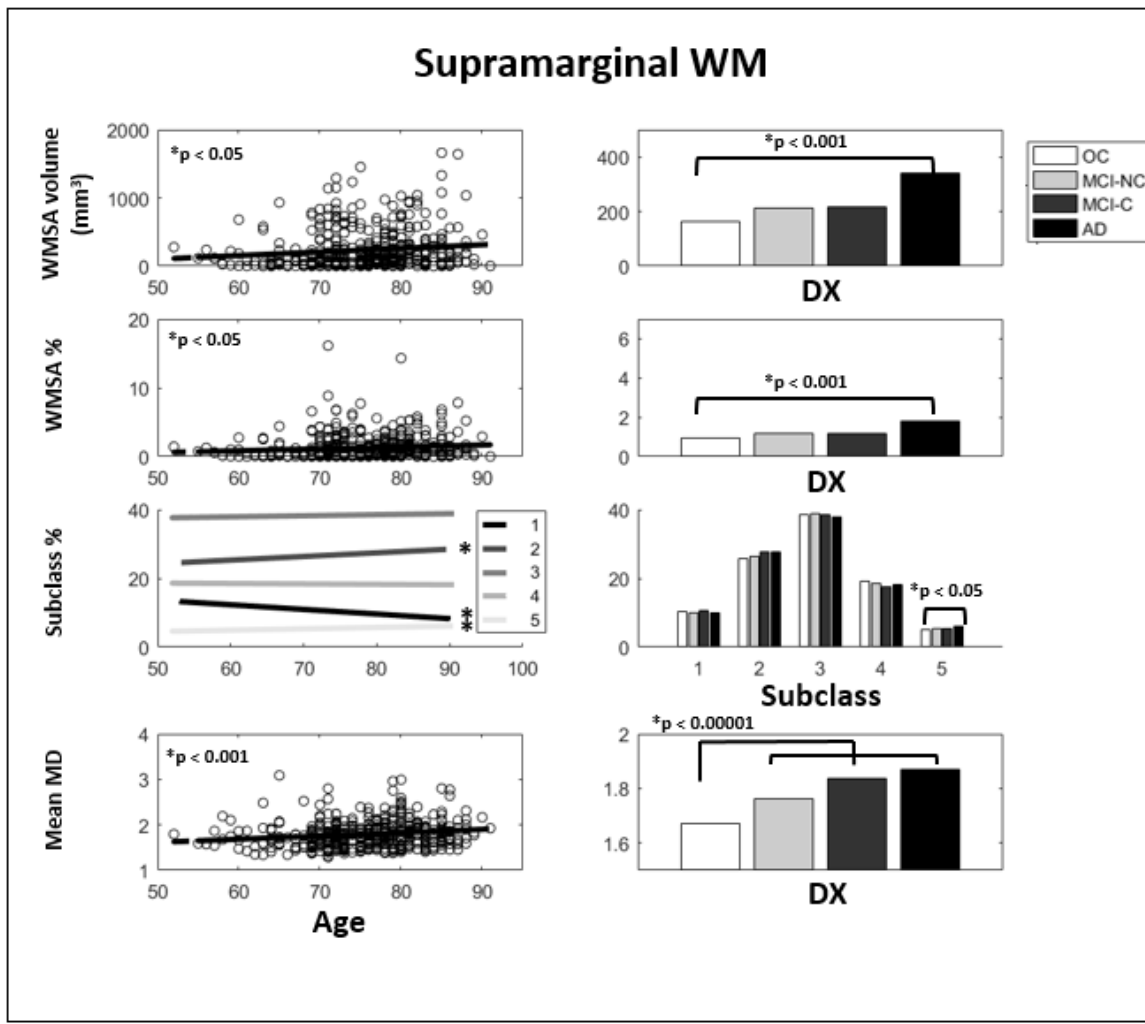


Figure 2-4: Descriptive statistics for rostral anterior cingulate WM (left) and for supramarginal WM (right) with respect to age as well as clinical diagnosis. p -values for analyses with age refer to one-sided t-tests for significance of the slope. p -values for analyses with diagnoses refer to one-way ANOVAs testing for group differences, with brackets indicating specific group differences as determined by follow-up tests. Top row: raw WMSA volume versus age and clinical diagnosis. Second row: WMSA volume as a percent of regional WM volume versus age and clinical diagnosis. Third row: Each subclass's volume as a percent of regional WM versus age and clinical diagnosis. Bottom row: Mean MD of entire WM region versus age and clinical diagnosis.

but this relationship is more statistically significant in supramarginal WM than rostral AC WM. Additionally, the overall MD values are higher in supramarginal WM indicating greater average damage in this region than in rostral AC WM.

Conclusions

In this section, I described a more in-depth tool that is capable of performing *continuous* damage labeling of the cerebral WM. In the past, it has been common practice in the literature to perform binary segmentation of WMSA from normal-appearing white matter (NAWM) and to quantify the total WMSA burden for individuals as a single metric. There are limitations to performing binary segmentation of WMSA, however, in that they often have fuzzy borders that are not clearly distinct from the surrounding NAWM. This can cause disagreement between automatic labels produced by different tools as well as by manual labeling which is considered the gold standard for WMSA segmentation [71, 74]. I provide here a tool that computes multiple different regional metrics of WM and WMSA within the confines of FreeSurfer, an already widely-used tool for structural segmentation of human brain MRI. As an example of this tool’s utility, I demonstrate that its output metrics are associated with age as well as clinical diagnosis in supramarginal and rostral AC WM. These ideas will be visited in more depth in **Chapters 3 and 4**.

2.3 Conclusions

Here I present a complete description of a novel set of tools for the multimodal segmentation of WMSA and description of WM quality. Many other studies have demonstrated the validity of binary segmentation of WMSA using automatic tools, but none have provided detailed qualitative or spatial statistics of the entire WM. The utility of the qualitative statistics of WMSA using the MD metric will be further described in a disease population in **Chapter 4** of this work. Along with this tool’s description, I provide example output for two WM regions whose characteristics differ as they relate to aging and clinical diagnosis. Supramarginal WM was chosen as parietal WM regions have been reported to increase in WMSA burden in AD [43, 44].

Rostral anterior cingulate WM was chosen as a second region, due to known associations between WMSA and age in WM regions close to the ventricles [5]. These regions were chosen to demonstrate how this tool could be replicated and applied to many different cohorts of individuals. The spatial specificity provided by this tool allows for a more granular spatial analysis of the WM than other existing tools to our knowledge. In general, most existing automatic segmentation tools use the classification of ‘deep’ versus ‘periventricular’ WMSA when explaining spatial statistics, and sometimes also include demarcation into the four major lobes of the brain [75, 76]. This is limiting to investigators who wish to study the functional impact of WMSA, as these large lobar WM regions each encompass many different functionally-specific gray matter regions. Additionally, there is conflicting evidence as to the spatial distribution of WMSA in diseases such as AD, and this may be in part due to the lack of precise spatial analysis. The use of large WM lobes alone as spatial regions dilutes results that may be subtle, but would be more appreciated in a finer-grained parcellation. Using the FreeSurfer WM parcellations [11, 56], I describe spatial WM statistics for each region of the WM that corresponds anatomically to a functional gray matter region.

Following from the limitations of binary WMSA segmentation, several studies have noted the heterogeneity of signal intensity within WMSA, highlighting their typically bright core on T2 and FLAIR imaging that then fades into the surrounding NAWM [5, 71, 77]. In addition to this, NAWM itself is quite heterogeneous in signal intensity, but these cerebrum-wide NAWM properties are often only assessed with diffusion imaging rather than classic structural imaging. In the tools described here, I implement a method for the assessment of WM integrity on a continuous scale using the Mahalanobis distance [63] metric with structural imaging alone. Further clinical utility of this metric will be described in **Chapter 4**. Using two regions of interest, I show that associations between MD and age as well as between MD and diagnosis differ between regions in the brain. In rostral AC WM, there is no age association with MD, but supramarginal MD increases with age, indicating greater decline in supramarginal WM quality with age. Additionally, there is a stronger association

between MD and AD diagnosis in supramarginal WM than in rostral AC.

The final metric included in this novel tool is a subclass demarcation of all WM into five classes of 'damage.' This metric has been implemented as a more exploratory option for future studies, as it has not been used before in any published work by our group. I show here, however, that even these subclasses show differing relationships with age and diagnosis across different regions of WM. In Section 2.1 I demonstrated that NAWM voxels that are subthreshold for being defined as WMSA often have 'pre-damage' properties, and reliably convert to WMSA in the future. I suggest that these subclasses could be used in the future in more exploratory ways to determine if WM in the middle-ground of damage (i.e. somewhere between completely healthy and WMSA) can be assessed to be another factor in disease prognosis and diagnosis. For example, in the two regions of interest, I show that the volume of WM in the second-lowest subclass of damage is associated with age in the supramarginal WM, while no subclasses show an age association in rostral AC. Additionally, the volume of WM in the highest-damage subclass shows a relationship with diagnosis in supramarginal WM, while not in rostral AC. The newly described tool presented here for the quantitative, qualitative, and spatial analysis of WM from structural imaging data is written in MatLab and will be available for public download and use.

Chapter 3

Assessing WMSA in Healthy Aging

*“Instead of asking him how much of your time is left,
Ask him how much of your mind, baby.”
-Prince, “Let’s Go Crazy,” 1984*

To date, the integration of WMSA into an understanding of both normal and diseased brain aging has been challenging. Prior studies have demonstrated that WMSA are associated with a range of altered neurological and psychological profiles and contribute to the profile of dementia in individuals with compounded neurological disease [14,67,78–84], yet they are often treated as a benign comorbidity of aging due to their high prevalence of 80-95% in older adults [14,85,86]. In order to better understand the development of WMSA without the complications of concurrent cognitive impairments, the aim of this chapter is to outline a staging procedure for WMSA in cognitively healthy older adults that can later be applied to disease populations such as Alzheimer’s disease (AD) and mild cognitive impairment (MCI) to determine how WMSA involvement relates to disease state.

Visual rating scales exist for describing the degree of WMSA within an individual [75, 76]. These scales have been useful in ranking individuals based primarily on the degree of periventricular compared to ‘deep’ WMSA. While individual variation exists, imaging studies have demonstrated that WMSA generally first appear and are most prominent in periventricular areas when total lesion burden is low, but they

progressively expand to include WM distal to the ventricles and proximal to the cortex with greater disease burden [87,88]. It is still unclear, however, whether or not aging individuals show a stereotypical pattern of WMSA development. This study investigates whether there exists a consistent relationship between global and regional WMSA burden and uses this information in the quantitative staging of WMSA based on vulnerable brain regions.

3.1 A Novel Staging Mechanism: Technical Development

Here we used an approach to perform an individual staging of WMSA that is inspired by prior neuropathological studies. In these studies, the degree of regional pathology in conditions such as Alzheimer’s disease is quantified by sorting individuals based on the severity of the given pathology and determining if a spatial pattern emerges [22, 89]. This creation of a WMSA staging procedure is limited to cognitively healthy older adults enrolled in the Alzheimer’s Disease Neuroimaging Initiative (ADNI) to avoid complications of comorbid neurodegenerative processes. In addition to this staging procedure, we devise a method to study the relationship between regional and global WMSA burden in order to understand how the WMSA burden in different regions of the WM scales with total WMSA, demonstrating specific regional vulnerabilities to WMSA. To provide an example of this method’s utility, the final staging procedure is then applied to individuals with AD and MCI to determine the relationship between disease prevalence and WMSA stage.

Data

As in **Chapter 2**, the data used in this work come from the ADNI-1 database. The following technical development was performed using 97 older controls (OC) from the ADNI-1 database. These individuals had no history of or current cognitive impairment, nor did they have any other neurological or psychiatric disease.

MRI acquisition, preprocessing, and WMSA segmentation methods reflect those

described in **Chapter 2** using ADNI data.

Methods

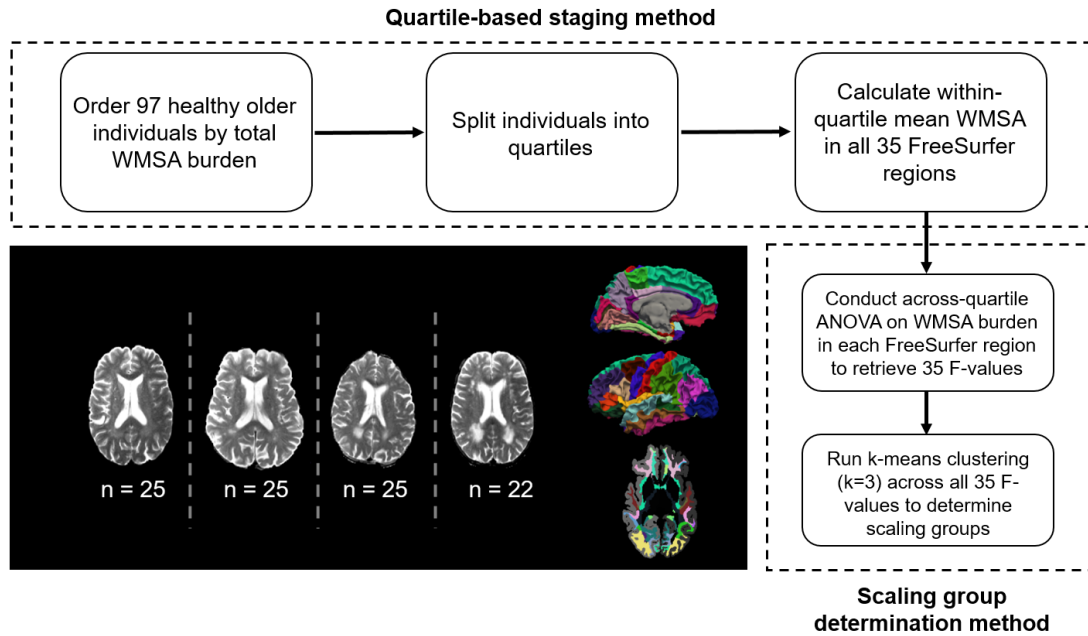


Figure 3-1: Visual representation of staging and scaling methods. In the scaling method, the three clusters from the k-means cluster analysis refer to ROIs that are non-scaling (low F-values), low-scaling(middle F-values),and high-scaling (high F-values) with global WMSA burden. Image shows examples of an individual in each of the four quartiles going from low to high total WMSA burden as well as FreeSurfer WM parcellations projected onto the brain's surface.

Quartile-Based Staging

After WMSA segmentation, the 97 OC individuals were sequentially ordered based on total global WMSA volume (rank ordered from lowest to highest WMSA volume) for an initial/preliminary staging. Four groups were defined by dividing individuals into simple quartiles corresponding to those with the lowest total WMSA (Quartile I, $n=25$), mid-low total WMSA (Quartile II, $n=25$), mid-high total WMSA (Quartile III, $n=25$), and highest total WMSA (Quartile IV, $n=22$) (Figure 3-1, image and first dashed box). Using quartiles is somewhat arbitrary however we found similar results when using tertiles, quartiles, and quantiles. Quartiles were settled on as a final choice as it allowed a compromise between statistical power and visualization of subtler differences between stages for spatial and temporal characterization. The

mean WMSA as a percent of total WM volume for each of the 35 bilateral FreeSurfer ROIs was calculated for each of the four quartiles. For visualization purposes, these mean values were mapped onto their corresponding cortical surface gyral regions (Figure 3-1, image). As with neuropathological studies [22,30,89], we infer staging based on cross-sectional information and use regional scaling relationships with total WMSA burden as the basis of this procedure. This is appropriate for the given study as age-associated WMSA volume has been demonstrated to be non-decreasing with longitudinal data [71,90] and therefore a staged process can be inferred cross-sectionally.

Regional Scaling

We are seeking a way to quantify how the WMSA burden in a given ROI scales with global burden. To do this, we first performed an ANOVA testing for a difference across the four quartiles in each of the 35 ROIs. As the quartiles were determined based on global WMSA, a high F-value indicates that the ROI's WMSA load strongly scales with global WMSA load. Next, we clustered the ROIs into three groups based on F-value using a k-means ($k=3$) algorithm. These three progression clusters correspond to: (1) non-scaling ROIs, (low F-valued ROIs), (2) mid-scaling ROIs (middle F-values), and (3) High-scaling ROIs (high F-values). The ROI make-up of the progression clusters gives an idea of how WMSA burden spatially manifests across the brain, which is the goal of this study (Figure 3-1, second dashed box).

Validation

To evaluate our scaling method statistically, we employed a permutation-knockout test to determine whether the spatial scaling pattern that we found was likely to appear by chance. We refer to this as "ROI-shuffling." Under the null hypothesis, no ROI scales higher than any other ROI with global WMSA load. In each permutation, we randomly reassigned the WMSA volume of an ROI for a given subject to another ROI in that subject, repeating for all subjects. The data were then staged, and the F-value was computed for the ROI that had the highest F-value in the real data. This was repeated 10,000 times. The p -value for this top-ranking ROI was then computed as the number of times out of 10,000 that the permutation F-value exceeded the

F-value in the true data. The same procedure was repeated for the ROI with the second-highest F-value except that the highest ranking ROI was removed (knocked out). This was repeated for all high-scaling ROIs, knocking out the previous highest-ranking ROI. If the pattern found in the true data is likely to be seen by chance, then the p-values should be relatively high. Note that we cannot simply use the *p*-values computed from the ANOVA F-test they would be biased by the staging procedure.

To test reliability, 10,000 permutations were performed in which random subsamples of 64 individuals were chosen for each permutation. The above methodology was then applied to each subsample, by first ordering the 64 subjects, splitting them into quartiles, and performing ROI-based ANOVAs on each ROI. F-stats from the ANOVAs were then clustered, and the number of times out of 10,000 that each ROI was placed into its true scaling cluster, as determined from the full dataset, was calculated as its reliability score.

Final Staging Mechanism

To provide a quantitative guideline by which to stage future individuals, we developed a cut-off-based staging system using information from the quartile-based staging. This was done by identifying high-scaling ROIs from the quartile-based analyses and working backwards from Stage IV to Stage I. More specifically, the high-scaling ROI that showed the greatest WMSA difference between the third and fourth quartiles was first identified. The mean and standard deviation of the WMSA burden in this ROI in the fourth quartile were used to determine a cut-off value (cut-off 1). This was then repeated with high-scaling ROIs that differed significantly between the second and third quartiles (cut-off 2), and the first and second quartiles (cut-off 3). These three cut-off values were then used to re-stage all individuals in the OC group. F-tests for the equality of variances between quartile-based and final stages for OC individuals in each ROI were performed to determine if within-stage variance decreased using the final staging method.

Quartile	I	II	III	IV
n	25	25	25	22
WMSA load (mm ³)	13,571 (425.5)	17,996 (205.7)	23,461 (478.4)	34,933 (1215)
Age	73.92 (1.2)*	74.72 (1.4)	78.4 (0.9)	79.0 (1.3)
Sex (% male)	40	52	40	55
Years education	15.44	15.64	15.8	15.68
% History hypertension	28	48	44	59
% Hypercholesterolemia	12	4	16	9
% History endocrine-metabolic disorder	44	40	40	36
MMSE	29.2 (0.2)	29.2 (0.1)	29.2 (0.2)	28.8 (0.2)
Ventricular volume (% ICV)	1.6 (0.1)**	2.6 (0.2)	2.7 (0.3)	2.6 (0.3)

Table 3.1: Demographic and imaging data for individuals in each quartile. Mean and standard error of the mean values are reported for continuous measures. *Significantly different from Quartiles III & IV ($p < 0.05$). **Significantly different from Quartiles II, III, & IV ($p < 0.05$).

3.2 Applications

3.2.1 WMSA Staging in Healthy Aging

Data

The dataset used in the application to healthy aging described here is comprised of the ninety-seven healthy older controls from the ADNI data set described above.

Results

Demographics

Demographic information for the OC individuals in each of the four quartiles are listed in Table 3.2.1. Quartiles differed in age, with individuals in Quartile I being significantly younger than individuals in Quartiles III and IV. As designed, there was a significant increase in total WMSA burden at each progressive quartile. Individuals in the four quartiles did not differ in MMSE, sex distribution, years of education, hypercholesterolemia, history of hypertension, or history of endocrine-metabolic dis-

order. Individuals in Quartile I had significantly lower lateral ventricular volume than Stages II-IV. As cognitive function has been associated with WMSA burden in prior literature, we assessed if there was a correlation within-quartile or across all 97 subjects between WMSA and MMSE. No correlation was significant (Quartile I: $R=-0.09$, $p=0.64$; Quartile II: $R=0.21$, $p=0.32$; Quartile III: $R=-0.11$, $p=0.61$, Quartile IV: $R=-0.19$, $p=0.40$).

Spatial Differences Across Quartiles

Within-quartile means and variances of percentages of ROIs occupied by WMSA are reported in Table 3.2.1. The table colors indicate the scaling cluster that the ROI belongs to (this will be described in more depth in the next section). Isthmus cingulate (retrosplenial cortex) is an example of a non-scaling cluster as its WMSA load does not change much across the four quartiles (1.51, 1.02, 1.52, and 1.22% of the total ROI volume). On the other hand, precuneus is a high-scaling cluster with the WMSA load increasing by a factor of 2.7 from quartile I to quartile IV (2.60, 3.05, 4.91, and 6.92% of total ROI volume). Figure 3-2 demonstrates mean values visually; Figure 3-3 shows variances and demonstrates generally low variance across ROIs suggesting consistency to the observed staging.

Individuals in Quartile I exhibited substantial WMSA in periventricular, frontal, cingulum, and medial occipital WM. Greater WMSA was found in Quartile II over Quartile I in all of these regions, with additional WMSA in rostral middle frontal, pars triangularis, pars opercularis, inferior and superior parietal, paracentral, and fusiform in Quartile II. Individuals in Quartile III had greater WMSA in all ROIs present in Quartiles I and II, with additional WMSA becoming apparent in lateral occipital and the banks of the super temporal sulcus WM. Quartile IV individuals demonstrated even more WMSA in all regions evident in Quartiles I - III, and additional WMSA was seen in supramarginal and postcentral WM. WM in medial orbitofrontal, cuneus, entorhinal, parahippocampal, pars orbitalis, and superior, middle, and inferior temporal WM never exceeded 1% WMSA to be included as quartile-associated ROIs.

Scaling Clusters

K-means clustering performed on F-statistics from one-way ANOVAs on each ROI's

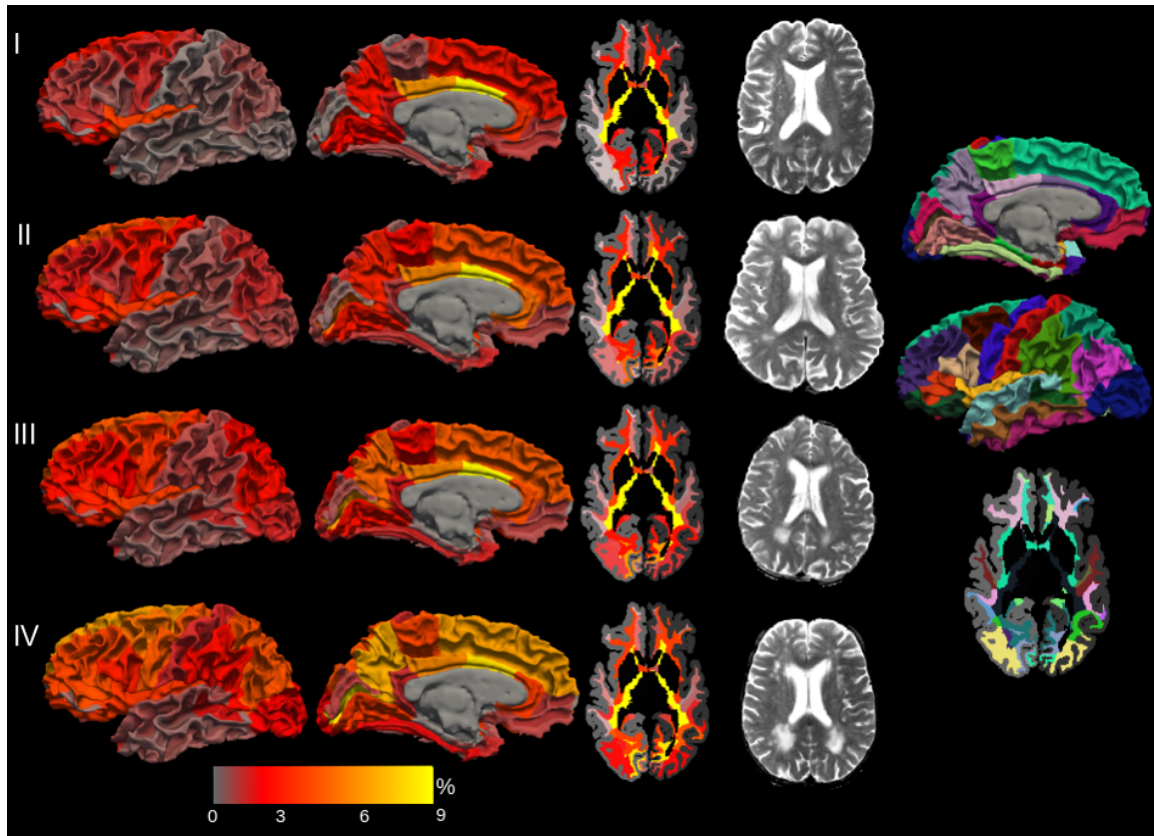


Figure 3-2: Left: Spatial staging of age-associated WMSA into four quartiles, using the percent of an ROI's total WM that is occupied by WMSA as a metric for comparison across quartiles. Surface maps showing the percent of each region's underlying WM that is occupied by WMSA (first and second columns) and an axial slice through the periventricular WM showing these values in a volume view (third column) for WM disease stages I-IV. Fourth column: an example individual from each quartile, taken from the 15th position within the quartile when ordered based on total global WMSA burden. Individuals in quartile I ($n=25$) demonstrate the lowest amount of global WMSA, with quartiles II and III ($n=25$, $n=25$) demonstrating higher global WMSA respectively, and quartile IV ($n=22$) demonstrating the highest overall WMSA burden. Right: surface images and axial slice of all atlas parcellations used in the present analyses [1-3].

Quartile	I	II	III	IV
Pars Triangularis*	1.05 (0.02)	2.76 (0.04)	3.10 (0.05)	4.26 (0.07)
Precentral	1.22 (0.01)	2.49 (0.06)	3.41 (0.09)	4.55 (0.10)
Caudal MF	1.35 (0.02)	2.71 (0.03)	3.56 (0.06)	5.30 (0.06)
Temporal Pole*	1.41 (0.05)	1.30 (0.03)	1.40 (0.04)	1.24 (0.04)
Isthmus cingulate*	1.51 (0.01)	1.02 (0.00)	1.52 (0.03)	1.22 (0.01)
Lingual*	2.28 (0.01)	2.73 (0.04)	2.52 (0.02)	3.71 (0.05)
Lateral Orbitofrontal*	2.52 (0.02)	2.90 (0.03)	3.03 (0.05)	3.68 (0.04)
Precuneus	2.60 (0.01)	3.05 (0.03)	4.91 (0.06)	6.92 (0.14)
Superior frontal	2.70 (0.01)	4.27 (0.06)	4.66 (0.08)	6.56 (0.14)
Pericalcarine	2.84 (0.03)	4.96 (0.15)	6.35 (0.30)	8.32 (0.25)
Rostral AC*	3.55 (0.02)	5.16 (0.06)	4.26 (0.08)	3.76 (0.06)
Insula*	3.91 (0.05)	3.67 (0.05)	3.79 (0.08)	3.58 (0.04)
Posterior cingulate*	6.35 (0.13)	5.89 (0.08)	5.78 (0.14)	5.87 (0.15)
Caudal AC*	9.09 (0.23)	10.24 (0.22)	9.12 (0.4)	8.20 (0.29)
Periventricular*	15.29 (0.08)	18.29 (0.15)	22.78 (0.37)	30.04 (0.93)
Pars opercularis*	—	1.02 (0.01)	2.15 (0.04)	2.92 (0.06)
Fusiform	—	1.08 (0.01)	1.28 (0.01)	1.71 (0.01)
Inferior parietal*	—	1.26 (0.01)	2.47 (0.02)	4.41 (0.10)
Superior parietal	—	1.26 (0.01)	2.24 (0.03)	4.36 (0.12)
Rostral MF	—	1.53 (0.01)	2.51 (0.03)	4.01 (0.04)
Paracentral*	—	2.28 (0.07)	2.29 (0.04)	3.99 (0.12)
Banks STS*	—	—	1.17 (0.02)	1.58 (0.02)
Lateral Occipital*	—	—	1.36 (0.05)	1.88 (0.04)
Postcentral*	—	—	—	1.33 (0.01)
Supramarginal*	—	—	—	2.38 (0.02)
Cuneus*	—	—	—	—
Entorhinal*	—	—	—	—
Cuneus*	—	—	—	—
Medial Orbitofrontal*	—	—	—	—
Middle temporal*	—	—	—	—
Parahippocampal*	—	—	—	—
Inferior temporal*	—	—	—	—
Superior temporal*	—	—	—	—
Transverse temporal*	—	—	—	—
Frontal pole*	—	—	—	—
Pars orbitalis*	—	—	—	—

Table 3.2: Mean and variance WMSA% values for each ROI for each of the four quartiles. For quartiles I-III, n=25; for quartile IV, n = 22. Cells with "—" indicate that <1% of the ROI was WMSA. (STS = superior temporal sulcus, AC = anterior cingulate, MF = middle frontal. Red = non-scaling, orange = mid-scaling, yellow = high-scaling). *Reliability score of at least 70% in cross-validation.

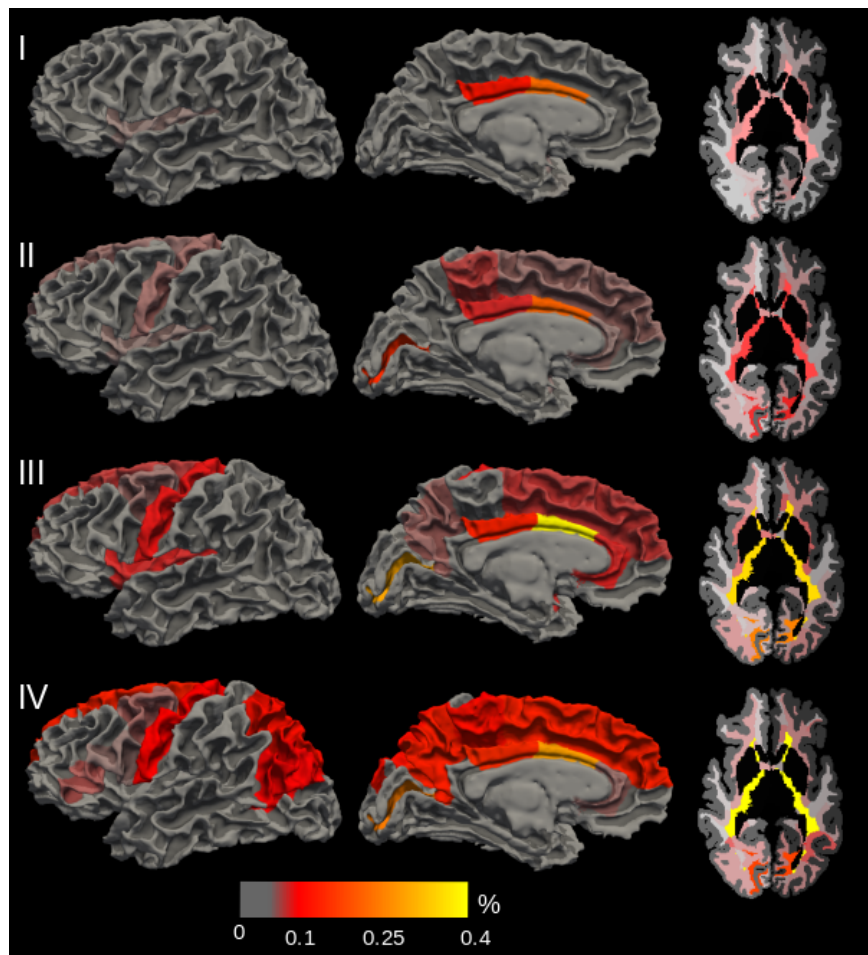


Figure 3-3: Within-quartile variance maps of the volume percent of WMSA in each ROI. Colorbar represents within-ROI variance in terms of the percent of the ROI. Values are reported in Table 2.

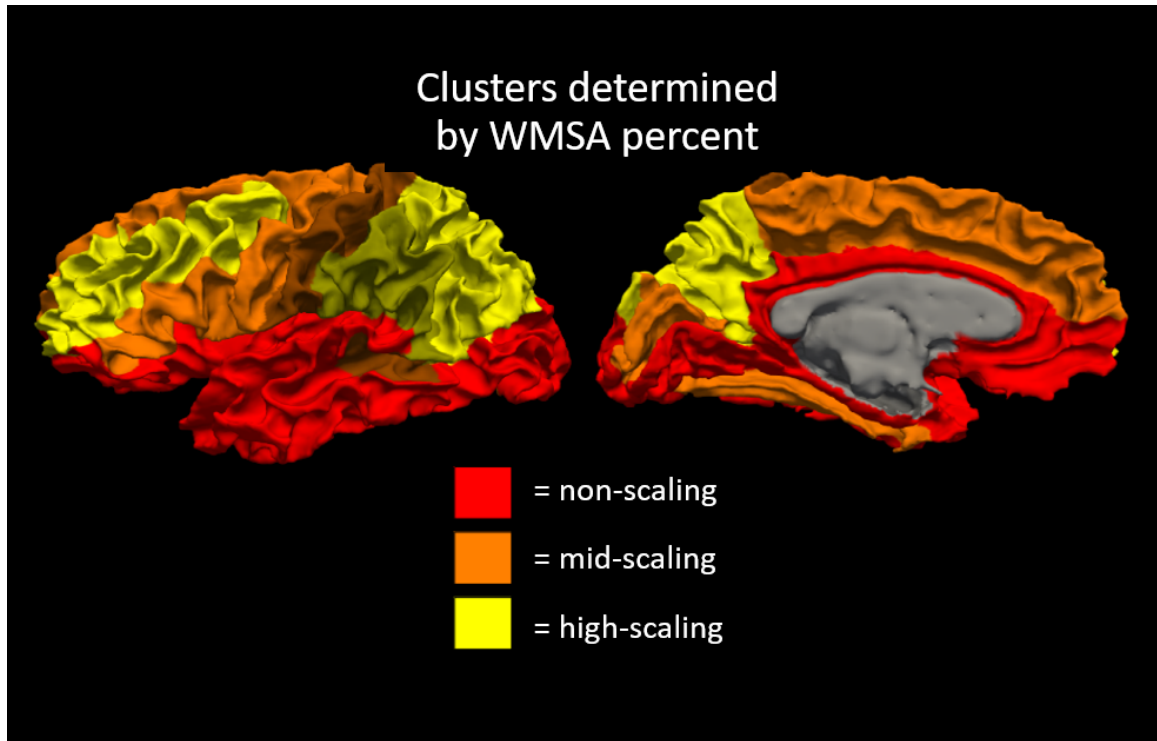


Figure 3-4: Surface maps depicting which scaling cluster each region's underlying WM belongs to, with respect to WMSA percent of total ROI WM (WMSA percent), as determined by statistically different WMSA measurements across all four quartiles of WMSA burden. Scaling here refers to the strength of the statistical significance when assessing WMSA burden across the four quartiles for a given region, where "high-scaling" indicates that the increase in regional WMSA with increasing quartile is highly significant

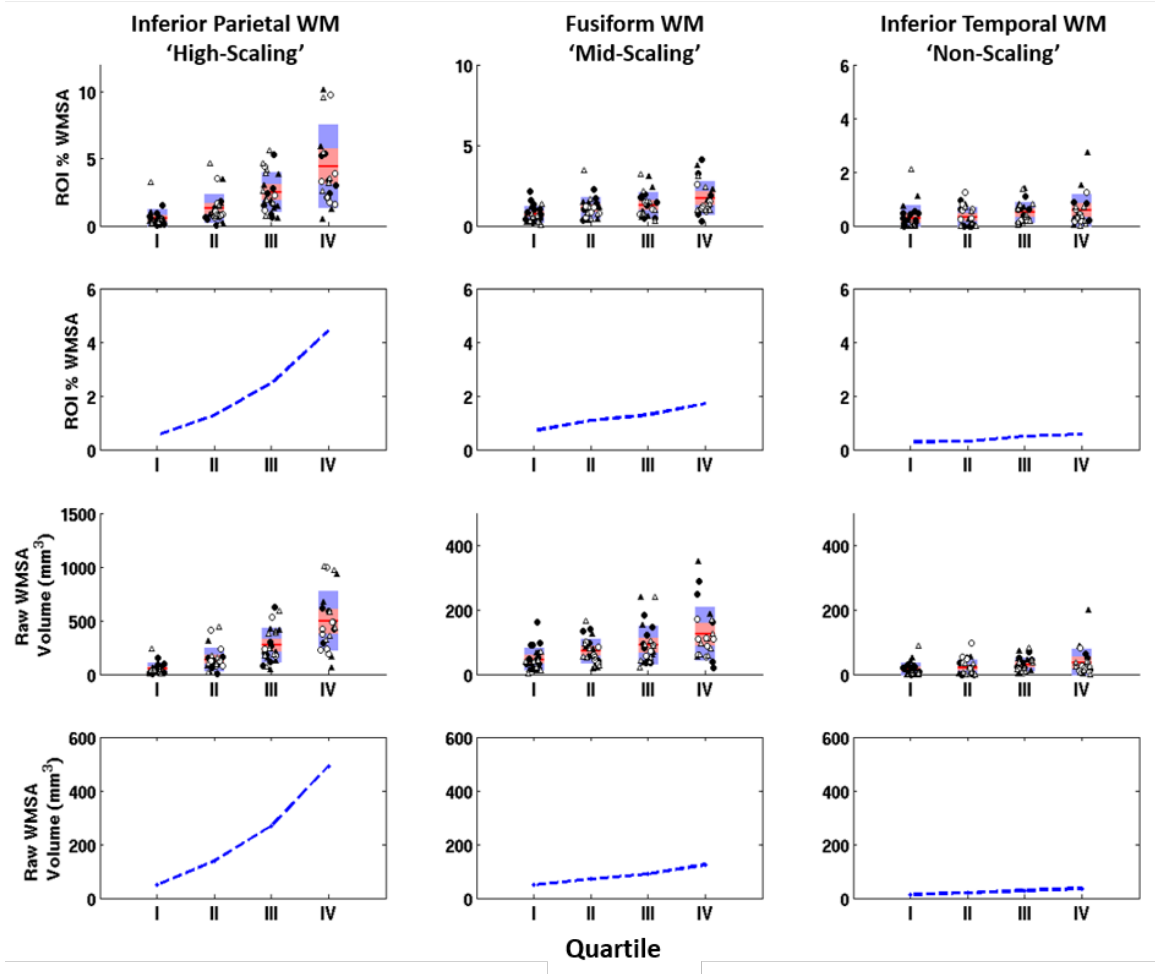


Figure 3-5: Left column: Individual subject data across all 4 quartiles showing the percent of the total WM occupied by WMSA in the inferior parietal region (top); a scaling curve for percent WMSA created by plotting mean values per quartile (second); individual raw WMSA volumes across the 4 quartiles in inferior parietal WM (third); a scaling curve for raw WMSA volume (bottom) (Individual data points: white=hypertensive, black=non-hypertensive, circle=male, triangle=female; red: mean, pink: 95% confidence interval of the mean; blue: 1 standard deviation). Middle column: Same data shown for fusiform WM, a mid-scaling region. Right column: Same data shown for inferior temporal WM, a non-scaling region.

across-quartile WMSA measure demonstrated three distinct clusters that differentially increased in WMSA volume with increasing quartile. We deemed ROIs in the cluster with the highest F-statistic centroid to be high-scaling, those in the middle cluster being mid-scaling, and those in the lowest cluster to be non-scaling (Figure 3-4; also denoted in Table 3.2.1). The high-scaling cluster was composed of rostral and caudal middle frontal, inferior and superior parietal, precuneus, supramarginal, and periventricular WM. Figure 3-5 shows actual progression curves along with boxplots for example ROIs from each cluster. Mean F-statistics for non-scaling, mid-scaling, and high-scaling clusters were 19.6383, 8.6318, and 1.6098, respectively. Notably, several ROIs did not have greater than 1% WMSA until Quartiles III or IV; supramarginal WM in the high-scaling cluster, and the postcentral and banks of the superior temporal sulcus WM in the mid-scaling cluster (dark regions in Figure 3-4). All high-scaling regions followed a more non-linear trajectory than mid-scaling regions, with greater amounts of WMSA increase occurring at each increasing quartile.

Noting the high variance in inferior parietal WMSA in Quartile IV individuals, we conducted a separate follow-up analysis using these 22 individuals to determine if the overall spatial pattern of WMSA differed between those with high ($n=11$) and low ($n=11$) inferior parietal WMSA. We determined the mean WMSA volume percent in each ROI for these two new subgroups, and subtracted the ROI-based mean values of the low inferior parietal WMSA individuals from the high inferior parietal WMSA individuals. These two splits did not differ in age, sex distribution, history of hypertension, hypercholesterolemia, or endocrine-metabolic disease. In the 'high' split individuals, WMSA volume percent was on average 7.84% higher in the periventricular WM, 4.5% higher in the inferior parietal WM, 3.7% higher in the precuneus WM, 2.3% higher in the paracentral WM, and 2% higher in the posterior and caudal anterior cingulate WM, but less than 0.5% higher in all other ROIs. These reflect the regions that demonstrated the highest degrees of variance across all quartiles. Importantly, the mean WMSA burdens of all of these regions in the 'low' split Quartile IV individuals were still higher than the means in the Quartile III individuals.

Cluster Validation

Reliability of these clusters was determined by performing 10,000 iterations of the quartiling and clustering technique with subsamples of the data. Twenty-seven of the 35 ROIs had reliability scores over 70% (starred ROIs in Table 3.2.1). All other ROIs had a reliability score above 60% with the exception of caudal middle frontal WM, whose score was 50.1%, and was equally assigned to mid-scaling and high-scaling. Periventricular WM demonstrated the highest F-statistic in the true data (26.1293) and was first tested for significance. Using the ROI-shuffling method, none of the 10,000 iterations produced a maximum F-statistic higher than 26.1293 and periventricular WMSA was deemed to be a significantly high-scaling ROI at $p < 0.0001$. For the remaining high-scaling ROIs, only two or fewer shuffling iterations generated an F-statistic higher than that generated for the true data, and therefore the F-statistics for all high-scaling ROIs are significant at $p < 0.0002$. These p -values are not corrected for multiple comparisons; however, they are so significant that they would still be significant even after Bonferroni correction across the 70 ROIs.

Cut-off Based Staging

For this final staging using ROI cut-off values, all individuals were considered for inclusion in any stage. Cut-off values for stage inclusion were based on the seven ROIs deemed high-scaling in the quartile-based staging, and a flowchart of this process is shown in Figure 3-6. The supramarginal WM showed the greatest difference between the third and fourth quartiles as determined by a t-test. Using the mean and standard deviation values reported in Table 3.2.1, a cut-off of one standard deviation below the mean of the fourth quartile (2.35%) was chosen and any individual with supramarginal WMSA above this amount was placed in Stage IV. Next, the remaining individuals were placed into Stage III based on an inferior parietal WMSA cut-off of one standard deviation below the mean of third quartile inferior parietal WMSA (2.45%). Finally, the remaining individuals were placed in Stage II based on a caudal middle frontal WMSA cut-off of one standard deviation below the mean of second quartile caudal middle frontal WMSA (2.68%).

Demographics for the individuals in final cut-off based stages are presented in

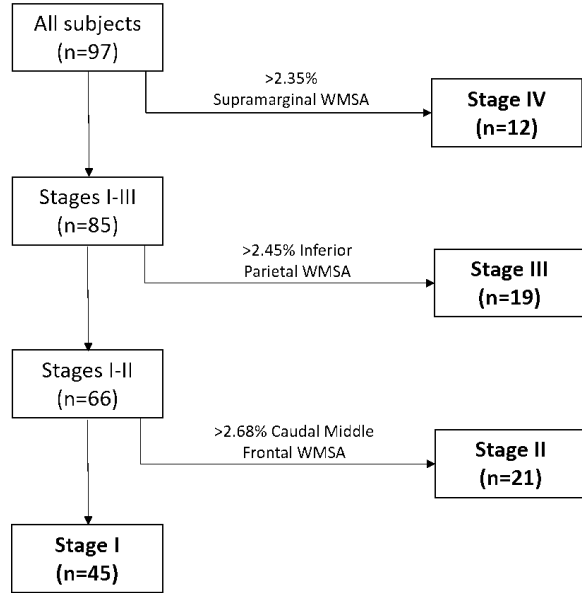


Figure 3-6: Flowchart demonstrating cut-off values for inclusion criteria for final staging in OC individuals, based on values derived from quartile-based staging.

Supplementary Table A.1 along with mean and variance values for the seven high-scaling clusters determined in the first part of the study. Individuals in these final stages did not differ significantly in age or MMSE, but they did differ in hypertension, with a greater proportion of individuals in increasing stages having hypertension. Furthermore, mean WMSA values for each ROI showed a similar spatial pattern across the four quartile-based stages as with the four final stages (Supplementary Figure B-1), but within-ROI variance significantly decreased in several ROIs across all stages (Supplementary Figure B-2), indicating greater similarity between individuals in each final stage.

3.2.2 Comparison to MCI and AD

Data

To compare the staging pattern of healthy older controls (OC) demonstrated in the previous section with patterns in disease states, two new diagnostic groups were introduced into this study: mild cognitive impairment (MCI; n=121) and Alzheimer's disease (AD; n=127). These data sets were also taken from the ADNI database and

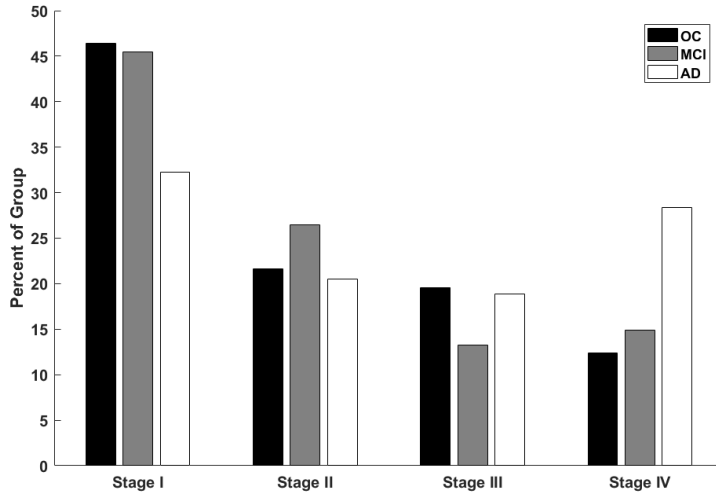


Figure 3-7: Within-group percentages of individuals in each WMSA Stage using secondary staging cut-off values across three diagnostic groups. Significant differences were found between AD and MCI and between AD and OC in Stages I and IV.

processed using the methods described in the above section for OC individuals.

Results

Using the staging cut-off values, we then staged our MCI and AD groups. Individuals in these groups did not differ significantly in age, education, or history of cardiovascular risk factors nor did they differ from the OC group. Results of the percent of individuals in each group and stage are shown in Figure 3-7. A chi-squared goodness-of-fit test indicated that within-stage percentages were different across the three diagnostic groups ($\chi^2 = 15.4490$, $p = 0.017$) and follow-up Marascuillo tests for multiple comparisons demonstrated that there were significant differences between AD and MCI, and AD and OC, in Stages I and IV ($p < 0.01$). As expected, the greatest percentage of the AD group fell into Stage IV, and the greatest percentage of the OC group fell into Stage I. Demographic data for these three diagnostic groups are presented in Supplementary Table A.2.

3.3 Conclusions

We present here a regional staging of age-associated WMSA based on MRI measures of WMSA quantified by their proximity to cortical landmarks. We demonstrate that the regional scaling of WMSA to global burden, which we infer is due to the pathologic course of WMSA development, follows a consistent spatial pattern in cognitively healthy older adults, implying differential regional vulnerability to disease. We then applied the staging method to a disease population. Individuals with AD showed an increase in prevalence in Stage IV over both OC and MCI groups, as well as a decrease in prevalence in Stage I. These results emphasize the need to better understand the factors that contribute to the pathophysiology of WMSA in older adults and diseases of aging. Collectively, this information may lead to a better understanding of the mechanisms contributing to age-associated WMSA and how this tissue damage compromises neurological function and clinical status in older adults.

As in post-mortem studies [22, 30, 89], the current work used single time point data to infer stages based on the examination of accumulating regional pathology. In contrast to prior work, we used the global burden of WMSA as a metric of overall disease and used this to determine the regional profile with increasing total lesion volume. Given that WMSA do not decrease or shrink in the context of aging [90, 91], we infer here that this regional scaling is linked to progression of disease burden. The results therefore suggest that in cognitively healthy aging, WMSA originate in periventricular WM as well as the WM underlying caudal frontal, superior frontal, precuneus, and cingulum gray matter. Secondary progression includes inferior parietal, occipital, and some medial temporal regions, followed by WMSA progression to superior parietal WM, and finally supramarginal WM. We observe a general sparing of lateral temporal, orbitofrontal, cuneus, parahippocampal, and entorhinal WM in aging without cognitive impairment.

The seven regions that were clustered as high-scaling with global burden were inferior and superior parietal, supramarginal, precuneus, periventricular, and caudal and rostral middle frontal WM. This pattern was found to be highly unlikely by

chance using the ROI-shuffling permutation method. The pattern persisted when using a random subsampling of the total subject pool. Of significance is that these regions align to known cerebrovascular boundary zones (also known as watershed regions), which are areas that are at the border of blood supply zones from two different major cerebral arteries and are thus most susceptible to hypoperfusion [92, 93]. Furthermore, these regions are in close proximity to cortical regions in which cerebral blood flow (CBF) is known to decrease with advancing age [94]. The relationship between reductions in WM integrity and reductions in cortical CBF have also been demonstrated [80, 95], supporting the idea that these high-scaling regions may be tightly linked to neighboring cortical perfusion changes. We conclude that the spatial patterns and degree of accumulation of WMSA across the defined stages are due to common age-associated processes including decrements in vascular health. However, we note that common clinical indicators such as hypertension are not particularly sensitive to detecting this burden based on WMSA staging.

High-scaling regions were used to determine cut-off values for 'final' staging of individuals. This method provided a non-quartile-based procedure for assigning individuals to WMSA stage, yet it followed a similar pattern of spatial WMSA development as seen in the quartile analysis. Furthermore, increases in hypertension with increasing stage *were* observed using this staging method, reflecting the extensive histological and epidemiological literature that has shown links between hypertension and WM integrity [90, 96], and regions of WM damage are often due to hypoperfusion of the surrounding tissue [97–99].

Overall, the current data demonstrate a regionally stereotyped increase in WMSA with increasing overall burden in cognitively healthy older adults. Cut-off values for supramarginal, inferior parietal, and caudal middle frontal WMSA have been proposed as staging guidelines, and these values demonstrated a decrease in within-stage variance over the quartile-based staging, as well as some relevant indication of disease stage. Information from this work will guide future efforts towards a better understanding of the impact of WMSA on functional properties of the brain and normal cognitive and behavioral variation in older adults.

Chapter 4

Assessing WMSA in AD

“Things fall apart, it’s scientific.”

-David Byrne (*Talking Heads*), “*Wild Wild Life*,” 1986

The previous two chapters demonstrate novel tools for the assessment of WMSA, a spatial description of WMSA in cognitively healthy aging, and a brief introduction to spatial differences seen in MCI and AD diagnostic groups. Although others have demonstrated relationships between WMSA and cognitive decline as well as AD development [41, 78, 100] , WMSA are not currently thought of as being pertinent to the AD disease process. The clinical significance of WMSA has been unclear as their prevalence has been reported to be as high as 80-95% in older populations without cognitive impairment [14, 86]. As AD itself is a *disease of aging*, parsing the components of WMSA that are solely related to aging apart from potential AD-related components is quite challenging. The understanding of if and how WMSA are significantly different in AD from typical aging is critical, however, as newer theories of AD emerge. Although histopathological studies have indicated a mix of heterogeneous findings that correlate with WMSA including demyelination and gliosis [46, 69], they are often denoted ‘white matter hyperintensities of presumed vascular origin’ [12, 13] and a loss of surrounding vascular integrity is typically indicated as the upstream pathogenic mechanism responsible for their manifestation in both cognitively normal aging as well as in Alzheimer’s disease (AD) [46, 67, 90]. The understanding of WMSA,

vascular pathologies, and AD will likely require more advanced techniques of WMSA assessment than the simple binary labeling methods that have been performed by others as the spatial distribution and quality of WMSA may also hold important, yet more subtle, information. This chapter aims to assess WMSA in AD in three separate ways: total volume, spatial distribution, and quality using the Mahalanobis distance metric described in **Chapter 2**.

4.1 Total WMSA Burden and Clinical Diagnosis

Previous studies have demonstrated there is an association between WMSA burden and the rate of cognitive decline in MCI and AD individuals [100–102]. The exact timing of WMSA development as it relates to clinical diagnosis remains unknown. This information is critical if the volume of WMSA are to be used as a biomarker of disease state, and this section assesses diagnostic differences in total WMSA volume both cross-sectionally and longitudinally.

Methods

Data

Data used in the preparation of this article were obtained from the Alzheimer’s Disease Neuroimaging Initiative (ADNI) database (adni.loni.usc.edu). A cross-sectional analysis was conducted using imaging data across four diagnostic groups, and a longitudinal analysis was then conducted on two of these groups. The first set of images was comprised of a single baseline scanning time point for 459 individuals. These data encompass individuals who fall into four cognitive categories: (1) older controls without clinical diagnosis (OC, n = 104), (2) mild cognitive impairment without conversion to Alzheimer’s Disease during the three-year course of the ADNI study (MCI-NC, n = 116), (3) mild cognitive impairment with conversion to Alzheimer’s Disease during the course of the ADNI study (MCI-C, n=115), and (4) those diagnosed with Alzheimer’s Disease throughout the study (AD, n = 124). Briefly, all MCI participants have reported a subjective memory concern either autonomously or via an informant or clinician, but do not have significant levels of impairment

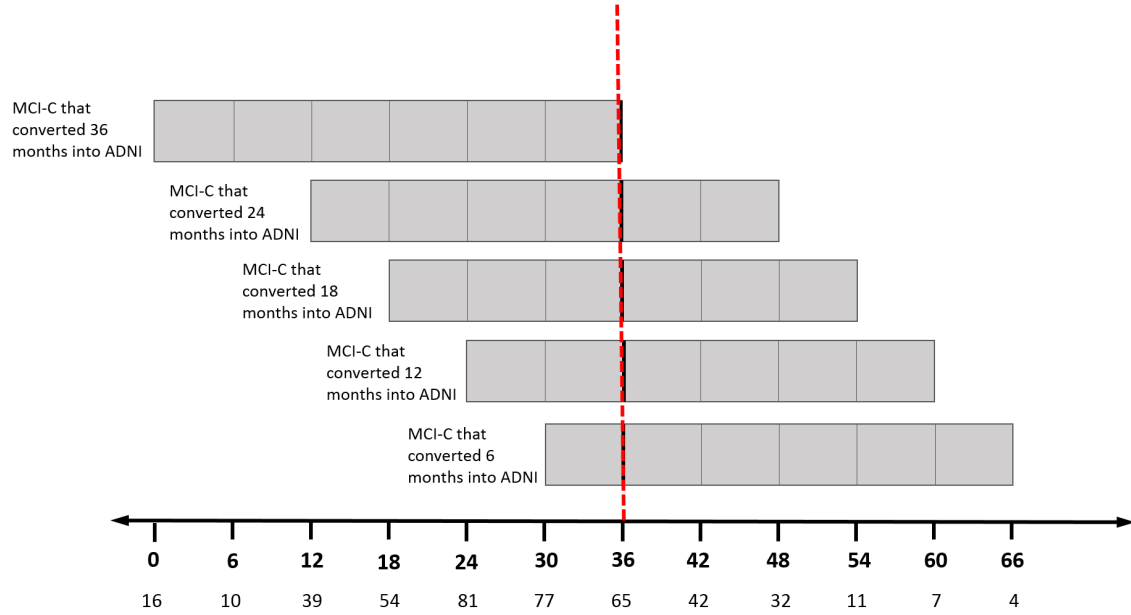


Figure 4-1: MCI-C individual alignment to point of AD conversion on a total-study timeline. Bold numbers on the x-axis are months. Light numbers represent the number of data sets from MCI-C individuals at each time point. Each gray bar represents the set of all MCI-C individuals who converted at the same time point on the ADNI timeline, and each dividing line represents a data collection point during the ADNI study. The red dashed line indicates the time of AD conversion. Each MCI-C was then matched for age and sex with an MCI-NC, and this MCI-NC was aligned with its MCI-C counterpart on the total-study timeline.

in other cognitive domains and have essentially preserved activities of daily living with no signs of dementia (i.e., all MCI individuals are amnestic MCI only). AD participants were evaluated and met the National Institute of Neurological and Communicative Disorders and Stroke/Alzheimer's Disease and Related Disorders Association (NINCDS/ADRDA) criteria for probable AD. Through this evaluation process, ADNI aims to reduce the risk of including subjects with vascular and other types of dementia.

The data for the longitudinal analysis was comprised of all 115 MCI-C individuals and 115 of the MCI-NC individuals from the cross-sectional analysis, and were used to study the progression of WMSA. These individuals all had between 3 and 6 sets of longitudinal imaging data that were acquired at months 0, 6, 12, 18, 24, and 36 during the ADNI study. Each MCI-C individual converted to AD at some point along this

time course. For the longitudinal analyses, all MCI-C data sets were aligned to each other based on time of AD conversion (Figure 4-1). Next, each MCI-C data set was age-matched to an MCI-NC data set and these were also aligned to the AD conversion time point of the corresponding MCI-C, for a total-study timeline of 66 months (36 months prior to MCI-C conversion to AD until 30 months post AD conversion; Figure 4-1). This matching procedure was done to analyze structural changes that occur in the time surrounding AD conversion in individuals with MCI while controlling for the strong effects that age is known to have on brain structure. For each time point, data were only included if both the MCI-C data set and the matched MCI-NC data set had imaging data, leading to a differing number of data points for each time point. Due to this, the month 60 and month 66 time points only had 7 and 4 subjects per group, respectively, and were not included in the subsequent analyses. Subjects in the current study were included from ADNI-1 based on the availability of at least three longitudinal T1, T2, and PD data sets that were of high enough quality for preprocessing through the robust FreeSurfer longitudinal registration stream [103].¹

MRI acquisition, preprocessing, and WMSA segmentation methods reflect those described in **Chapter 2** using ADNI data.

Statistical Analyses

All statistical analyses were conducted in MATLAB version R2013b [104]. Cross-sectional analyses with age, years of education, Mini Mental State Examination (MMSE), and baseline WMSA volume were conducted using a one-way ANOVA with follow-up Tukey tests in cases where the ANOVA resulted in a significant group difference. Cross-sectional group differences in sex, history of hypertension, hypercholesterolemia, and history of endocrine-metabolic disorders were determined using a chi-squared test. Tests for group differences in WMSA were subsequently controlled for the effects of all other demographic variables. For each time point of the MCI-C v. MCI-NC longitudinal analyses, a two-sample t-test was conducted to determine if there existed a difference in total WMSA volume between the two groups. Next, for each set of three consecutive time points (1 year), a repeated-measures ANOVA

¹Note: the longitudinal design for this section is the same as that for Section 4.3

was conducted to determine if there was a significant difference between groups in the rate of change in the variable of interest.²

Results

Demographics

The four groups (OC, MCI-NC, MCI-C, and AD) did not differ significantly in age, sex distribution, history of hypertension, hypercholesterolemia, or endocrine-metabolic disorder, but there existed a significant difference in years of education between AD and MCI-NC as well as between AD and OC ($p < 0.05$) (Table 4.1). As expected, significant differences in MMSE score existed between AD, OC, and MCI groups, but not between the MCI-C and MCI-NC ($p < 0.05$). Distribution of sex, history of hypertension, history of hypercholesterolemia, and history of endocrine-metabolic disorder did not differ between groups. Although data presented in this study comprise only a subset of all available ADNI data, this subset did not differ significantly from the overall ADNI-1 cohort in terms of age, sex, years of education, history of hypertension, history of hypercholesterolemia, history of endocrine-metabolic disorder, or cognitive scores (data not shown).

Cross-sectional Findings

WMSA volume was evaluated both as an absolute number and as a ratio of total WM volume. Total WMSA was significantly different across the four groups ($p < 0.0001$) as was total WMSA/total WM ($p < 0.0001$) (Figure 4-2). These results remained at their significance levels after controlling for all demographic variables in Table 1. Total WM did not differ between groups (including between MCI-C and MCI-NC). Post hoc Tukey tests demonstrated that OC, MCI-NC, and MCI-C had significantly lower values compared to AD for both WMSA measures.

Longitudinal Findings

We next examined whether WMSA volume differed between MCI-C and MCI-NC across the timeframe 36 months prior to MCI-C conversion to AD until 18 months post conversion. Volume was measured both in raw mm³ units, as well as a ratio of

²The same longitudinal statistical methods are employed in Section 4.3 with the same set of subjects.

	Older Controls (OC)	Mild Cognitive Impairment (MCI-NC)	Mild Cognitive Impairment (MCI-C)	Alzheimer's Disease (AD)
Number of Subjects	104	116	115	124
Age (y), mean (SD)	76.6 (5.8)	75.6 (6.8)	75.2 (6.9)	77.0 (5.7)
Sex (% Male)	50	62.93	55.65	50.81
Years of education mean (SD)	15.9 (2.7) ^a	15.7 (3.2) ^a	15.7 (3.0)	14.7 (3.1)
MMSE score, mean (SD)	29.1 (0.9) ^b	27.1 (1.8)	26.5 (1.7)	23.2 (2.0) ^b
History of hypertension (% of total)	42.31	47.41	50.43	46.77
History of hypercholesterolemia (% of total)	11.54	13.79	13.04	16.94
History of endocrine-metabolic disorder (% of total)	40.38	31.90	39.13	47.58

Table 4.1: Demographic information for individuals in the four diagnostic groups. MMSE = Mini-Mental State Examination; SD = standard deviation. ^aSignificantly different from AD, $p < 0.05$. ^bSignificantly different from MCI-C, $p < 0.05$.

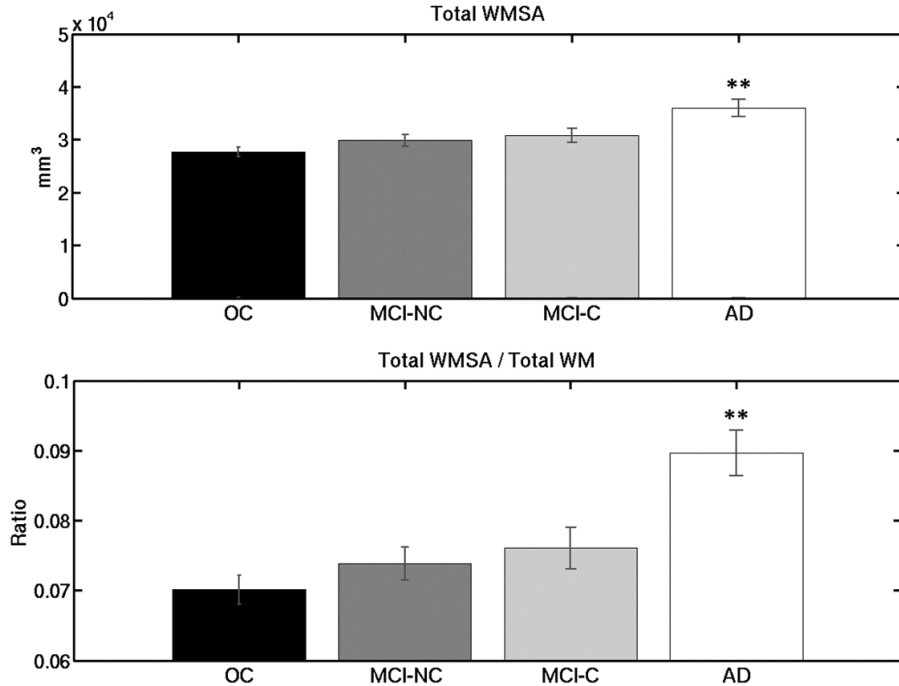


Figure 4-2: Cross-sectional group differences in total WMSA volume and WMSA/total WM volume ratio. **Significantly different from OC, MCI-NC, and MCI-C ($p < 0.0001$). Error bars are standard error of the mean.

WMSA volume to total WM volume. The time courses of these two measurements were extremely similar and so only the ratio of WMSA volume to total WM is shown in Figure 4-3. No single time point demonstrated a significant difference in volume or ratio between MCI-C and MCI-NC, but there was a trend-level difference at 18 months and at 30 months ($p = 0.07$). Additionally, no consecutive three time points demonstrated a significant difference in rate of growth. We note, however, that of the 32 MCI-C individuals depicted at time point 48 months, 18 individuals actually had an increase in volume ratio from 42 months, and we attribute the dip in Figure 4-3 to a loss of data from individuals with the highest ratios at time point 42 months.

Conclusions

The above work demonstrates that while there is an apparent increase in total WMSA in individuals who already have a clinical diagnosis of AD, this increase is not seen in pre-AD individuals who have a diagnosis of MCI. Furthermore, we do not see a WMSA increase in MCI individuals who convert to AD until months after their

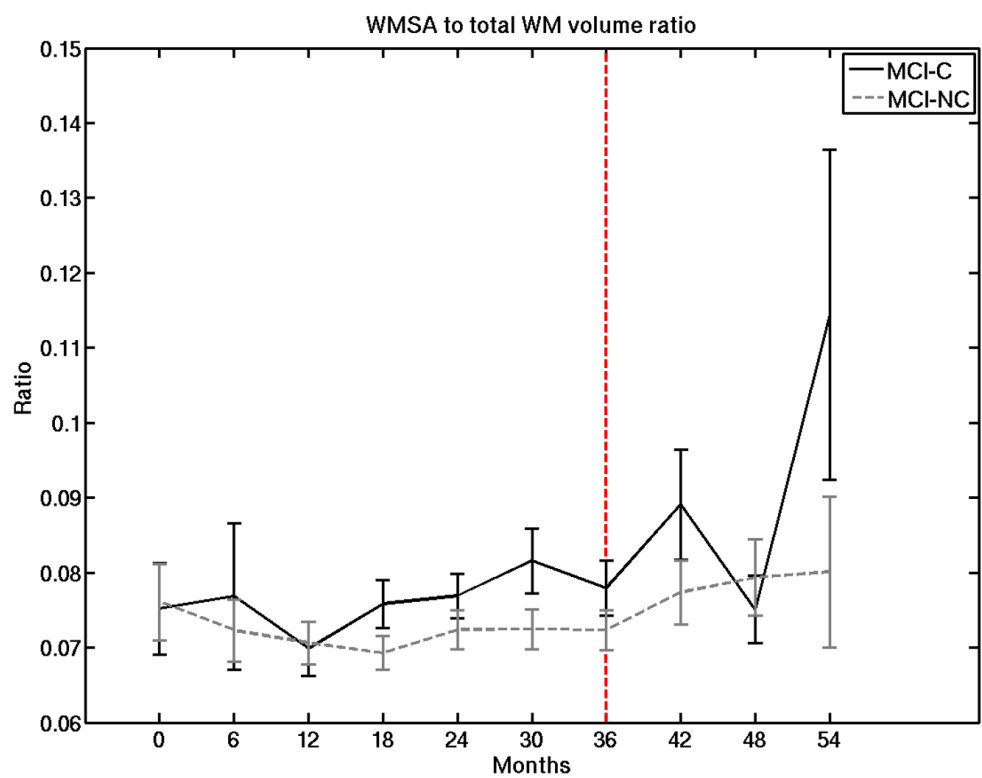


Figure 4-3: Time courses of WMSA/total WM volume ratio in MCI-C and MCI-NC individuals. Error bars are standard error of the mean. Red vertical line indicates time of AD conversion in MCI-C group.

clinical diagnosis is given.

4.2 Regional WMSA Burden and Diagnosis

In **Chapter 3**, we assessed the juxtacortical staging of WMSA in OC individuals with a brief staging comparison of MCI and AD individuals. Beyond this, no juxtacortical localization of WMSA in AD has been performed to date, and it is unknown whether such cortically proximal regional distributions differ in typical aging compared to AD. Several studies have demonstrated WMSA localized to parietal [43, 44] and periventricular regions [82, 84, 105–107] as being indicators of AD, yet other studies have found limited or no spatial differences between AD and healthy older adults in terms of distribution of WMSA [41, 42]. A consensus on this spatial distribution is critical in that it may provide new mechanisms for identifying individuals at risk for the development of AD. It may also yield a clearer picture of the underlying pathologies of the disease which is becoming increasingly recognized as a heterogeneous process with potential vascular contributions [108, 109]. In addition, associating WMSA with proximal cortex may be important for understanding the functional consequences of damaged WM as well as for designing and testing potential therapeutic interventions.

Methods

Data

A subset of ADNI subjects from the previous section were used for this study. Three hundred and eight individuals were used in the following analyses; 127 of these had a diagnosis of AD, 107 were cognitively healthy age-matched older controls (OC), and 74 had a diagnosis of amnestic MCI (Table 4.2). ADNI-1 follows individuals every 6 months and so MCI individuals were stratified by ADNI-1 into three groups based on their distance in time from AD conversion: those who were 6 months away from converting (MCI-6; n=16), those 12 months away from converting (MCI-12; n=35) and those 24 months away from converting (MCI-24; n=23). Demographic data such as age, sex, years of education, history of hypertension, history of endocrine-metabolic disorder, and Mini Mental State Examination (MMSE) scores were additionally ac-

	OC	AD	MCI-6	MCI-12	MCI-24
<i>n</i>	107	127	16	35	23
WMSA load (mm ³)	21,184 (830.5)	28,351 (1,462.6) ^a	28,607 (6,759.3)	23,511 (1,917.2)	20,795 (2,206.3)
Age	76.2 (6.2)	76.4 (6.2)	72.5 (7.3)	75.7 (6.6)	74.0 (7.9)
Sex (% Male)	47	51	75	57	74
Years Education	15.9 (2.9)	41.6 (3.2)	15.2 (3.6)	15.0 (2.8)	16.1 (2.9)
% History	43	46	56	49	57
Hypertension					
% History	11	17	6	11	9
Hypercholesterolemia					
% History	40	48	38	43	61
Endocrine-metabolic disorder					
MMSE	29.1 (0.9) ^b	23.2 (2.0) ^c	26.3 (1.8)	26.7	

Table 4.2: Mean and standard error values are reported for continuous measures.

^aSignificantly higher than OC group ($p < 0.001$). ^bSignificantly higher than all other groups ($p < 0.0001$). ^cSignificantly lower than all other groups ($p < 0.0001$).

quired from the ADNI database (Table 4.2).

MRI acquisition, preprocessing, and WMSA segmentation methods reflect those described in **Chapter 2** using ADNI data. For each of the 70 FreeSurfer-based WM ROIs, total WMSA burden was calculated and then combined across hemispheres for a total of 35 bilateral WMSA ROI measures.

Statistical Analyses

A general linear model (GLM) was implemented to test the difference in WMSA burden in each ROI between AD ($n=127$) and OC ($n=107$) groups while controlling for age. This was performed using both raw WMSA volume and WMSA as a percent of each ROI. To insure that regional increases were not simply due to greater global WMSA volume, these GLMs were also conducted using regional WMSA burden normalized to the individual's total WMSA burden. In total, each ROI was tested for group differences four times using two different WMSA metrics (raw WMSA volume and WMSA % of ROI) with and without normalization for total WMSA. Results are reported with and without correction for multiple comparisons using the false discovery rate (FDR) method [110], correcting for 140 tests.

Since raw WMSA volume and WMSA as a percent of each ROI showed similar

results when comparing AD to OC, the WMSA percent of each ROI was calculated for each MCI ($n=74$) individual. A linear regression was performed on WMSA burdens in each ROI across the three MCI subgroups, and a linear hypothesis test was conducted to determine if there was a significant increase in WMSA burden in MCI individuals who were closer in time to AD conversion.

Correction for global WMSA reduced the number of regions exhibiting group differences in WMSA volume between AD and OC. We therefore conducted secondary analyses to determine whether regional group by global WMSA burden interactions could be detected. This would indicate differential scaling of regional WMSA with global WMSA between the groups suggesting differential regional damage propensity.

Results

Demographics

Demographic information for the individuals in each of the diagnostic groups is listed in Table 4.2. As determined by a one-way ANOVA with post-hoc pairwise comparisons, groups did not differ significantly in age or years of education, but the AD group had significantly higher total WMSA ($p<0.001$). As expected due to the use of MMSE score in diagnoses, AD individuals had lower scores over OC and all MCI subgroups, and OC were significantly higher than all MCI subgroups. Chi-squared goodness-of-fit tests demonstrated that there were no significant differences in group distributions of sex, history of hypertension, hypercholesterolemia, or endocrine-metabolic disorders. In the OC group, age was significantly correlated with total WMSA burden ($R=0.3299$, $p<0.001$) but not in AD ($R=0.1369$, $p=0.1248$), nor in the combined group of MCI individuals ($R=0.1512$, $p=0.1985$). There was no significant group by global WMSA interaction with age. Due to these findings, all further group comparisons with WMSA were controlled for age.

Spatial Differences in Raw WMSA Volume

Out of the 35 ROIs, 26 demonstrated significantly greater raw WMSA volume in AD compared to OC ($p<0.05$ uncorrected; Figure 4-4, Top Left). All of these survived FDR correction except for the banks of the superior temporal sulcus, lateral orbitofrontal, precuneus, and superior temporal WM ($p=0.02$). After normalizing

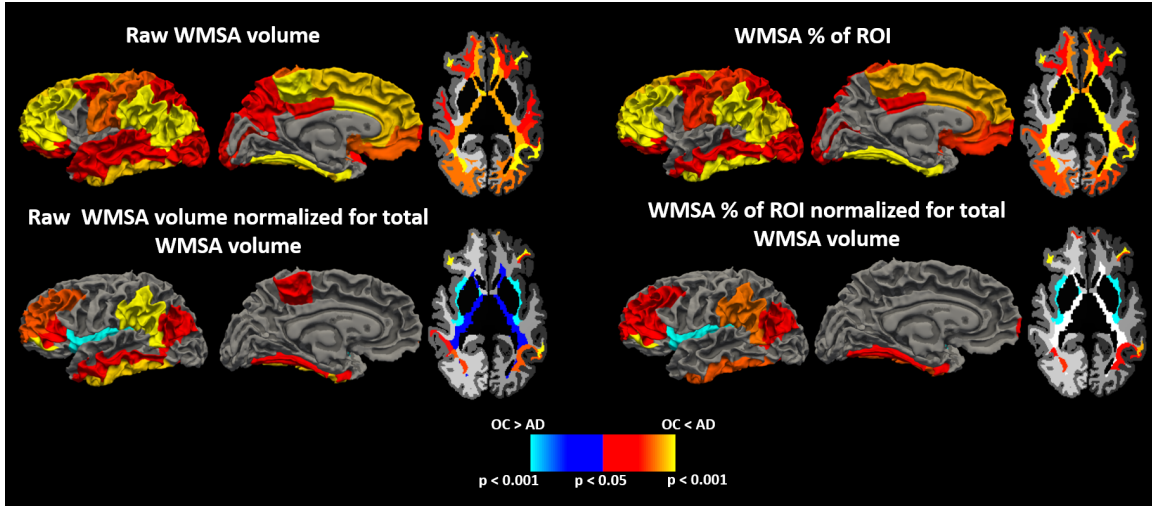


Figure 4-4: Regions demonstrating group differences in WMSA between AD and OC individuals when using raw WMSA volume as a metric (top left), raw WMSA volume normalized to total WMSA volume (bottom left), WMSA percent of ROI WM (top right), and WMSA percent of ROI WM normalized for total WMSA volume (bottom right). Warm colors indicate where AD have higher WMSA burdens than OC, and cool colors represent where OC have higher WMSA burdens than AD.

the WMSA volume in each ROI by each individual's total WMSA burden, nine regions remained significant at $p < 0.05$ (Figure 4-4, Bottom Left). Of these, fusiform, inferior parietal, inferior temporal, pars orbitalis, rostral middle frontal, and supramarginal WM survived FDR correction. Insular and periventricular WMSA showed greater normalized WMSA volumes in OC compared to AD, but only insular WM survived FDR correction.

There was a significant group by global WMSA interaction for WMSA within several regions including cuneus, fusiform, inferior parietal, inferior temporal, lateral occipital, middle temporal, periventricular and frontal pole WM ($p < 0.05$). This indicates that increasing global WMSA is linked to a greater accumulation of local WMSA in these regions compared to the accumulation in OC, demonstrating differential WMSA properties in these groups.

Follow-up analyses assessed whether spatial differences were seen when examining only individuals with hypertension as well as only individuals without hypertension in each diagnostic group. In AD individuals with hypertension there was a significantly higher WMSA burden in caudal anterior cingulate WM than in those without

hypertension. In OC individuals with hypertension there was a significantly higher WMSA burden in the banks of the superior temporal sulcus, lateral orbitofrontal, middle temporal, precuneus, superior temporal, supramarginal, and periventricular WM over those without hypertension.

Spatial Differences in WMSA as a percent of total ROI WM

The prior results were based on raw WMSA within a region. WMSA volumes corrected for regional total tissue volume is likely a more relevant marker of the degree of regional damage and compromise. We therefore repeated the ROI comparisons using a corrected measure of regional WMSA as a % of total WM volume in the region. Results remained essentially unchanged except in precuneus and superior temporal regions, which no longer reached significance (Figure 4-4, Top Right). Of the 24 significant ROIs, only lateral orbitofrontal, posterior cingulate, and superior parietal did not survive FDR correction. We next performed a secondary normalization of the WMSA percent measure to each individual's total WMSA (normalization for global WMSA) and found 8 ROIs to have significantly higher WMSA in AD, and insular WM to have higher WMSA in OC (Figure 4-4, Bottom Right). Of these, only inferior parietal and frontal pole regions did not survive FDR correction. When comparing individuals with and without hypertension in each diagnostic group, only precuneus WM showed a greater WMSA/total WMSA ratio in the OC group with hypertension over the OC group without hypertension.

Spatial WMSA and MCI Time to Conversion

Of the 35 ROIs tested, all but four exhibited the highest mean WMSA in the MCI-6 group (the MCI closest to conversion) relative to the other groups. A linear regression demonstrated that there was a significant relationship between regional WMSA burden and time-to-AD-conversion in fusiform, inferior temporal, pericalcarine, rostral middle frontal, and superior frontal WM ($p<0.05$ uncorrected) (Figure 4-5). After normalizing for total WMSA, only inferior temporal and rostral middle frontal regions exhibited a significant relationship with time-to-AD-conversion.

Conclusions

We demonstrate here for the first time a set of juxtacortical WM regions where a

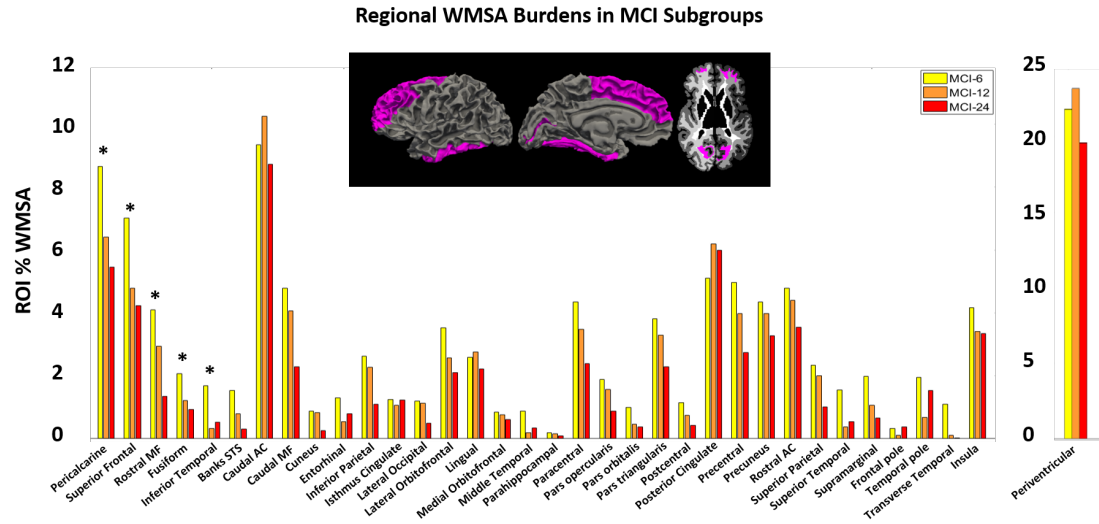


Figure 4-5: Mean WMSA burdens as a percent of total ROI WM volume in all 35 ROIs in the three MCI subgroups. Inset surface and volume images represent regions showing a significant relationship between WMSA and time-to-AD-conversion which are also starred on the graph (* $p < 0.05$).

greater WMSA volume is found in individuals with AD, where the scaling of WMSA with global WMSA is different in patients with AD compared to OC, and where larger regional volumes of WMSA are indicative of individuals with MCI who are temporally close to conversion. These results provide unique insight into the pathological basis of AD dementia and demonstrate the utility of the regional WMSA mapping procedure based on proximity to specific cortical regions. In addition to the regional analyses, we explored the relationship between regional and global WMSA volume and also measure WMSA as a percent of the ROI's total WM to account for WM tissue atrophy that is known to occur in aging and dementia [11]. While prior studies have demonstrated regional differences in periventricular [82,105] and parietal [43,44] WMSA between the two diagnostic groups, we provide evidence for more widespread increases in WMSA in AD that include temporal and frontal WM.

Our results indicate that as MCI individuals are closer in time to AD conversion, WMSA burden increases in regions that demonstrate higher WMSA in AD over OC. We demonstrate that the regions showing a statistically significant relationship between WMSA and time-to-AD-conversion are limited to the inferior temporal and

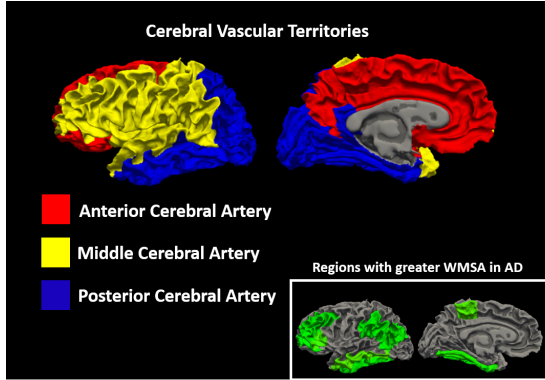


Figure 4-6: Cerebral vascular territories depicted with FreeSurfer parcellations, demonstrating which major cerebral vessels provide the main vascular supply for each ROI. Regions where two supplies meet are known as cerebrovascular boundary zones (or 'watershed' regions) and are most susceptible to hypoperfusion. Inset shows results from manuscript where there is a greater WMSA burden in AD over OC individuals.

the frontal WM. We note that this does not include parietal WM, which did show significantly increased WMSA in AD individuals over the OC group, and has also been shown by other groups to be predictive of AD conversion[26]. We interpret this finding to suggest that perhaps parietal WMSA follow a different time course than temporal and frontal WMSA, as we see a significant relationship in these regions within the two years prior to AD conversion, but the duration of MCI can be much longer depending on the individual.

Interestingly, the regions demonstrating higher WMSA in AD as well as a relationship in the MCI individuals regardless of the WMSA metric used and after normalizing for total WMSA align to known cerebrovascular boundary zones (also known as watershed regions; Figure 4-6), which are areas that are at the border of blood supply zones from two different major cerebral arteries and are thus most susceptible to hypoperfusion [111]. These same regions were noted to most readily accumulate WMSA in healthy aging in **Chapter 3**. Specifically, these include superior frontal, supramarginal, inferior temporal, and cuneus regions. Furthermore, these regions are in close proximity to cortical regions in which cerebral blood flow (CBF) is known to decrease with advancing age [94]. The relationship between reductions in WM integrity and reductions in cortical CBF has also been previously demonstrated [80,95],

supporting the idea that the effects seen in these regions may be linked to neighboring cortical perfusion changes. We therefore interpret our findings to suggest that there may be vascular changes in AD that are at least regionally accelerated relative to global changes in comparison to those seen in normal aging. Our initial findings with WMSA, hypertension, and AD diagnosis suggest that this relationship is complex and future work will examine whether or not there are interactive effects between vascular risk factors and a clinical diagnosis of AD on the manifestation of WMSA, and how these effects are spatially represented.

4.3 Longitudinal WM Quality Changes in AD Con- version

In the previous two sections, we use WMSA volume as a metric by which to study its associations with the AD disease process. However, the notion of differing levels of WM damage [112], particularly a penumbra encircling a central damage region, have been addressed before [70, 71]. There is also an extensive body of literature of the heterogeneous histological profiles of WM lesions that appear similar on MRI [68, 69, 90]. Taken together, these studies suggest that WMSA contain more information than just their overall volume, and that the subtle heterogeneities within lesions may provide further information to help differentiate between clinical populations.

Methods

All data used in this section are the same as the MCI-C and MCI-NC longitudinal data that were used in Section 4.1, and statistical analyses also follow the methodology described in Section 4.1. In this section, however, total and regional WMSA were not assessed. Rather, we revisit one of the WMSA metrics described in **Chapter 2** that assessed the *continuous* nature of WM damage rather than binary segmentation of WMSA from normal-appearing white matter (NAWM). For this, each WMSA voxel that was segmented in an individual’s ADNI baseline scan was re-labeled with its Mahalanobis distance (MD) from that individual’s NAWM. These original WMSA

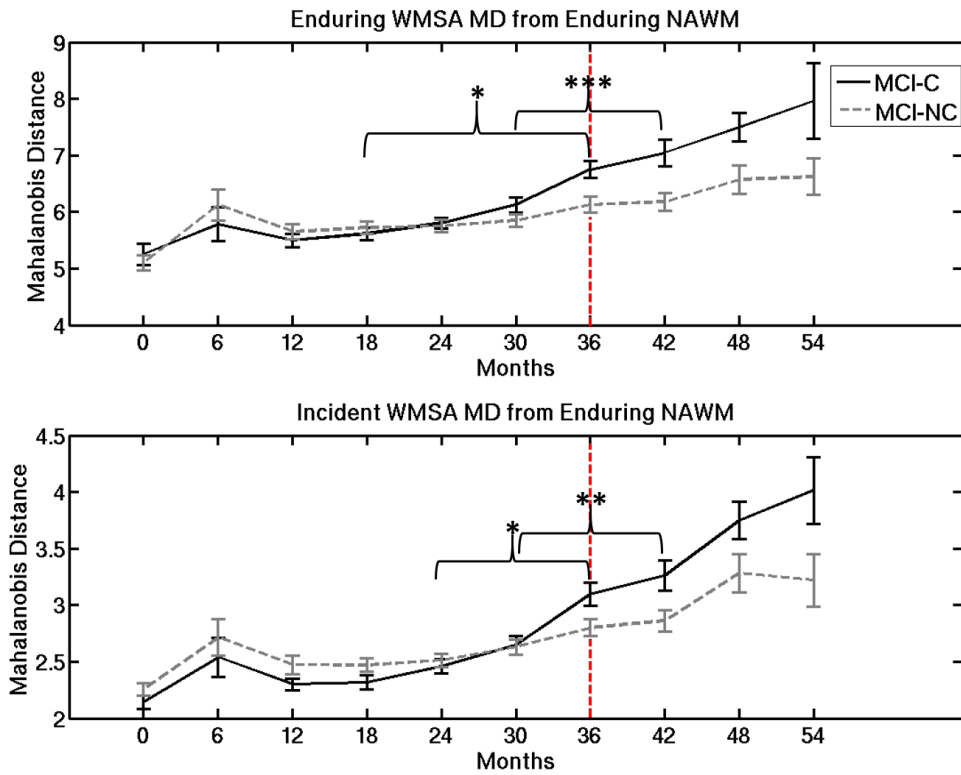


Figure 4-7: Time courses of enduring WMSA MD from enduring NAWM (top) and incident WMSA from enduring NAWM (bottom) in MCI-NC and MCI-C individuals. *Significant interaction ($p < 0.05$), **($p < 0.01$), ***($p < 0.0001$). Error bars are standard error of the mean. Red vertical lines indicate time of AD conversion in MCI-C group.

voxels that existed at ADNI baseline are referred to as "enduring WMSA." Voxels that transitioned from NAWM to WMSA during the three-year ADNI duration were also assessed in this way and are referred to as "incident WMSA."

In this section the longitudinal change in hippocampal volume in the MCI-C and MCI-NC cohorts is also assessed. Hippocampal volumes are automatically extracted using FreeSurfer at each longitudinal time point and volumes were corrected for partial volume effects.

Results

Longitudinal WMSA Quality Findings in MCI-C and MCI-NC

For all individuals, WM damage expanded outwards from an initial WMSA region over a 3-year period. This expansion consisted of the progression of NAWM to

WMSA, generally in voxels that neighbored an existing WMSA. To analyze the qualitative changes of WMSAs over time, we tracked two different sets of voxels: (1) voxels that started out as WMSA in each individual's first scanning session (enduring WMSA) and (2) voxels that started out as NAWM in the first scanning session but progressed to WMSA by the end of the individual's enrollment in ADNI (incident WMSA). Voxels that remained NAWM from the first scanning session through the last scanning session were also isolated (enduring NAWM), and their baseline T1/T2/PD values alone were extracted as a reference NAWM distribution with which to calculate MD values for the two WMSA groups. Both WMSA sets were followed over time, and at every available time point the mean MD of these voxels to the reference NAWM distribution was calculated. The time courses of these changes in enduring WMSA MD and incident WMSA MD are depicted in Figure 4-7.

The MD of enduring WMSA from enduring NAWM was significantly different between groups at the point of AD conversion and at 42 months ($p < 0.01$) as well as at 48 months ($p < 0.05$). A significant difference between groups in the rate of enduring WMSA MD change was observed between 18 months and 30 months ($p < 0.05$), between 24 months and AD conversion ($p < 0.05$), and between 30 months and 42 months ($p < 0.001$). The MD of incident WMSA from enduring NAWM was significantly different between groups at the point of AD conversion, at 42 months, and at 54 months ($p < 0.05$). A significant difference in the rate of MD change in incident WMSA was observed between 24 months and AD conversion ($p < 0.05$) as well as between 30 months and 42 months ($p < 0.01$). We note that the T1/T2/PD trajectory of change in both NAWM and WMSA is generally consistent within subject; i.e. the compression of the intensity vector into a single MD value does not exaggerate differences between NAWM and WMSA.

Longitudinal Hippocampal Volume Findings in MCI-C and MCI-NC

As hippocampal volume is a known marker of AD, we analyzed its volumetric trajectory in both MCI-C and MCI-NC for a comparison to WMSA trajectories. Hippocampal volume measurements were corrected for total intracranial volume and were produced automatically by FreeSurfer with no manual intervention. These time

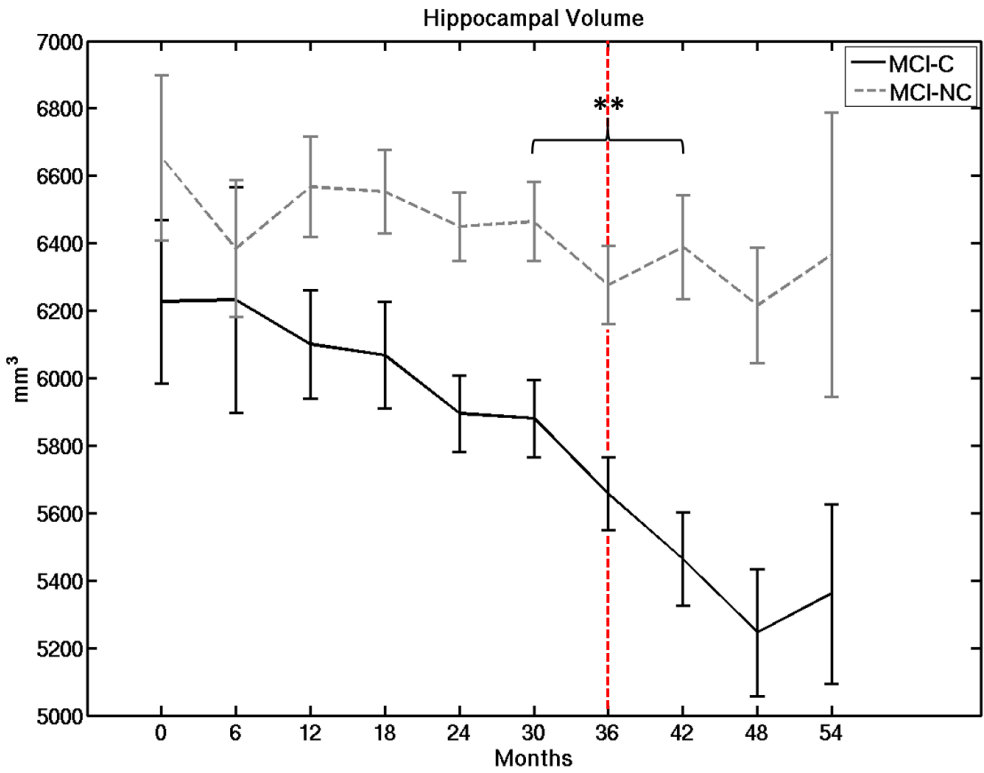


Figure 4-8: Time courses of hippocampal volume change in MCI-NC and MCI-C individuals. **Significant interaction in rate of change ($p < 0.01$). Error bars are standard error of the mean. Red vertical line indicates time of AD conversion in MCI-C group.

courses are demonstrated in Figure 4-8. Hippocampal volume was significantly different at 12 and 18 months ($p < 0.05$) and at all consecutive time points until 48 months ($p < 0.001$). A significant difference in the rate of hippocampal volume change was observed between 30 months and 42 months ($p < 0.01$).

Conclusions

In the above work we employ MD as a novel image quantification procedure to demonstrate that although WMSA do not differ at baseline, there is a difference in the trajectory of WMSA progression and accumulation in individuals with MCI that convert to AD compared with MCI that do not convert. It is important to compare these findings to the longitudinal WMSA *volume* findings in the same population of individuals, depicted in Figure 4-3. We additionally show that the progression of healthy

WM to damaged WM demonstrates a distinct temporal dynamic synchronized to the period just before conversion to a clinical diagnosis of AD, with greater deviation from normal T1, T2, and PD intensities based on MD. This suggests that this change may be a direct determinant of this conversion. The associations presented between these labels and clinical profiles indicate that there are subtle changes in the WM that can be detected on MRI before a diagnosis of AD. The significant increase in WMSA volume in individuals with an AD diagnosis (seen in the first section of this chapter) provides additional support for this interpretation.

We compare our longitudinal WMSA findings to longitudinal hippocampal volume measures, a known marker of AD, in the same MCI-C and MCI-NC individuals. Conflicting evidence has been presented about when a significant difference in hippocampal volume can be seen between these 2 groups before MCI-C conversion to AD [113,114]. Others have demonstrated that the combination of hippocampal atrophy and WMSA burden can differentiate between different subtypes of MCI [115], and furthermore that both of these changes are associated with brain hypoperfusion in MCI [116]. Our findings indicate that a difference in hippocampal volume can be seen 24 months before MCI-C conversion to AD. A significant group difference in the rate of hippocampal volume decline is not seen until 6 months before AD conversion, which is when the greatest change in rate of WMSA quality progression is seen. We interpret this finding to mean that some triggering event for hippocampal volume decrease in MCI-C individuals occurs >3 years before AD onset, and a second event potentially occurs 6 months before AD onset as seen in Figure 4-8. As this second event is timed to the change in WMSA progression rate as well as MCI-C conversion to AD, we speculate that these different biological indicators are both important to AD, and future work will attempt to determine whether these events are independent or related to one another.

4.4 Conclusions

The work in this chapter describes novel WMSA findings in AD specific to their total global volume (**Section 4.1**), their spatial distribution (**Section 4.2**), and their quality or continuous damage level (**Section 4.3**). Many biological indicators have been proposed for tracking AD progression [117], yet little attention has been given to the use of WMSA as a biomarker. Furthermore, the only structural measures that have been robustly indicated as a predictor of AD development thus far have been hippocampal and entorhinal volumes [113, 114, 118–121]. The information presented here in the context of MCI may be critical to understanding the biological differences between individuals with MCI that are subsequently diagnosed with AD and those who are not.

To synthesize the findings described in **Sections 4.1 and 4.3**, Figure 4-9 shows a new predictive model of WMSA and AD. This model contains several key components that differentiate MCI-C individuals from MCI-NC individuals. First, the data in Figure 4-9 suggest that the rate at which WM tissue becomes damaged differs between the 2 groups during a time frame that begins roughly around 18 months before MCI conversion to AD. This is captured in the new model by showing the MCI-NC damage profiles as a slow progression and the MCI-C individuals exhibiting a steeper slope starting 18 months before AD onset. The second critical component of this model is the increase in WMSA volume that occurs in the MCI-C group relative to the MCI- NC group after MCI-C conversion to AD. In the model, line width corresponds to global WMSA burden. Figure 4-3 demonstrates that as a percent of total WM, differences in WMSA volume demonstrate only trend-level significance before MCI-C conversion to AD. In our cross-sectional analyses, shown in Figure 4-2, individuals with AD show a significant increase in WMSA volume from individuals with MCI. This is consistent with previous reports in which AD individuals show higher levels of WMSA than either subjects with MCI or healthy controls [122–125]. We speculate that the increase in WMSA volume occurs gradually after the onset of AD, as the AD individuals in the ADNI cohort have had a clinical diagnosis of AD for a varying

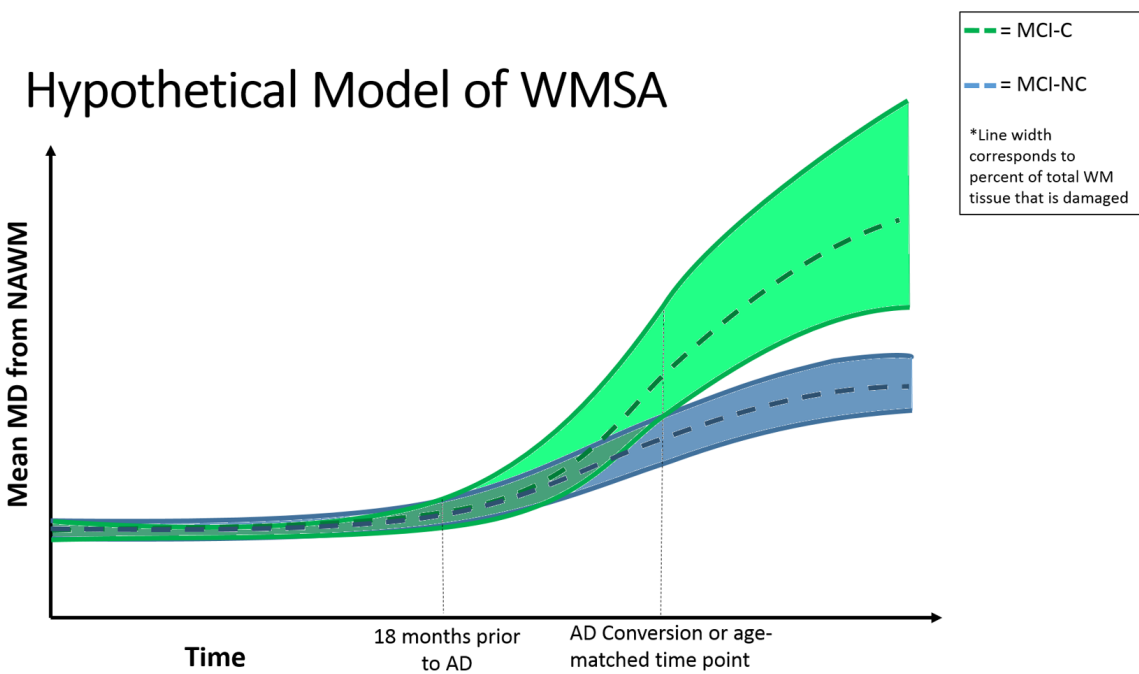


Figure 4-9: Hypothetical model of the trajectories of WM damage progression over the course of MCI development in populations that do and do not convert to AD. The width of each bounded region corresponds to the percent of the total WM that is damaged (WMSA to total WM volume). The dashed line in the middle of each region corresponds to the mean MD of all WMSA from NAWM (degree of damage within lesions). At 18 months before AD conversion, the MCI-C group exhibits a faster increase in WMSA development than the MCI- NC group. After AD conversion in the MCI-C group, volume differences start to be seen between the groups, and the MCI-C group exhibits a larger volume increase. Abbreviations: AD, Alzheimer's disease; MCI-C, mild cognitive impairment converters; MCI-NC, mild cognitive impairment nonconverters; MD, Mahalanobis distance; NAWM, normal-appearing white matter; WM, white matter; WMSA, white matter signal abnormality.

number of years. Our findings suggest that a change in WMSA quality precedes a change in WMSA quantity.

In **Section 4.2** we demonstrate for the first time a set of juxtacortical WM regions where a greater WMSA volume is found in individuals with AD, where the scaling of WMSA with global WMSA is different in patients with AD compared to OC, and where larger volumes of WMSA are indicative of individuals with MCI who are temporally close to conversion. While prior studies have demonstrated regional differences in periventricular [82, 105] and parietal [43, 44] WMSA between AD and OC, we provide evidence for more widespread increases in WMSA in AD that include temporal and frontal WM. To ensure that global WMSA increases are not solely responsible for any regional increases, our technique in which we normalize for global WMSA describes what we believe to be true regional increases in cuneus, inferior temporal, middle frontal, and inferior parietal WM. To our knowledge, with the exception of parietal WMSA, these regions have not been reported to demonstrate higher WMSA in AD and we attribute these findings to our methodology which normalizes regional WMSA for global WMSA burden. WMSA in temporal WM fit into the classic picture of AD that demonstrates marked cortical changes in relation to memory loss symptoms, but whether these are two separate processes or part of the same pathological pathway is currently unknown. The increase in frontal WMSA in AD may explain some of the executive dysfunction seen in AD [126, 127] which is highly dependent on frontal lobe function. Furthermore, others have shown that increased WMSA anywhere in the brain is associated with greater executive dysfunction [128]. A deeper investigation of AD, WMSA, and cognitive function will be a focus in **Chapter 5**.

THIS PAGE INTENTIONALLY LEFT BLANK

Chapter 5

Relating WMSA to Classic AD Biomarkers

“Take care of all your memories ... for you cannot relive them.”

-Bob Dylan, “Open the Door, Homer,” 1975

For neurologists who treat AD patients, disease diagnosis presents as a particularly unique challenge. There are two types of AD diagnosis: the clinical diagnosis made by a neurologist while the patient is still living, and the pathological diagnosis based on brain abnormalities made at autopsy. While an autopsy is necessary for the definitive diagnosis, there are several biomarkers that can be extracted *in vivo* to aid the clinical diagnosis. Estimates ranging from 10-30% of individuals who present with AD-like cognitive symptoms, however, do not demonstrate AD-like biomarker profiles while living or after death [25, 108]. The underlying cause of these patients’ symptoms is a mystery and poses a problem not only in the clinical treatment process, but also suggests that there is a significant amount of information about AD and dementia that is yet to be understood. For the final portion of this work, I aim to demonstrate the utility of WMSA metrics to fill in some of these gaps by relating them to known AD biomarkers and generating new ideas about the underlying disease processes.

Established clinical biomarkers of AD consist of both cerebrospinal fluid (CSF) markers as well as imaging markers acquired using positron emission tomography

(PET) to visualize relevant pathologies in the cerebral cortex *in vivo*. Of the CSF biomarkers, amyloid- β_{1-42} ($A\beta_{1-42}$) and phosphorylated tau_{181p} (ptau_{181p}) are the most well established and clinically utilized [28, 117, 129, 130]. These CSF markers are related to the presence of $A\beta$ plaques and tau neurofibrillary tangles (NFTs) in the cerebral cortex [131], which are thought to be responsible for the disruption of neuronal synapses that ultimately cause cognitive decline. While these markers are well established and provide a strong basis for clinical judgment, autopsy studies have demonstrated high rates of both pathologies in the cerebral cortices of individuals who passed away with fully intact cognitive functioning, as well as the lack of both pathologies in the cerebral cortices of individuals who passed away with a clinical diagnosis of AD [108, 109]. Previous studies have demonstrated relationships between WMSA and CSF markers of AD, but the results are conflicting in that some studies suggest a synergistic role of WMSA and ptau_{181p} on cognition [132–136], some suggest independent influences of WMSA and $A\beta_{1-42}$ in affecting cognition [137, 138], and some suggest no relationship between WMSA and other AD pathologies [139, 140]. Importantly, it is unclear whether or not WMSA play a prominent role in future cognitive decline and how they are related to CSF biomarkers in the context of disease prognosis.

The most well-established genetic marker of AD lies within the APO ϵ genetic sequence. There are three possible allele types: APO ϵ 2, APO ϵ 3, and APO ϵ 4, and each individual has two separate alleles. APO ϵ 4 is the allele most associated with AD. Individuals with a single APO ϵ 4 allele demonstrate a 2-fold increased risk of developing AD, and individuals with two APOE ϵ 4 alleles have up to a 10-fold increased risk. Several studies have found that WMSA are more prevalent in APO ϵ 4 carriers, suggesting a potential genetic link between their presence and AD [47, 48].

5.1 Diagnostic Classification

Researchers have long been attempting to classify between individuals with AD and healthy older adults using biomarkers and imaging data alone [141–144]. These indi-

viduals can be classified based on clinical interviews with the patient and their family as well as assessment with neuropsychological exams, yet classification experiments with biological data can lead to new insights about the underlying disease process. Reflecting the clinical-pathological mismatch stated above, results of these classification experiments with biological data never demonstrate a 100% correspondence with clinical diagnoses [145, 146]. Another goal that has yet to be attained is the ability to classify between individuals with MCI who will or who will not convert to AD within a given window of time. This is still an open problem using both biological data as well as the results of neuropsychological exams. This section demonstrates the utility of CSF measures of A β ₁₋₄₂ and ptau_{181p} in classifying between AD and healthy older adults, as well as between MCI individuals who will and who will not convert to AD within three years. WMSA are then added as a biomarker into both classification experiments to determine if there is any added utility for diagnostic or prognostic classification.

Methods

Participants

Data used in the preparation of this article were obtained from the Alzheimer's Disease Neuroimaging Initiative (ADNI) database (adni.loni.usc.edu) and described here as directed by ADNI. Two hundred and thirty-eight individuals were used in the following analyses; 61 of these had a diagnosis of AD, 56 were cognitively healthy age-matched older controls (OC), and 119 had a diagnosis of amnestic MCI. Within the 36-month duration of the ADNI-1 study, 64 of the MCI subjects converted to AD creating a further stratification of MCI individuals who converted to AD within 36 months (MCI-C; n=64) and those who did not convert (MCI-NC; n=55). All individuals underwent genetic screening for the present of 0, 1, or 2 APO ϵ 4 alleles. Demographic data such as age, sex, years of education, history of hypertension, history of endocrine-metabolic disorder, composite memory scores (ADNI-MEM) and composite executive function scores (ADNI-EF) were additionally acquired from the ADNI database (Table 5.1).

MRI acquisition, preprocessing, and WMSA segmentation methods reflect those described in **Chapter 2** using ADNI data.

	AD	MCI	OC
Age	75.98	75.18	75.20
Sex (% Male)	56	66	38
Years Education	14.95	15.70	15.45
% Hypertension	48	45	45
% Hypercholesterolemia	20	9	11
CSF ptau_{181p} (pg/mL)^b	42.45	36.90	23.55
CSF Aβ₁₋₄₂ (pg/mL)^b	144.28	156.76	208.80
Total WMSA^a	10.07	9.96	9.86
Hippocampal Volume	0.34	0.37	0.46
APOE ε4 -/-	28	45	75
APOE ε4 -/+	47	41	23
APOE ε4 +/+	25	14	2
Baseline ADNI-MEM^c	-0.89	-0.24	0.94
Baseline ADNI-EF^c	-0.77	-0.11	0.69
One-year ADNI-MEM Change^d	-0.20	-0.07	0.04
One-year ADNI-EF Change^b	-0.30	-0.17	0.20

Table 5.1: Demographic information for individuals in the four diagnostic groups. Total WMSA values are the log of the total WMSA volume in mm³. Hippocampal volume values are reported as % of total intracranial volume. APOE ε4 values correspond to the percent of each diagnostic group that carries each of the three possible genetic profiles. ^aAD and OC significantly different ($p<0.05$), ^bAD and MCI significantly different from OC ($p<0.05$), ^cAll three groups significantly different from each other ($p<0.05$), ^dAD significantly different from MCI and OC ($p<0.05$).

CSF Biomarker Data

In the ADNI study, participants receive a lumbar puncture at their baseline visit to obtain CSF for assays of amyloid β 1-42 ($A\beta_{1-42}$), total tau, and phosphorylated tau_{181p} (ptau_{181p}). Sample collection and analysis procedures are described in detail in [147]. In the present study, I created CSF biomarker quadrants across all individuals based on the median $A\beta_{1-42}$ and ptau_{181p} values in the MCI participants. For $A\beta_{1-42}$ this median value was 144 pg/mL, and for ptau_{181p} this median value was 35 pg/mL. While there is no definitive consensus for clinical cut-off points for CSF biomarkers in determining AD diagnosis, these two values are reflective of what is typically used in the clinical setting [148–150].

In these data, it is important to note that ADNI diagnosis of individuals is done *independently of CSF biomarker profile*.

Classification

We conducted support vector machine (SVM) classification experiments to determine whether CSF biomarkers and WMSA volumes were capable of identifying subject diagnoses. In these experiments, we implemented a k-fold cross-validation scheme in which we used 90% of subjects to train an SVM to classify between two diagnostic groups, and then tested this SVM on the remaining 10% of subjects. For each SVM experiment, this process was repeated 1000 times with a random training subset of 90% of subjects and tested on the remaining 10%. The average accuracy of all 1000 iterations is the classification accuracy for a given paradigm. Likewise, we calculated true positive rate (TPR) and the true negative rate (TNR) as the average percent of times that subjects in each of the two groups of interest were classified correctly.

Results

Biomarker Relationships

Figure 5-1 demonstrates the relationship between $A\beta_{1-42}$, ptau_{181p}, and WMSA across all 238 individuals in all three diagnostic groups at baseline. The Pearson product-moment correlation coefficient was computed between each pair of measures and demonstrated that ptau_{181p} and $A\beta_{1-42}$ are highly correlated across all individuals ($r = -0.4757$, $p < 0.0001$). There was no observed significant correlation between $A\beta_{1-42}$

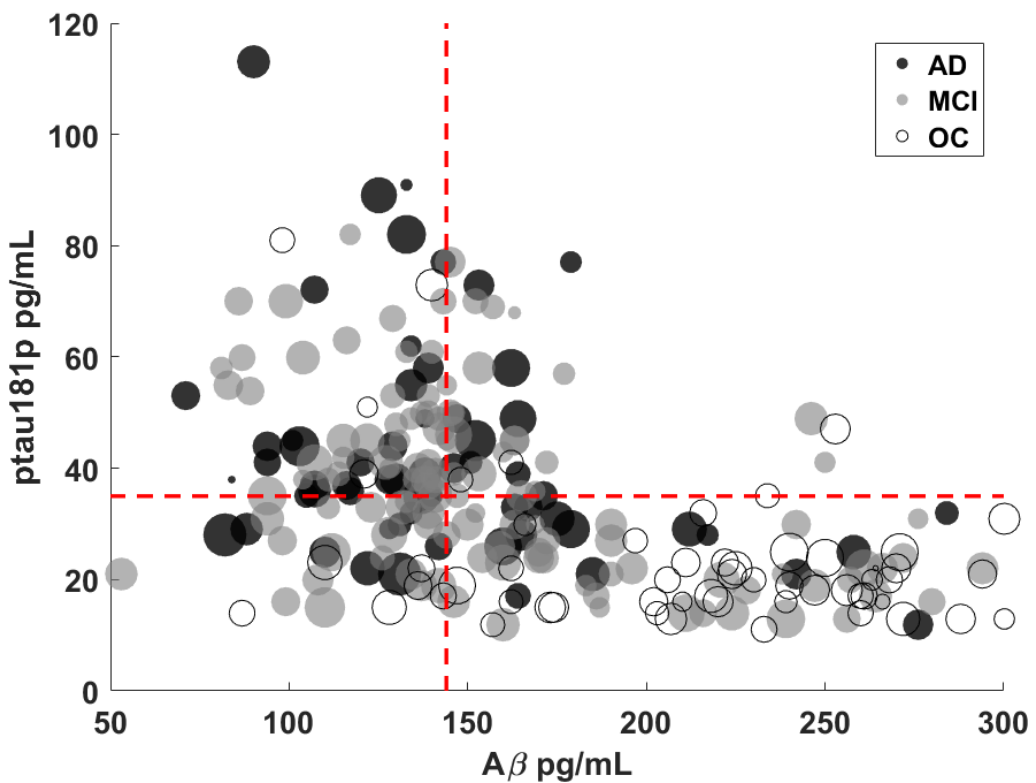


Figure 5-1: CSF biomarker data for all 238 study individuals. Points are weighted by individual total WMSA burden.

Accuracy	77%	79%	82%	58%	83%
TPR	80%	67%	80%	79%	79%
TNR	75%	89%	84%	40%	86%
ptau_{181p}	x		x		x
Aβ₁₋₄₂		x	x		x
Total WMSA				x	x

Table 5.2: Results of SVM Classification experiments between AD and OC groups. TPR = true positive rate (correct AD classifications) and TNR = true negative rate (correct OC classifications). Each column is a separate SVM experiment, and X's represent whether or not a given biomarker was used in that classification experiment.

Accuracy	52%	64%	59%	43%	57%
TPR	70%	35%	46%	52%	48%
TNR	37%	88%	70%	36%	65%
ptau_{181p}	x		x		x
Aβ₁₋₄₂		x	x		x
Total WMSA				x	x

Table 5.3: Results of SVM Classification experiments between MCI-C and MCI-NC groups. TPR = true positive rate (correct MCI-C classifications) and TNR = true negative rate (correct MCI-NC classifications). Each column is a separate SVM experiment, and X's represent whether or not a given biomarker was used in that classification experiment.

and total WMSA ($r = -0.0559$, $p = 0.39$) nor was there a significant correlation between ptau_{181p} and total WMSA ($r = -0.1206$, $p = 0.06$) across all 238 individuals at baseline.

Diagnostic Classification

Five separate SVM experiments were conducted to classify AD and OC individuals and then again to classify MCI-C and MCI-NC individuals. The variables used in each experiment and final accuracies are reported in Tables 5.2 and 5.3. As expected based on our previous work, adding total WMSA volume to our classification experiments only incrementally increased accuracies when classifying between AD and OC individuals, and showed no improvement when classifying between MCI-C and MCI-NC individuals. CSF biomarkers alone achieved a maximum classification accuracy of 82% when classifying between AD and OC individuals, they were only able to classify MCI-C vs. MCI-NC individuals at an accuracy of 59%.

Conclusions

As expected based on WMSA results presented in **Chapter 4.1** as well as in previous works by others [142], WMSA did not add value in experiments to classify between AD and OC, nor between MCI-C and MCI-NC. It is of note, however, that using only $\text{ptau}_{181\text{p}}$ and $\text{A}\beta_{1-42}$, accuracy rates for classifying between AD and OC still only reach 82%. This is a number that is reflected in the literature, where reports of AD misdiagnosis rates have been cited to be between 10 - 20% due to the non-specificity of CSF biomarkers [108, 151].

It is not surprising that the MCI-C vs. MCI-NC classification was also not helped by the addition of WMSA as a biomarker into the SVM experiments. It is also not surprising to see the low accuracy rate of 59% when using the two CSF biomarkers alone. This is reflected in work by Jack et al [117] which suggests that the development of these biomarkers is too late-stage to predict time-to-conversion.

5.2 Associations with Cognitive Measures

Alzheimer’s Disease is not a discrete process, but rather, a gradual decline in cognitive abilities over time. Despite this, discrete diagnoses are clinically necessary in order to stratify patients into treatment groups. Continuous metrics of cognitive functioning are still critical metrics in both clinical and research settings however, and may provide more robust results when predicting outcome metrics. This is in part due to the complex nature of the AD diagnostic process, which often requires a consensus diagnosis by several clinicians who take into account numerous different aspects about a patient. Cognitive scores from neuropsychological exams, however, provide robust, objective, continuous metrics that change over time and can be used to measure meaningful changes in patient status. While diagnosis will remain a component of the methodology and discussion, this section will focus primarily on continuous metrics of cognition derived from neuropsychological examinations.

Methods

All methodology described above for the extraction of CSF measures, MRI acquisition, MRI processing, and WMSA segmentation remains true for the analyses de-

scribed below. The subject population is also the same. In this section, however, rather than using statistical classification methods to predict clinical diagnosis with biomarker data, we use these biomarker data to predict cognitive measures.

Cognitive Measures

To assess cognition in participants in the current study, we utilized the ADNI-MEM and ADNI-EF composite scores of memory and executive functioning that are available in the ADNI dataset (Table 5.1). These scores were created and rigorously validated in previous works [152, 153]. Briefly, the ADNI-MEM score is a composite score of results from the Rey Auditory Verbal Learning Test (RAVLT), AD Assessment Schedule - Cognition (ADA-Cog), Mini-Mental State Examination (MMSE), and Logical Memory neuropsychological exams. This composite memory score has been shown to detect changes in memory functioning over time in individuals with MCI and AD, and is also a strong predictor of conversion from MCI to AD. Furthermore, it is strongly associated with neuroimaging markers of AD such as hippocampal volume and cortical thickness in the fusiform, parahippocampal, and entorhinal gyri, and can detect differences in changes over time for individuals with MCI who demonstrate CSF biomarker profiles suggestive of an AD signature. The ADNI-EF score is a composite score of results from Trails A and B, Category Fluency, Clock Drawing, WAIS-R Digit Symbol Substitution, and Digit Span Backwards exams. Similarly to the ADNI-MEM composite score, ADNI-EF has been shown to be a strong predictor of AD conversion in an MCI cohort, is associated with MRI-derived measures of structures involved in frontal systems, and is associated with baseline CSF measures of amyloid β_{1-42} , total tau, and phosphorylated tau $_{181p}$.

Statistical Analyses

To assess the relationship between CSF biomarkers, WMSA, and continuous measures of cognition, we used a general linear model (GLM) with cognitive scores as the dependent variables in each separate model. Significance values are reported for each independent variable in each different model to reflect that variable's contribution to the model. For each model, the overall deviance is calculated as the sum of squares of the residuals.

Baseline ADNI-MEM as Outcome Measure							
ptau _{181p}		Aβ ₁₋₄₂		WMSA		Model Deviance	
β	p	β	p	β	p		
-0.0187	<0.0001	—	—	—	—	140.99	
—	—	0.006	<0.0001	—	—	138.56	
-0.0121	<0.0001	0.004	<0.0001	—	—	129.99	
—	—	—	—	-0.3409	<0.01	162.51	
-0.0137	<0.0001	0.004	<0.0001	-0.3807	<0.001	123.85	

Baseline ADNI-EF as Outcome Measure							
ptau _{181p}		Aβ ₁₋₄₂		WMSA		Model Deviance	
β	p	β	p	β	p		
-0.0160	<0.0001	—	—	—	—	169.18	
—	—	0.004	<0.0001	—	—	173.05	
-0.0119	<0.001	0.002	<0.05	—	—	164.80	
—	—	—	—	-0.3910	<0.01	182.10	
-0.0138	<0.0001	0.002	<0.05	-0.4423	<0.001	156.52	

Table 5.4: Results of GLM experiments conducted using baseline memory scores (top) and baseline executive function scores (bottom) as dependent variables across all study subjects, regardless of diagnosis.

5.2.1 High-level view across all stages of AD

To begin, we assessed the relationships between the three biomarkers of interest in this chapter ($A\beta_{1-42}$, $ptau_{181p}$, and WMSA) and cognitive function (ADNI-MEM and ADNI-EF) across all 238 individuals regardless of diagnosis. This was performed with both cross-sectional cognitive measures as well as with one-year changes in cognitive measures.

Results

Continuous Measures of Cognitive Functioning: Cross-sectional Analyses

To assess the relationship between CSF biomarkers, WMSA, and cognitive functioning, five separate GLM experiments were conducted across all subjects in all

One-year ADNI-MEM Change as Outcome Measure						
ptau _{181p}		$\text{A}\beta_{1-42}$		WMSA		Model Deviance
β	p	β	p	β	p	
-0.0047	<0.001	–	–	–	–	23.7442
–	–	0.0007	0.07	–	–	24.9310
-0.0047	<0.001	0.000	0.98	–	–	23.7441
–	–	–	–	-0.0378	0.47	25.2409
-0.0049	<0.001	-0.0001	0.91	-0.0599	0.24	23.5961

One-year ADNI-EF Change as Outcome Measure						
ptau _{181p}		$\text{A}\beta_{1-42}$		WMSA		Model Deviance
β	p	β	p	β	p	
-0.0057	0.0011	–	–	–	–	46.8124
–	–	0.0019	<0.0001	–	–	46.5989
-0.0037	0.06	0.0013	0.03	–	–	45.8592
–	–	–	–	-0.1770	0.01	47.7883
-0.0045	0.02	0.0011	0.07	-0.1889	<0.01	44.3885

Table 5.5: Results of GLM experiments conducted using one-year changes in memory scores (top) and one-year changes in executive function scores (bottom) as dependent variables across all study subjects, regardless of diagnosis. Bold values indicate variable coefficients and p -values that attained statistical significance.

four diagnostic groups using baseline ADNI-MEM as a dependent variable. These five experiments were then repeated using baseline ADNI-EF as a dependent variable. Results of these GLM experiments are reported in Table 5.4. As expected based on the studies in which ADNI-MEM and ADNI-EF were created and validated, both CSF biomarkers demonstrated significant contributions to the predictive models. Importantly, however, the addition of WMSA into both models predicting baseline ADNI-MEM and ADNI-EF demonstrated significance of the WMSA model coefficient ($p < 0.001$) for both cognitive domains.

Continuous Measures of Cognitive Functioning: Longitudinal Analyses

We next assessed the relationships between CSF biomarkers, WMSA, and cogni-

tive changes over a one-year duration using GLM experiments. The results of these experiments are reported in Table 5.5. Only ptau_{181p} demonstrated a significant contribution to predicting a one-year change in ADNI-MEM. The additions of A β ₁₋₄₂ and WMSA did not significantly decrease the model deviance, nor did either variable render a significant model coefficient. When assessing one-year changes in ADNI-EF, however, all three independent variables (A β ₁₋₄₂, ptau_{181p}, and WMSA) significantly contributed to the model.

Conclusions

The above analyses demonstrate that across all individuals, regardless of diagnosis, there appear to be independent associations of ptau_{181p}, A β ₁₋₄₂, and WMSA on baseline measures of memory and cognitive function. In the longitudinal analyses, however, only ptau_{181p} is associated with a one-year change in memory. When assessed individually, however, all three biomarkers appear to have an association with a one-year change in executive function, but when modeled together A β ₁₋₄₂ drops out of significance. Furthermore, WMSA shows the strongest association with a one-year change in executive function when modeled with both CSF biomarkers.

5.2.2 A closer look in a ‘healthy’ biomarker subset

An interesting clinical situation arises when a patient enters the clinic complaining of cognitive symptoms, yet whose CSF biomarker profile appears "normal." This can be seen in Figure 5-1 where we see a heterogeneous mix of clinical diagnoses in the four quadrants that are created by using the clinical cut-off values for our two CSF biomarkers. Noting the diagnostic distributions of subjects in the four CSF biomarker quadrants depicted in Figure 5-1, we investigated within-quadrant relationships between biomarkers and cognitive changes. We specifically aimed to assess these relationships in the top left quadrant (Q1) whose subjects' biomarker profiles are the most clinically significant (low A β and high ptau_{181p}) and in the bottom right quadrant (Q3) whose subjects' biomarker profiles were the least clinically significant (high A β and low ptau_{181p}). (Note: *low* levels of CSF A β are considered pathological as they reflect high levels of A β deposited in the cerebral cortex.) Within each of these

	Q1 OC	Q1 Impaired	Q3 OC	Q3 Impaired
n	4	65	43	55
Age	77.8	73.8	74.9	76.2
Sex (%Male)	75	57	30	64
% Hypertension	0	42	49	51
% Hypercholesterolemia	25	12	10	16
CSF ptau_{181p} (pg/mL)	61.0	51.9	19.5	23.5
CSF Aβ₁₋₄₂ (pg/mL)	120.3	120.7	230.4	204.4
Total WMSA	9.8	9.9	9.9	10.1
Hippocampal Volume	0.43	0.36	0.47	0.36
APOE ε4 -/-	25	22	88	69
APOE ε4 -/+	75	49	12	29
APOE ε4 +/+	0	29	0	2
Baseline ADNI-MEM	0.35	-0.61	0.97	-0.23
Baseline ADNI-EF	0.24	-0.23	0.73	-0.16
One-year ADNI-MEM Change	0.09	-0.14	0.03	-0.04
One-year ADNI-EF Change	0.10	-0.21	0.20	-0.12

Table 5.6: Demographic information for individuals in CSF biomarker quadrants Q1 and Q3, delineated in Figure 5-1. MCI and AD individuals in each quadrant are combined in the above table into one "Impaired" group. Hippocampal volume is % of intracranial volume. WMSA are taken as the log-transform of the total volume in mm³. APOE ε4 values represent the percent of the within-quadrant diagnostic group that carry each possible allele combination. For example, 25% of the OC individuals in Q1 are APOE ε4-/-.

two quadrants, the GLM analyses from the whole-group study were repeated using both baseline and one-year change in cognitive measures.

Results

Quadrant Demographics

Demographic information for individuals in these two quadrants are reported in Table 5.6. While Q3 impaired individuals showed significantly less-impaired memory scores than their Q1 counterparts, we note that this is due to the higher contribution of MCI individuals to the Q3 impaired group than to the Q1 impaired group. When ADNI-MEM and ADNI-EF scores are compared between AD individuals in the two

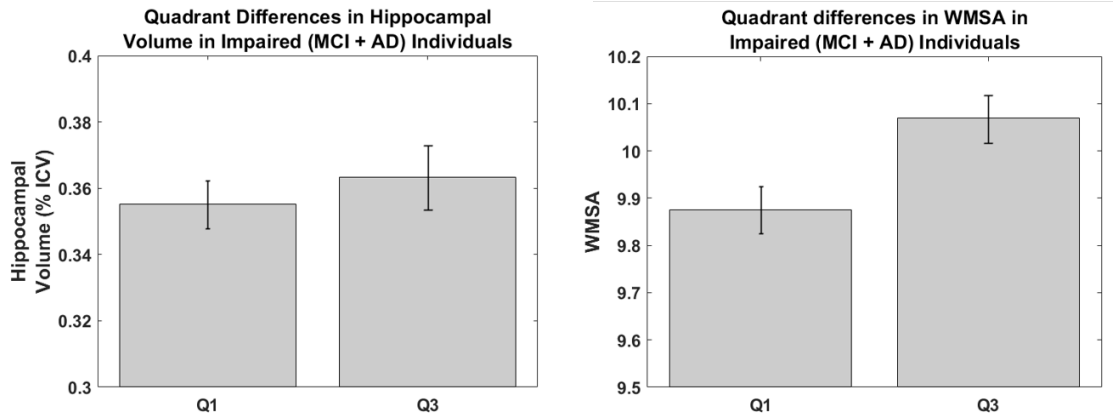


Figure 5-2: Left: Hippocampal volumes in impaired (MCI + AD) individuals in Q1 vs. Q3, showing no significant difference ($p=0.50$); Right: WMSA volumes in impaired (MCI + AD) individuals in Q1 vs. Q3, showing significantly higher WMSA in Q3 individuals ($p<0.01$).

quadrants there is no statistically significant difference, nor is there between MCI individuals in the two quadrants.

Quadrant Structural Differences

When assessing structural differences between impaired (MCI + AD) individuals in Q1 versus those in Q3, hippocampal volume showed no significant difference ($p=0.50$, Figure 5-2; left and Figure 5-3). Impaired individuals in these two quadrants did, however, differ in total WMSA volume ($p<0.01$, Figure 5-4; right) with those in Q3 having higher overall WMSA burdens. WMSA burden between impaired and OC individuals in Q3 was also assessed, and Figure 5-4 shows significantly higher WMSA in the Q3 impaired individuals than Q3 OC individuals ($p<0.01$), similar to findings of higher WMSA volume in a larger and more heterogeneous group in **Section 4.1**.

Quadrant Genetic Differences

The two quadrants of interested showed strikingly different genetic profiles. Of the impaired individuals in Q1, 29% were homozygous APOE $\epsilon 4$ carriers (APOE $\epsilon 4$ $+/+$) and only 2% of impaired individuals in Q3 were homozygous carriers. This imbalance was also seen in heterozygous APOE $\epsilon 4$ carriers where 49% of Q1 impaired individuals fit this profile and only 29% of impaired individuals in Q3 did.

Biomarkers and Cognitive Outcomes

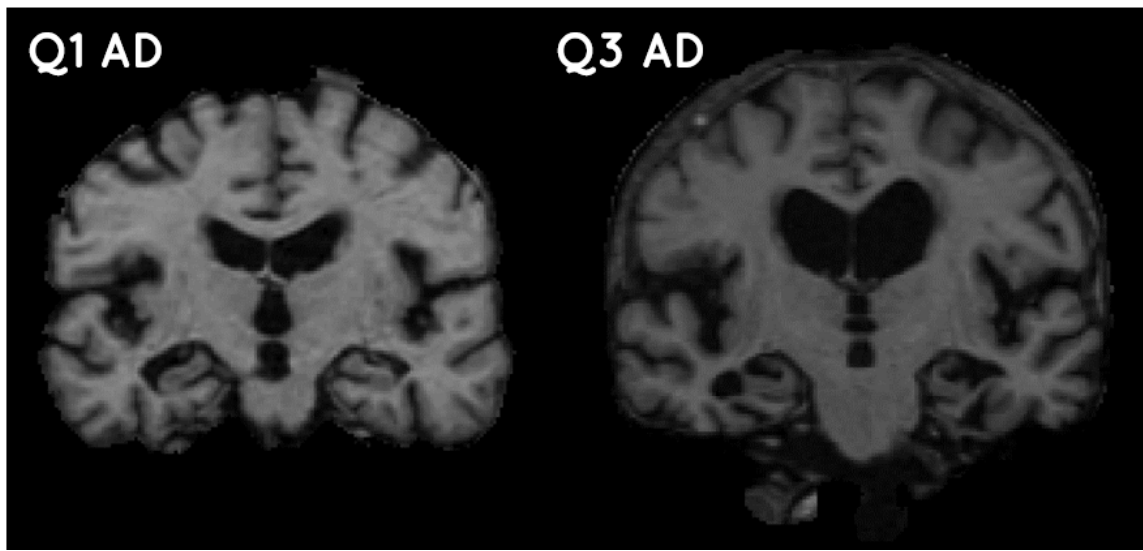


Figure 5-3: Left: Example AD individual from Q1 with hippocampal atrophy; Right: AD individual with similar hippocampal atrophy from Q3. Both individuals are from the bottom quartile of individuals ranked by hippocampal volume in each quadrant.

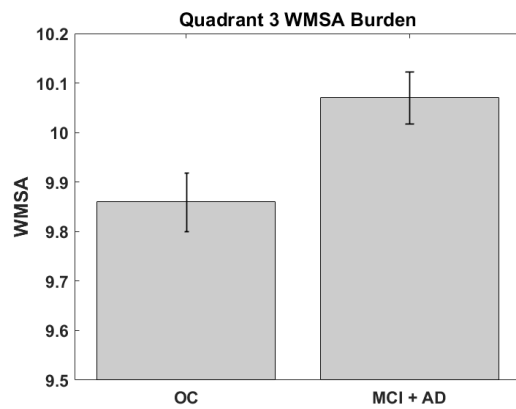


Figure 5-4: WMSA volumes in impaired (MCI + AD) vs. OC individuals in Q3, showing significantly higher WMSA in the impaired individuals ($p < 0.01$).

One-year ADNI-MEM Change as Outcome Measure						
ptau _{181p}		Aβ ₁₋₄₂		WMSA		Model Deviance
β	p	β	p	p		
-0.0025	0.359	—	—	—	—	7.4587
—	—	-0.0003	0.89	—	—	7.5576
-0.003	0.346	-0.001	0.778	—	—	7.4491
—	—	—	—	0.094	0.378	7.4664
-0.003	0.318	-0.0001	0.834	0.100	0.354	7.344
One-year ADNI-EF Change as Outcome Measure						
ptau _{181p}		Aβ ₁₋₄₂		WMSA		Model Deviance
β	p	β	p	p		
-0.0004	0.913	—	—	—	—	13.3760
—	—	-0.0003	0.923	—	—	13.3765
-0.001	0.90	-0.0003	0.91	—	—	13.3731
—	—	—	—	-0.3054	0.03	12.3867
0.00	0.99	-0.0001	0.77	-0.309	0.03	12.3692

Table 5.7: Results of GLM experiments for individuals in **Q1** sconducted using one-year changes in memory scores (top) and one-year changes in executive function scores (bottom) as dependent variables across all study subjects, regardless of diagnosis. Bold values indicate variable coefficients and *p*-values that attain statistical significance.

One-year ADNI-MEM Change as Outcome Measure							
ptau _{181p}		Aβ ₁₋₄₂		WMSA		Model Deviance	
β	p	β	p	β	p		
-0.0114	0.04	—	—	—	—	9.81	
—	—	0.0004	0.6515	—	—	10.27	
-0.0116	0.04	-0.0001	0.9161	—	—	9.80	
—	—	—	—	-0.2072	0.01	9.64	
-0.0117	0.04	-0.0003	0.7182	-0.2061	0.01	9.17	
One-year ADNI-EF Change as Outcome Measure							
ptau _{181p}		Aβ ₁₋₄₂		WMSA		Model Deviance	
β	p	β	p	β	p		
-0.0144	0.06	—	—	—	—	18.80	
—	—	0.002	0.07	—	—	18.87	
-0.0116	0.1375	0.0015	0.1721	—	—	18.41	
—	—	—	—	-0.2922	0.01	18.29	
-0.0116	0.1256	-0.0013	0.2494	-0.2732	0.02	17.30	

Table 5.8: Results of GLM experiments for individuals in **Q3** sconducted using one-year changes in memory scores (top) and one-year changes in executive function scores (bottom) as dependent variables across all study subjects, regardless of diagnosis. Bold values indicate variable coefficients and *p*-values that attain statistical significance.

When assessing one-year changes in ADNI-MEM in Q1, there were surprisingly no significant relationships with either CSF biomarker nor with WMSA. However, when assessing one-year change In ADNI-EF in Q1, only WMSA demonstrated a significant coefficient and adding both CSF biomarkers into the model did not significantly decrease model deviance (Table 5.7). In Q3, when each of the CSF biomarkers and WMSA were tested individually in modelling one-year changes in ADNI-MEM, WMSA alone showed the lowest model deviance and most significant model coefficient. $\text{A}\beta_{1-42}$ did not show a significant relationship with one-year change in ADNI-MEM in any model configuration, but inclusion of all three measures into the model rendered the lowest model deviance. Findings were similar for one-year changes in ADNI-EF in Q3, although here only WMSA demonstrated a significant relationship with cognitive outcome, yet inclusion of all three measures into the model rendered the lowest model deviance (Table 5.8).

Conclusions

When stratifying individuals into quadrants based in CSF biomaker levels, greater associations between WMSA and cognitive decline are seen in the "least pathological" quadrant (Q3). In a one-year follow-up, only baseline WMSA shows a significant association with a one-year change in both cognitive domains. In the "most pathological" quadrant (Q1) only baseline WMSA shows a significant association with a one-year change in ADNI-EF. When comparing impaired (MCI + AD) individuals across Q1 and Q3, we might expect to see higher hippocampal volumes in Q3 as these individuals also have far lower levels of AD-associated CSF pathologies. Interestingly, however, we see no difference in hippocampal volume in these individuals. We do, however, see greater WMSA in the impaired individuals in Q3 than we do in impaired individuals in Q1. When comparing impaired and non-impaired individuals in Q3, we see the expected increase in WMSA in the impaired group, demonstrating the robustness of the WMSA volume findings in **Section 4.1** even within a CSF-biomarker subset. The genetic make-up of the two quadrants is also of interest. In line with a reduction in CSF pathologies, the impaired individuals in Q3 also show a reduction in APO ϵ 4 prevalence. Aside from the similarities in hippocampal volume

between impaired individuals in the two quadrants, all other AD-related biomarkers suggest that impaired individuals in Q3 would not fit the pathological diagnosis for AD at autopsy and these findings suggest a role for WMSA in the development of their cognitive symptom profiles.

5.3 Conclusions

The results presented in this chapter provide new insights into the role that WMSA play in the clinical presentation of AD. Along with these new insights, our results confirm much of what is already known regarding the clinical-pathological mismatch seen in AD diagnosis. The results of the classification experiments presented in the first section of this chapter demonstrate that with ptau_{181p} and Aβ₁₋₄₂ alone, AD and OC individuals can only be classified with an accuracy of 82%. In the clinical literature, misdiagnosis rates have been reported as high as 25%, reflective of our classification results. Our findings combined with others' suggest that other factors must be at play for the manifestation of AD-like symptoms. The results of our classification experiments between MCI-NC and MCI-C individuals provide added support for the argument that the classic biomarkers of AD do not present a full picture of the disease process and hold minimal utility in understanding an MCI patient's future clinical trajectory. All of the MCI-C individuals in this study converted to AD within three years of the time that CSF measurements were taken. Our findings suggest that this three-year time window is not a sensitive period for Aβ₁₋₄₂ and ptau_{181p} in the CSF, and this is supported by the work of Jack et al who showed that CSF levels of both markers do not differ significantly between MCI patients who are 0-2.5 years away from conversion and those who are 2.5-5.0 years from conversion [117]. While our findings presented in **Chapter 4** indicate that WMSA do in fact demonstrate differences between diagnostic groups, the results presented in this chapter show that they do not hold utility in diagnostic classification.

With the understanding that some of the individuals enrolled in ADNI likely fall into the clinical-pathological diagnosis mismatch cohort seen in other studies and in

typical clinical settings, we moved towards studying cognitive function rather than diagnosis. While memory is the most significantly affected cognitive domain in AD, cognition is universally effected as the disease progresses. Based on previous studies of WMSA and cognitive decline as well as our own findings presented in **Chapter 4** we hypothesized that WMSA would hold predictive power for changes in continuous cognition measurements. Across all subjects, regardless of diagnosis, WMSA showed a strong relationship with a one-year change in executive function but was not a robust predictor of memory decline.

An interesting pattern emerged in our data when plotting the two CSF biomarkers against each other (Figure 5-1). Reflective of the accuracy levels that were revealed by our classification experiments, 25% of individuals with an AD diagnosis fell into the biomarker quadrant whose ptau_{181p} and Aβ₁₋₄₂ levels fell into a normal clinical range (Q3). Similarly, 34% of MCI individuals fell into this quadrant. These individuals presented an opportunity for deeper study and possible discovery of novel biomarkers to explain their cognitive symptoms. In these individuals, WMSA were the strongest predictor of a one-year change in memory when assessed against the CSF biomarkers, and were the *only* predictor of a one-year change in executive function.

Two interesting findings that add to the complexity of the current picture are the lack of difference in hippocampal volumes of impaired individuals in Q1 and Q3, and the increase in APOε4 prevalence in impaired Q1 individuals over Q3. While hippocampal atrophy is typically considered to be a hallmark structural biomarker of AD, it is also associated with other unrelated neurodegenerative conditions such as hippocampal sclerosis [154], and it is possible that the impaired individuals in Q3 reflect this process. It is also possible, however, that this is AD-like hippocampal atrophy is due to the same upstream process in all impaired individuals, but that the cognitive symptom manifestation necessary for a clinical AD diagnosis requires a second hit [155]. Under this hypothesis, the second hit could be the development of tau and amyloid pathologies *or* it could be a cerebrovascular process such as those that lead to WMSA. The low prevalence of APOε4 in the impaired Q3 individuals further suggests that these individuals are protected from the development of classic AD

pathologies. It is interesting to note however that previous studies have demonstrated a relationship between APO ϵ 4 and WMSA yet our findings of higher WMSA in Q3 suggest otherwise.

Taken together, we interpret our results to suggest the following. Impaired individuals in Q1 embody the classic AD pathologic profile with high levels of CSF ptau_{181p}, low A β ₁₋₄₂, and prevalent APO ϵ 4. These pathologies are the main drivers of memory loss leading to a clinical AD diagnosis in Q1. In these individuals, tau and amyloid have a saturating effect on memory loss and WMSA do not further contribute to impairment. In the Q3 impaired individuals who lack classic CSF biomarkers, however, WMSA are the dominating pathology that drive memory loss and their effect can be appreciated in the absence of ptau_{181p} and A β ₁₋₄₂ saturation. This is further supported by the finding that Q3 impaired individuals have a greater WMSA burden than those in Q1 which would presumably have a greater effect on memory. Across all individuals and even within quadrants, WMSA demonstrate a longitudinal relationship with executive function. This has been reported in other studies as well [83,156], and is perhaps a more robust and general association between WMSA and cognitive function that exists even in the presence of other strong neurodegenerative pathologies.

THIS PAGE INTENTIONALLY LEFT BLANK

Chapter 6

Discussion

“...there are known knowns; there are things we know we know. We also know there are known unknowns; that is to say we know there are some things we do not know. But there are also unknown unknowns – the ones we don’t know we don’t know.”

-Donald Rumsfeld, Former U.S. Secretary of Defense, February 12, 2002

This body of work provides a comprehensive – but by no means exhaustive – study of white matter integrity in aging and Alzheimer’s Disease. The findings presented here suggest that while WM changes are a common part of brain aging, they are not always benign, and that deviations from the ‘normal’ WM aging trajectory may hold critical insight into neurodegenerative processes. This work paints a comprehensive picture that begins with technological development in **Chapter 2** and ends with clinical applications that address specific gaps in our understanding of AD in **Chapter 5**. To bridge the gap between technical development and clinical application, several important questions about WM, aging, and cognitive decline are addressed in **Chapters 3 and 4**. This final chapter synthesizes a full discussion of the findings in this work, their potential clinical implications, study limitations, and future studies that should be conducted as a result of the questions left unanswered by this work.

6.1 Technical Developments

I began by addressing an important technical limitation. Despite a growing body of evidence that WMSA are elevated in AD and cognitive decline, the only tools in existence to study these lesions are limited in their quantitative abilities. Existing tools only measure global WMSA volume and are generally only applicable to one or two imaging modalities [72]. In **Chapter 1** I posed the question: *Is there novel information that we can extract from WMSA?* In **Chapter 2** I took observations from the works of others as well as my own research about the apparent continuous nature of WM integrity to develop a tool that measures not only the total volume of WMSA in an individual’s brain, but also the voxel-by-voxel degree of damage and the spatial distribution of change. In a brief exploratory analysis, I demonstrated that there are differences in all of these metrics that correlate with aging and clinical diagnosis. Not only had these metrics never been described and implemented before, but these basic associations with age and clinical status had also never been explored. They suggest that there are still unexplored dimensions of WM integrity as it can be appreciated *in vivo* on MRI and open the door for the studies conducted in **Chapters 3 through 5.**

The power of this tool is also of note. It allows researchers with any multimodal combination of T1-weighted, T2-weighted, PD-weighted, or FLAIR images to explore their own data and assess WM changes at a more granular level than is allowed by existing WMSA segmentation tools. There are still limitations to this tool, particularly in the output of different subclasses of WM damage. While these subclasses are based on continuous damage measures, which I show in **Chapter 4** are related to AD-conversion, the clinical significance of damage subclasses is still unknown. The optimal number of subclasses is also still an open question, and I demonstrated the use of five subclasses in **Chapter 2** as an example. It is possible that there is a more optimal number of subclasses that could be used to pull out the most meaningful effects in aging, AD, or other diseases, or that a continuous damage metric is more powerful.

An interesting question that results from this work relates to the underlying nature of different levels of WM damage. While histopathological studies describe WMSA as being primarily vascular in origin, other processes such as gliosis and demyelination are also described in the literature [69, 157]. My findings as well as others' show that WMSA are typically described as having a highly damaged core on MRI with a penumbra that gradually transitions into healthy, normal-appearing white matter (NAWM). It is likely that these signal intensity differences in MRI correspond to different types of cell-level pathologies, some perhaps being more vascular in nature than others. Future work will better characterize how MD properties relate to histological properties through histological-imaging correlation studies.

6.2 Aging

One of the central questions that motivated this body of work was whether or not WMSA are simply a benign comorbidity of aging. Their prevalence is high in aging populations, with reports as high as 92% in individuals aged 60-90 [14]. It is extremely common for clinical neuroradiology reports to describe “diffuse white matter changes” in elderly individuals with no comment on their implications or potential interventions. In short, they are so common that they have become overlooked. Despite this high-level acceptance of the natural occurrence of WMSA, there has yet to be an established baseline of how they occur with age and without this, their assessment in disease states is not possible. In **Chapter 1** I specifically asked, *What do WMSA look like in “normal” aging?* The lack of baseline understanding in aging motivated the study described in **Chapter 3**.

Our WMSA staging study is to our knowledge the first attempt to treat WMSA as an actual neuropathology. Other neuropathologies such as tau in AD and α -synuclein in Parkinson’s Disease have robust, well-established staging mechanisms that demonstrate their stereotyped spatial spread in disease progression [22, 158]. While the general consensus is that WMSA begin in periventricular WM and expand outwards over time, there has never been an in-depth study that describes whether or not

there is a true spatial pattern in their development. This knowledge would enable the identification of deviations from what is normal in the aging process and potentially reveal novel components of pathological processes at an early stage.

The staging results presented in **Chapter 3** describe a clean and concise spatial progression of WMSA in aging, a relatively uncommon finding in biological science. Not only is this a clear finding, but there is also a well-supported potential pathological explanation for the described spatial pattern. The regions that we found to most readily accumulate WMSA align closely to cerebrovascular boundary zones. These regions are most susceptible to hypoperfusion injury due to their vascular anatomy. This ties into the histopathological findings of WMSA being primarily vascular in origin. As systemic vascular integrity declines with normal aging, it makes sense that this would extend to and be reflected in the brain. It is interesting to note that the regions that were mainly spared of WMSA in the staging performed with healthy aging (such as the temporal lobes) are regions that are known to be susceptible to classical Alzheimer's neurofibrillary pathology [22]. It is possible that regions showing rapid accumulation of WMSA may have a particularly appreciable influence on cognitive status as a 'second hit' [137, 159] to regions being used in a compensatory manner to overcome the primary neurodegenerative deficits. This speculative idea will be examined in future work. A portion of the regions examined appear to be inevitably affected by WMSA, even in the early stages, but do not show increases in WMSA with increasing global burden and were categorized as non-scaling. These regions include the cingulum, insular, inferior frontal, and pericalcarine regions. A subset of the non-scaling regions also appear to be protected entirely from WMSA, including the lateral temporal, lateral orbitofrontal, cuneus, entorhinal and parahippocampal WM. Interestingly, these areas have been shown to have a dual-blood supply [111]. A dual-blood supply decreases a region's susceptibility to hypoperfusion, and therefore may explain why these regions do not show increased damage with increased global WMSA. Studies have demonstrated hypoperfusion in normal-appearing white matter that precedes the development of WMSA [160]. Due to the differing levels of perfusion throughout the WM, it is likely that different WM regions become damaged at

different rates, depending on the regional susceptibility to hypoperfusion.

6.3 Alzheimer’s Disease

The final two questions that I posed in the beginning of this work were *Do WMSA differ from the “normal” aging trajectory in the progression to AD?*, and *Do WMSA matter?* A strong theme that has been carried throughout this work is that the diagnosis of AD is challenging, and our understanding of the disease’s underlying pathologies is incomplete. The significant clinical-pathological diagnosis mismatch rates in AD beg the question, *Is there something else going on that causes these symptoms?* Many signs point towards WMSA as being an important part of the cognitive decline process, but the lack of standardization and depth of their study has limited their clinical utility. The developments in **Chapters 2 and 3** set the stage for the clinical utility of WMSA in AD to be possible.

Chapter 4 described three major findings about WMSA in AD. It assessed global WMSA volume differences in MCI and AD both cross-sectionally and longitudinally, spatial differences in WMSA in AD, and qualitative changes in WMSA in MCI. Confirming what others have previously demonstrated [82, 105, 161, 162], we found that individuals with AD had greater global volumes of WMSA in **Section 4.1**. A more elusive question, however, was whether or not there are spatial differences in this pathology. A spatial specificity in WMSA accumulation would suggest a more AD-specific vascular pathologic process, whereas simple global increases in WMSA could support the argument that AD individuals exhibit accelerated aging. To ensure that the global increase was not responsible for regional increases, our technique in which we normalize for global WMSA describes what we believe to be true regional increases in cuneus, inferior temporal, middle frontal, and inferior parietal WM. These analyses demonstrated that regional differences between groups are strongly influenced by total WMSA burden. Prior to normalization for global WMSA burden, there were widespread regions where AD had greater WMSA volume compared to OC including medial frontal, postcentral and precentral WM. This finding perhaps demonstrates

a vascular comorbidity of AD that is expressed more strongly than in cognitively healthy older controls but which is not a unique component of the AD disease process itself. Based on our findings, we hypothesize that the spatial distribution of WMSA may be important to the understanding of the pathological processes that occur separately from normal aging during the development of AD. This is supported by the relationship between increasing regional WMSA burden and decreasing time-to-AD-conversion in MCI individuals.

Interestingly, some of the regions demonstrating higher WMSA in AD as well as a relationship in the MCI individuals align to the cerebrovascular boundary zones discussed in **Chapter 3**. These regions include superior frontal WM and inferior temporal WM. We therefore interpret our findings to suggest that there may be vascular changes in AD that are at least regionally accelerated relative to global changes in comparison to those seen in normal aging. Studies that compare the histopathological profiles of WMSA between AD and OC individuals have demonstrated that they are similarly comprised of lacunes, arteriosclerosis, cerebral amyloid angiopathy, and microinfarcts [163]. Individuals with AD, however, demonstrate more marked deep white matter demyelination as well as nearly doubled thickness of the adventitia of deep white matter arteries over OC individuals [46] and WM atherosclerosis as well as WMSA burden are associated with higher Braak [22] scores in aging populations [164]. Thus, our findings, together with previous studies, provide evidence that vascular pathologies may be contributing factors to AD development, acting either independently from more classically known AD pathologies or due to a common upstream process. The findings of increased regional WMSA volume independent of global volume suggests that there is something unique about AD that results in this regional WMSA accumulation, and that WMSA do not simply represent a comorbid vascular condition that is found to be heightened in individuals with AD. Our initial findings with WMSA, hypertension, and AD diagnosis suggest that this relationship is complex and future work will examine whether or not there are interactive effects between vascular risk factors and a clinical diagnosis of AD on the manifestation of WMSA, and how these effects are spatially represented.

The final section of **Chapter 4** introduces the utility of our novel continuous-damage WMSA metric in clinical populations. In this study, we demonstrate that while differences in global WMSA volume do not predate MCI conversion to AD, there are differences in the *quality* of these lesions that can be seen as early as 18 months prior to AD conversion. Differences in cerebrovascular integrity may help to explain these differences in WM damage progression, and this issue has gained increasing interest in the AD community [66, 165, 166]. WMSA have long been used as an indirect marker of small-vessel disruption [167–169], and it is possible that the differences in damage progression rate that occur before AD conversion are linked to differences in small-vessel vulnerability to damage. There is also evidence that WM damage burden is related to future amyloid accumulation [138, 170] as well as neurofibrillary tangles [90], both of which are classic markers of AD. These are particularly novel findings in that they present the possibility that between MCI-C and MCI-NC individuals, different biological processes may occur at the sub-voxel level before clinical symptoms of AD are present, and may be valuable as a prognostic tool or as a marker of therapeutic intervention efficacy. Future research will focus on regionally specific changes in WMSA quality over time, as the current MD findings are limited to whole-brain analyses and do not specify whether or not these changes are driven by specific types of WMSA, namely periventricular lesions.

To fully understand our WMSA findings in the context of what is currently understood and accepted about AD, we turned our focus to more classic AD biomarkers in **Chapter 5**. As expected based on previous studies and our own findings in **Chapter 4**, we immediately saw that WMSA did not have an appreciable contribution to classifying individuals by their clinical diagnosis. Regardless of diagnosis or cognitive status, however, we also saw that WMSA had a significant predictive power in future decreases in executive function. We have reiterated the complexities of *in vivo* AD diagnosis over and over again in this work, and the most obvious individuals in which to study this issue are in those who present with AD-like symptoms but do not have classic AD biomarkers. In **Chapter 5** we isolate these individuals by dividing a large heterogeneous population into quadrants using CSF measures of

$\text{A}\beta_{1-42}$ and $\text{ptau}_{181\text{p}}$. There were a significant number of impaired individuals who fell into the “least pathological” quadrant (Q3), some of whom had a full-blown clinical diagnosis of AD and some of whom were classified as MCI. What is even more interesting about these individuals is that they also appeared to be genetically protected from AD based on their low levels of APOE $\varepsilon 4$. Their CSF profiles combined with their low genetic risk factor may suggest that they are not in fact AD patients, yet they demonstrated low hippocampal volumes that matched those seen in their “most pathological” Q1 counterparts. As these individuals appeared to have only partial AD pathologic profiles, yet full AD cognitive profiles, we sought to determine if WMSA could fill in the pathological gaps. Indeed, we found that in these individuals there was a higher WMSA burden and that WMSA were the strongest predictor of future cognitive decline in both memory and executive function domains.

Taken together, our findings of WMSA in AD and how they relate to classic biomarkers suggest that WMSA play a significant role in the AD pathological process. This is most appreciated in individuals who lack classic AD pathologies such as tau and amyloid. WMSA may be the source of a “second hit” that is responsible for the clinical manifestation of cognitive impairment in these individuals. Our findings suggest that the clinical presentation of AD is complex and heterogeneous, and that in individuals who do not fit the classic profile, WMSA can be an important and powerful tool in determining patient prognosis. If we are to accept that these cerebral lesions are indicative of poor cerebrovascular health, then the findings in this work motivate future studies of AD prevention and treatment that focus on cerebrovascular integrity rather than only amyloid and tau. Findings from epidemiological studies that show that vascular risk factors increase the likelihood of AD development already support this notion. Potential therapies to prevent or slow WM damage progression and therefore potentially AD development could include lifestyle modifications, anti-hypertensive medications, and other pharmacological agents that could be developed to target the cerebrovasculature specifically.

Appendix A

Supplementary Tables

Stage	I	II	III	IV
n	45	21	19	12
WMSA load (mm ³)	17,679 (760.1)	22,101 (1,644.4)	25,730 (1,926.8)	32,974 (2,406.3)
Age	74.3 (0.9)	75.5 (1.4)	78.5 (1.1)	79.2 (2.1)
Sex (% male)	53	43	32	50
Years education	15.6 (0.5)	15.7 (0.6)	15.8 (0.7)	15.3 (1.0)
% History hypertension	36	33	58*	75*
% Hypercholesterolemia	9	10	21*	0*
% History endocrine-metabolic disorder	42	38	26	58
MMSE	29.2 (0.1)	29.2 (0.2)	29.0 (0.3)	28.8 (0.3)
Ventricular volume (% ICV)	2.2 (0.2)	2.4 (0.2)	2.5 (0.3)	2.8 (0.4)
Caudal MF	1.33 (0.0)	4.31 (0.0)	4.39 (0.1)	6.10 (0.1)
Inferior Parietal	–	1.03	4.61	4.69
Precuneus	–	(0.0)	(0.0)	(0.1)
Rostral MF	2.94 (0.0)	3.68 (0.0)	6.18 (0.1)	7.46 (0.2)
Superior Parietal	–	2.47 (0.0)	3.63 (0.0)	3.35 (0.0)
Supramarginal	–	1.67 (0.0)	3.13 (0.0)	5.18 (0.2)
Periventricular	–	1.15	3.57 (0.0)	– (0.0)
	18.47 (0.3)	19.57 (0.3)	23.74 (0.9)	31.38 (1.0)

Table A.1: Demographics for individuals in secondary staging with mean and standard error of the mean values (above gray row) and mean and variance values for WMSA % in each of the high-scaling ROIs (below gray row). *Significantly different from all other stages ($p < 0.05$)

Group	OC	MCI	AD
n	97	121	127
WMSA load (mm ³)**	22,106 (858.5)	23,957 (1,249.6)	28,351 (1,462.6)
Age	76.4 (0.6)	75.1 (0.6)	76.4 (0.5)
Sex (% Male)	46	64	50
Years Education*	15.6 (0.3)	15.6 (0.3)	14.6 (0.3)
% History Hypertension	44	51	47
% History Hypercholesterolemia	10	12	17
% History endocrine-metabolic disorder	40	41	50
MMSE***	29.1 (0.1)	26.2 (0.2)	23.2 (0.2)
Ventricular Volume (% ICV)**	2.4 (0.1)	2.8 (0.1)	3.0 (0.1)

Table A.2: Demographics for individuals in each of the three demographic groups with mean and standard error of the mean values. AD significantly different from OC ($p<0.05$)* and ($p<0.01$)**. All groups significantly different ($p<0.001$)***

THIS PAGE INTENTIONALLY LEFT BLANK

Appendix B

Supplementary Figures

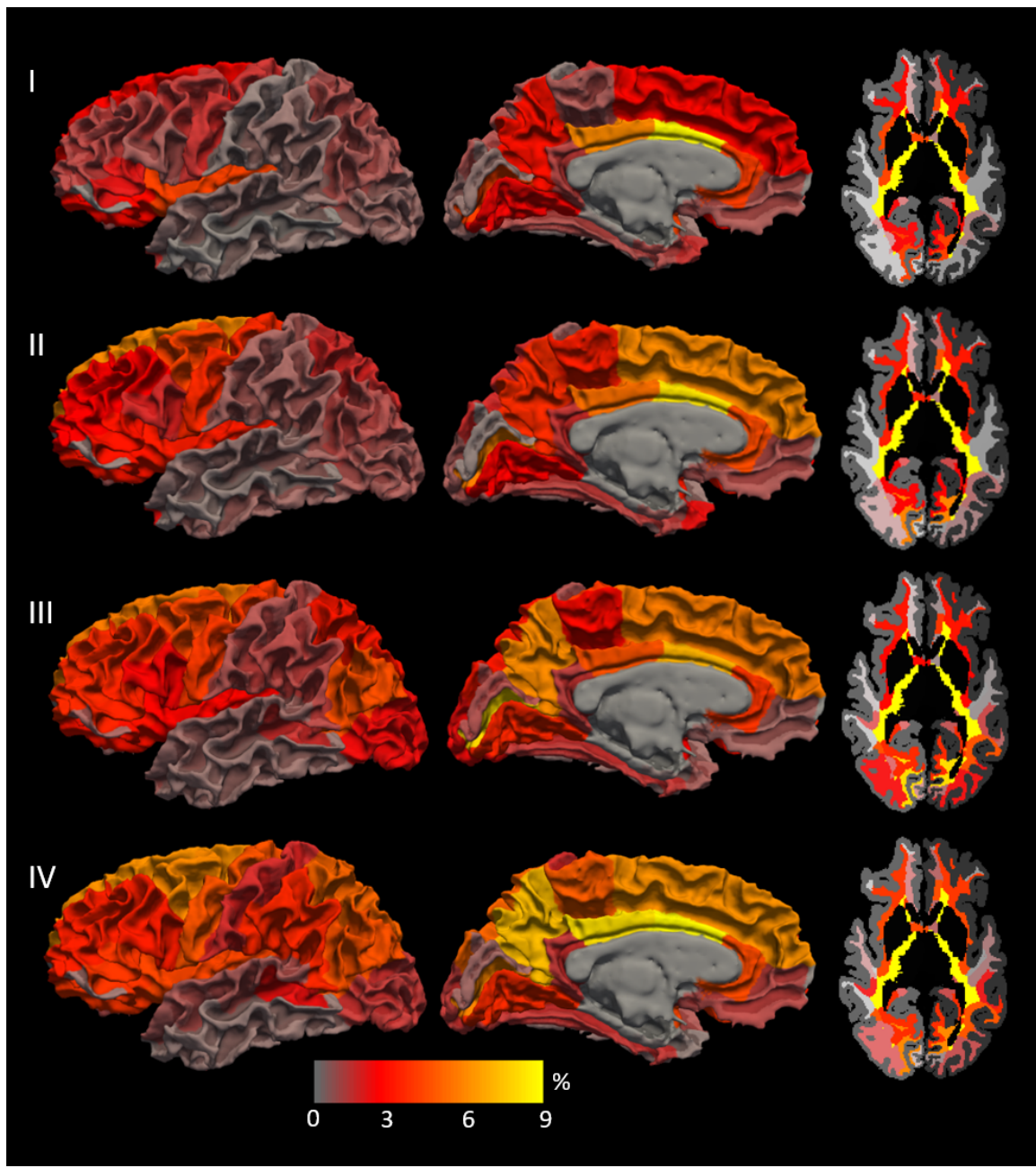


Figure B-1: Spatial staging of age-associated WMSA into four stages using ROI cut-off values derived from quartile-based staging and described in 3-5. Percent of an ROI's total WM that is occupied by WMSA is used as a metric for comparison across stages (color bar). Surface maps showing the percent of each region's underlying WM that is occupied by WMSA (first and second columns) and an axial slice through the periventricular WM showing these values in a volume view (third column) for WM disease stages I - IV. Demographics for these individuals are reported in Supplementary Table 1.

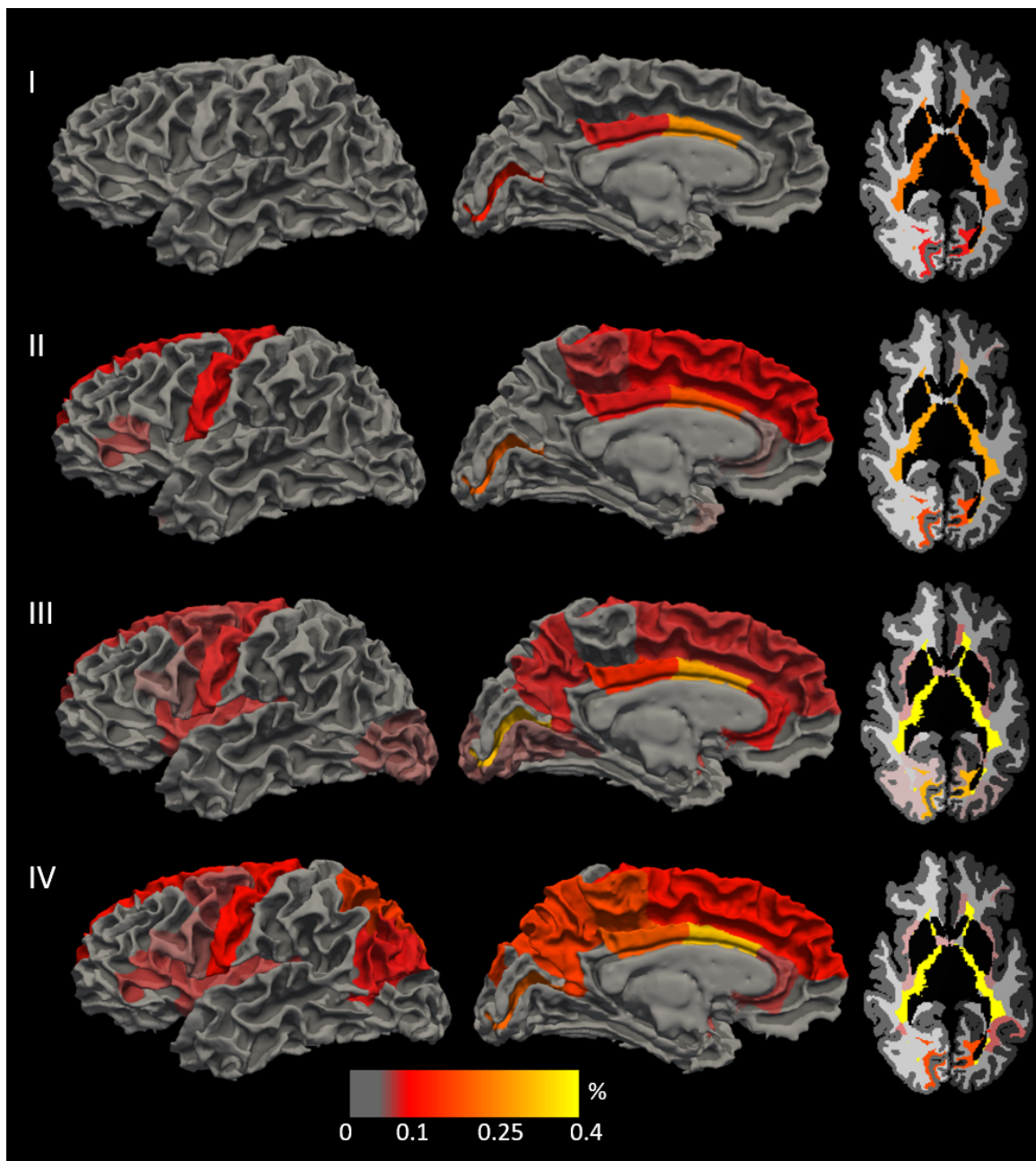


Figure B-2: Within-stage variance maps of the volume percent of WMSA in each ROI for staging using ROI cut-off values derived from quartile-based staging and described in 3-5. Colorbar represents within-ROI variance in terms of the percent of the ROI. Values for the seven high-scaling ROIs are reported in Supplementary Table 1. Compared to their quartile-based counterpart stage (i.e. quartile-based Stage I vs. final Stage I), an F-test for equality of variance determined that variance was significantly lower ($p < 0.05$) in the secondary staging for the following ROIs: Stage I: caudal MF; Stage II: caudal MF, cuneus, inferior parietal, lingual, frontal pole, & transverse temporal; Stage III: entorhinal, parahippocampal, temporal pole; Stage IV: entorhinal, inferior temporal, middle temporal, & temporal pole. Variance was not significantly higher in any ROI at any stage compared to the quartile-based staging.

THIS PAGE INTENTIONALLY LEFT BLANK

Appendix C

Complete List of Work

Some of the work presented in this thesis has been published in peer-reviewed scientific journals and presented at international conferences, and some has yet to be published. The bibliographic listing of published work is below. In addition to the results put forth in this document, my graduate research career also produced several other pieces of work that are not included here. Those works are presented in abstract after the bibliographic listing below.

Publications

Lindemer, E.R., Greve, D.N., Fischl, B.R., Augustinack, J.C., Salat, D.H., "Regional Staging of White Matter Signal Abnormalities in Aging and Alzheimer's Disease." *NeuroImage: Clinical* 14 (2017): 156.165.

Lindemer, E.R., Greve, D.N., Fischl, B.R., Augustinack, J.C., Salat, D.H., "Differential Regional Distribution of Juxtacortical White Matter Signal Abnormalities in Aging and Alzheimer's Disease." *Journal of Alzheimer's Disease* 57.1 (2017): 293:303.

Coutinho, A.M., Coutu, J., **Lindemer, E.R.**, Rosas, D.H., Rosen, B.R., Salat, D.H., "Differential Associations between Systemic Markers of Disease and Cortical Thickness in Healthy Middle-Aged and Older Adults," *NeuroImage* 146.1 (2017): 19-27.

Coutu, J., **Lindemer, E.R.**, Konukoglu, E., Salat, D.H., "Two distinct classes of degenerative change are independently linked to clinical progression in Mild Cognitive Impairment." *Neurobiology of Aging* 54 (2017): 1-9.

Lindemer, E.R., Salat, D.H., Smith, E.E., Fischl, B., Greve, D.N., "White matter signal abnormality quality differentiates mild cognitive impairment that converts to Alzheimer's disease from nonconverters." *Neurobiology of Aging* 36.9 (2015): 2447-57.

Poster Presentations and Conference Abstracts

Poster Presentation, "White matter, CSF biomarkers, and cognitive decline in aging and Alzheimer's disease," *Annual HST Forum*, Boston, MA, April 2017.

Poster Presentation, "Anatomically-specific associations between connectivity nodes of the default mode network and a novel metric for structural white matter integrity in cognitively healthy older individuals," *Fifth Biennial Conference on Resting State Brain Connectivity*, Vienna, Austria, September 2016.

Poster Presentation, "Regional Staging of Age-Associated White Matter Disease," *Annual Meeting of the Organization for Human Brain Mapping*, Geneva, Switzerland, July 2016.

Poster Presentation, "Regional White Matter Quality Changes in Alzheimer's Disease," *Alzheimer's Association International Conference*, Toronto, ON, July 2016.

Poster Presentation, "White Matter Integrity Changes Preceding Alzheimer's Disease in Mild Cognitive Impairment," *Annual Meeting of the Organization for Human Brain Mapping*, Honolulu, HI, June 2015.

Poster Presentation, "White Matter Integrity Changes Preceding Alzheimer's Disease in Mild Cognitive Impairment," *Alzheimer's Disease Research Center Conference*, Boston, MA, February 2015.

	AD	OC
n	127	107
Sex (% male)	50	47
Age	76.36 (6.19)	76.21 (6.17)
Hippocampal Volume (% of ICV)	0.34 (0.06)	0.45 (0.06)
WM Lesion Volume (mm ³)	28,351 (16,482)	21,184 (8,590)
AD-region Cortical Thickness (mm)	2.32 (0.23)	2.60 (0.18)
Years Education	14.65 (3.16)	15.65 (2.98)
MMSE	23.21 (1.99)	29.12 (0.95)

Table C.1: Demographics of individuals from ADNI used in the present study. mean and standard deviations are reported for each group. (ICV = Intracranial Volume, WM = white matter, AD = Alzheimer's disease, MMSE = Mini Mental State Examination).

Regional WM Quality Changes in Alzheimer's Disease

Presented at the Alzheimer's Association International Conference in Toronto, ON, July 2016

Background

Changes in cerebral white matter (WM) as seen on MRI are common in normal aging but are found to a greater degree in individuals with Alzheimer's disease (AD). Several studies have examined regional WM damage in AD [171, 172], yet limited information exists about the interplay between large lesions, tissue changes in 'normal appearing' tissue, and their spatial relationships with known patterns of cortical degeneration in AD. We present here a new method for evaluating WM damage on a continuous scale and show the spatially-specific profile of this damage as it relates to clinical diagnosis, hippocampal volume, total WM lesion volume, and cortical thickness.

Methods

Data consisted of T1-weighted, T2-weighted, and proton density (PD)-weighted images from healthy older controls (OC) and individuals with AD acquired from the Alzheimer's Disease Neuroimaging Initiative (ADNI) (Table C). WM lesions were automatically segmented using our previously described FreeSurfer-based lesion segmentation tool [77]. FreeSurfer was also used to compute cortical thickness in AD signature regions [31], hippocampal volume [173], and WM volume in 35 bilateral

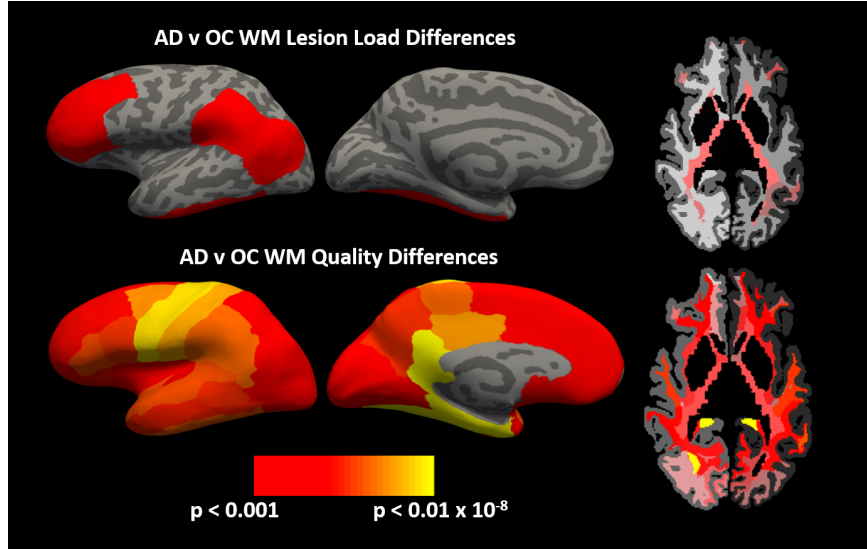


Figure C-1: Top: WM regions that demonstrated a significant increase in total WMSA load in AD individuals over OC individuals at the Bonferroni-correction threshold of $p < 0.0014$. Bottom: WM regions that demonstrated significantly poorer overall WM quality in AD individuals over OC individuals. Significance values for WM ROIs have been projected onto inflated brain surfaces for ease of viewing. Images on right represent a single slide through the center of the brain to highlight changes in periventricular WM.

regions of interest (ROI) [11]. Using a WM atlas created from ten separate OCs, the Mahalanobis distance [63] was calculated in each WM ROI in each individual and used as a metric of WM quality [77]. All statistical analyses were conducted using a general linear model (GLM), controlled for age effects, and Bonferroni-corrected.

Results

Individuals with AD had significantly poorer WM quality than OC in all 35 ROIs, but a greater WM lesion load was only seen in eight ROIs (Figure C-1). WM quality was associated with hippocampal volume in medial temporal and limbic regions, with total WM lesion load in a frontal-parietal pattern, and with cortical thickness in a widespread fashion (Figures C-2 & C-3).

Conclusions

The WM quality procedure demonstrated here is a sensitive metric of tissue deterioration in AD showing widespread alterations compared to WM lesion load. The pathologic basis of this new metric is unknown, but we speculate that it may be reflective of vascular integrity based on its relationship with WM lesions, as well as Wallerian degeneration due to upstream gray matter atrophy. Future work will assess limitations of these procedures as well as advance the implementation through

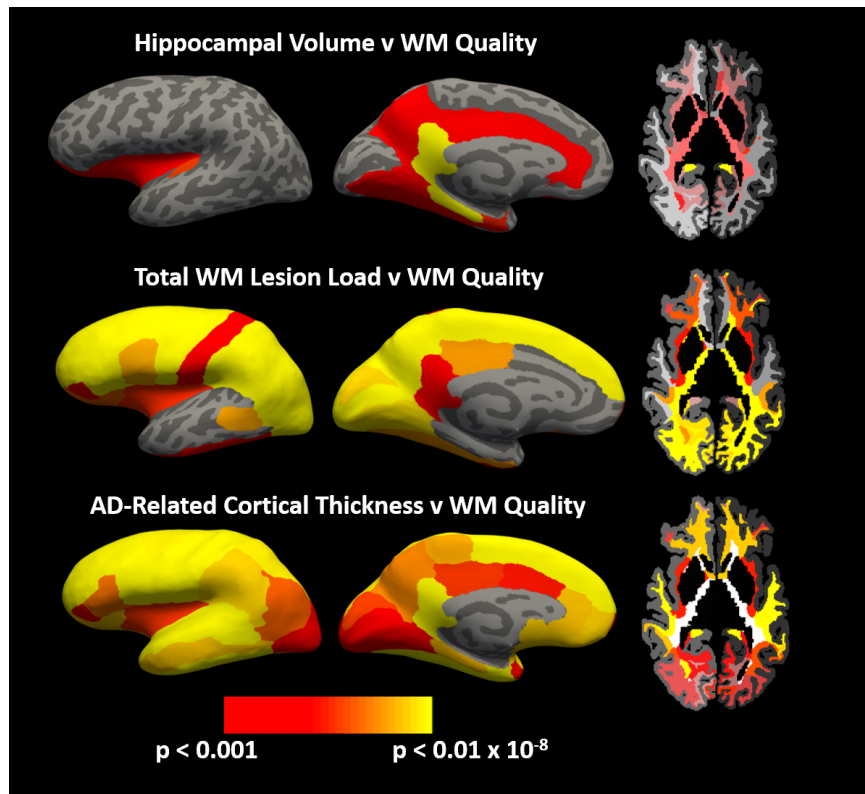


Figure C-2: Top: WM regions that demonstrated a significant relationships between hippocampal volume and WM quality across all 234 individuals at the Bonferroni-correction threshold of $p < 0.0014$. Middle: WM regions that demonstrated a significant relationship between whole-brain WM lesion load and WM quality. Bottom: WM regions that demonstrated a significant relationship between cortical thickness in AD-related regions and WM quality. Significance values for WM ROIs have been projected onto inflated brain surfaces for ease of viewing. Images on right represent a single slice through the center of the brain to highlight changes in periventricular WM.

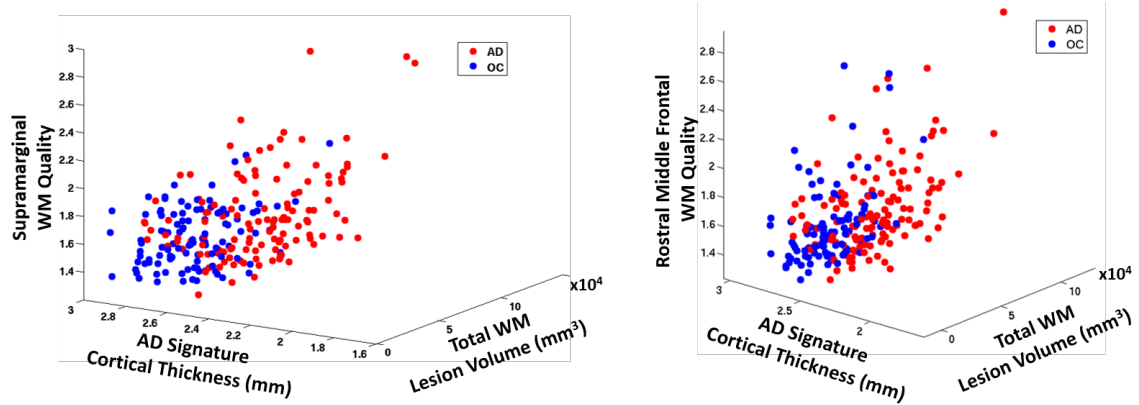


Figure C-3: Relationship between cortical thickness in AD signature regions, total WM lesion volume, and WM quality in supramarginal WM (left) and rostral middle frontal WM (right). Higher WM quality values reflect lower tissue integrity. When controlling for total WM lesion volume, these two regions still demonstrated a significant relationship between WM quality and cortical thickness, as well as a significant relationship between WM quality and WM lesion volume when controlling for cortical thickness. These results suggest that in these regions as well as others demonstrating similar relationships (Figure C-2), both WM lesions and cortical thickness may be contributing to the quality of the WM in its entirety. (Red = AD, Blue = OC).

addition of partial volume correction to account for regional atrophy.

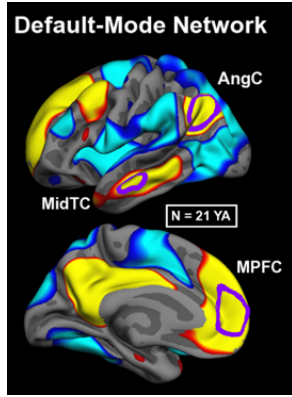


Figure C-4: Default mode network extracted from 21 young healthy individuals and ROIs used for FC-WM analysis. (Seed region not shown)

Anatomically-specific associations between connectivity nodes of the default mode network and a novel metric for structural white matter integrity in cognitively healthy older individuals

Presented at the bi-annual Brain Connectivity and Resting State conference in Vienna, Austria, September 2016

Background

Deterioration of the cerebral white matter (WM) is a common phenomenon of aging leading to decreased structural connectivity (SC) of the fiber bundles connecting different cortical regions, but how WM deterioration is linked to alterations in functional connectivity (FC) is currently unclear. Prior work examined associations between FC and SC using microstructural measures obtained via diffusion weighted magnetic resonance imaging (MRI) procedures. Although such studies have demonstrated associations between structural and functional markers in aging samples, the anatomical specificity of such associations to specific functional nodes has not been demonstrated. We present here a novel method for assessing WM integrity from multi-spectral structural MRI and use this procedure to demonstrate associations with FC in anatomically-specific regions of the default mode network (DMN) in older individuals.

Methods

Posterior cingulate cortex was used as a seed region to calculate DMN connectivity from resting-state BOLD data in 21 young adults.

Four regions of interest (ROIs) were created in regions demonstrating positive correlation to the seed region (Figure C-4) and partial correlation coefficients with the

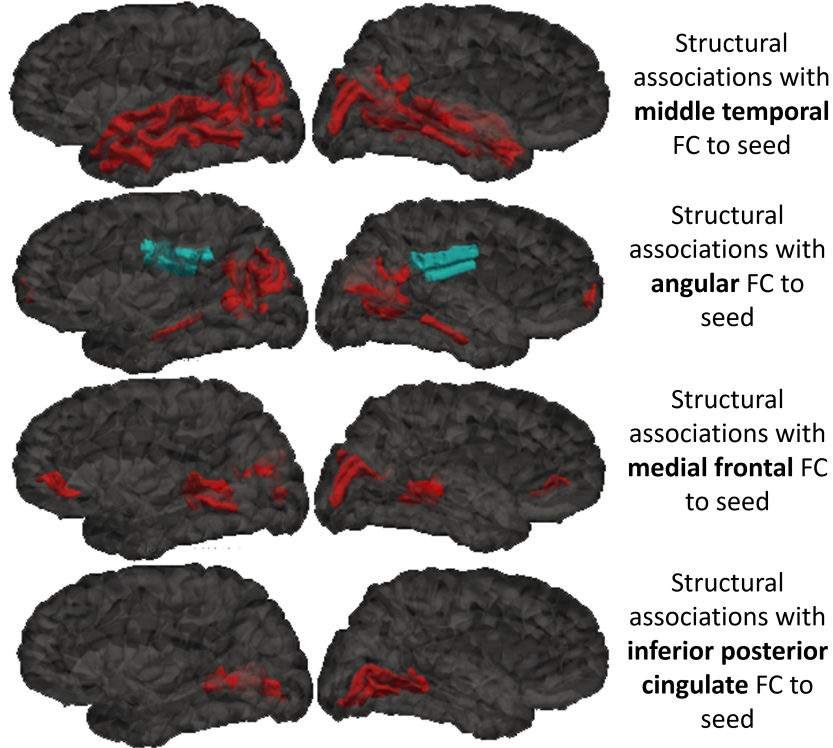


Figure C-5: Glass brain representations of WM regions whose structural integrity is significantly correlated with the specified functional connectivity measure after correcting for age and for multiple comparisons ($p < 0.05$.) Regions in red indicate decreased MD with decreased functional connectivity, and blue indicates the opposite relationship.

seed were extracted from these regions in a separate group of 45 cognitively healthy older individuals between the ages of 40 and 80 with BOLD data. Continuous measures of WM integrity were created using a method described in previous work, which calculates the Mahalanobis distance (MD) of each WM voxel from healthy WM with three structural modalities (T1, T2, FLAIR). FreeSurfer was used to automatically parcellate the WM into 35 ROIs and the mean MD for each ROI was calculated. A general linear model (GLM) was implemented to determine significant associations between WM integrity in each structural ROI and FC measures in each DMN ROI after controlling for age.

Results

Significant decreases in WM integrity were seen with decreased functional connectivity in WM regions underlying the specified functional pathway for all four FC ROIs ($p < 0.05$). Strikingly, these preliminary data suggest that the results were specific to tissue structure of regions anatomically supporting the functional nodes (Figure C-5).

Conclusions

These preliminary data demonstrate that a novel metric of WM integrity with is anatomically specifically associated with variation in FC of the nodes of the DMN. Future work will compare these results to similar analyses utilizing diffusion MRI to assess the unique utility of this metric compared to traditional imaging measures.

THIS PAGE INTENTIONALLY LEFT BLANK

Appendix D

A CV of Failures

"You miss 100% of the shots you don't take."

-Wayne Gretzky

What Wayne didn't say, right after he said this, was that you also miss about 99% of the shots that you *do* take. He was a pro, so maybe his miss rate was lower, but for most people, life is full of misses. The day-to-day of graduate school, like life, has far more failures than successes. It is only at the end, when we organize and compile and polish that we walk away with a story about the rare moments that worked. This is something that I wish I had understood at the beginning. And so, for posterity, I write here a CV of all of my failures beginning with my initial attempts at even applying to graduate school, in the hopes that those who come after me will understand that success is built on failures, and that failures are the small nudges that *actually* get you to where you were supposed to go all along.

Education

MIT (Take 1)

In 2011, I applied to PhD programs in both MIT's Media Lab and MIT's Brain and Cognitive Sciences departments. I was rejected from both without an interview. If I were to go back and read my personal statements, it would take everything in me to not cringe at the apparent lack of direction in interests and goals that I outlined in these applications.

MIT (Take 2)

After being accepted to MIT's HST program in 2013, I chose computer science to be my concentration area in which I would have to pass my Technical Qualifying

Examination (TQE). I spent my first two years at MIT regretting this decision, failing my TQE on the first attempt and losing sleep over the theoretical underpinnings of support vector machines, Fibonacci heaps, and Poisson distributions. I now would have it no other way, but of course, I say this with the ability to look backwards and polish up the shiny parts.

Work Experience

For every one experiment with an interesting result that is described in this dissertation, there were at least 50 experiments that resulted in absolutely nothing interesting or interpretable. In addition to these failed experiments there were entire abandoned and unfinished projects. Some of my favorite involved 7T data, vascular imaging, low-resolution imaging-histopathological comparison experiments, and graph cut algorithms. There's some good stuff in those abandoned projects – I hope that someone picks them up one day and can learn from my mistakes.

Awards and Honors

During my graduate school career I applied to a total of 12 academic fellowships of which I was awarded two. The failed applications included NSF, NDSEG, and other major nationwide graduate funding agencies. The two that I successfully secured funding from were NIH-sponsored programs funded through HST and the Martinos Center, and for these opportunities I am forever grateful.

Publications

I produced three first-author publications during my time in graduate school. Ten separate submissions were required to bring the following three works to publication. Below are the rejections to these works.

White matter signal abnormality quality differentiates mild cognitive impairment that converts to Alzheimer's disease from nonconverters

This manuscript was rejected from three separate journals before it was reviewed by *Neurobiology of Aging*, after which it went through two rounds of major revisions before final publication.

Regional staging of white matter signal abnormalities in aging and Alzheimer's disease
This manuscript received a scathing rejection from an unnamed high profile journal that led to an unsuccessful rebuttal with the editor followed by six months of being set on the back burner. It was later submitted to a second journal, and then a third, rejected both times without review. After these rejections, the manuscript was completely revised into an essentially new work. On its fourth submission, this work received a major revision and was finally published in *NeuroImage: Clinical*.

*Differential Regional Distribution of Juxtacortical White Matter Signal Abnormalities
in Aging and Alzheimer's Disease*

This manuscript was only rejected by one journal before undergoing major revisions at the second journal. It was finally published in *Journal of Alzheimer's Disease*.

THIS PAGE INTENTIONALLY LEFT BLANK

Bibliography

- [1] B. Fischl, D. H. Salat, E. Busa, M. Albert, M. Dieterich, C. Haselgrove, A. Van Der Kouwe, R. Killiany, D. Kennedy, S. Klaveness, A. Montillo, N. Makris, B. Rosen, and A. M. Dale, “Whole brain segmentation: Automated labeling of neuroanatomical structures in the human brain,” *Neuron*, vol. 33, pp. 341–355, 2002.
- [2] D. H. Salat, S. Lee, A. J. W. van der Kouwe, D. N. Greve, B. Fischl, and H. D. Rosas, “Age-Associated Alteration in Cortical Gray and White Matter Signal Intensity and Gray to White Matter Contrast,” *NeuroImage*, vol. 48, no. 1, pp. 21–28, 2010.
- [3] R. S. Desikan, F. Segonne, B. Fischl, B. T. Quinn, B. C. Dickerson, D. Blacker, R. L. Buckner, A. M. Dale, R. P. Maguire, B. T. Hyman, M. S. Albert, and R. J. Killiany, “An automated labeling system for subdividing the human cerebral cortex on MRI scans into gyral based regions of interest,” *NeuroImage*, vol. 31, pp. 968–980, 2006.
- [4] Alzheimer’s Association, “2016 Alzheimer’s disease facts and figures,” *Alzheimer’s & Dementia*, vol. 12, pp. 459–509, 2016.
- [5] J. M. Wardlaw, M. C. Valdés Hernández, and S. MuñozáRManiega, “What are White Matter Hyperintensities Made of? Relevance to Vascular Cognitive Impairment,” *Journal of the American Heart Association*, vol. 4, no. 6, p. 001140, 2015.
- [6] D. Carmelli, C. DeCarli, G. E. Swan, L. M. Jack, T. Reed, P. A. Wolf, and B. L. Miller, “Evidence for genetic variance in white matter hyperintensity volume in normal elderly male twins,” *Stroke*, vol. 29, no. 6, pp. 1177–1181, 1998.
- [7] H. Schmidt, M. Zeginigg, M. Wiltgen, P. Freudenberger, K. Petrovic, M. Cavalieri, P. Gider, C. Enzinger, M. Fornage, S. Debette, *et al.*, “Genetic variants of the notch3 gene in the elderly and magnetic resonance imaging correlates of age-related cerebral small vessel disease,” *Brain*, p. awr252, 2011.
- [8] C. R. French, S. Seshadri, A. L. Destefano, M. Fornage, C. R. Arnold, P. J. Gage, J. M. Skarje, W. B. Dobyns, K. J. Millen, T. Liu, *et al.*, “Mutation of foxc1 and pitx2 induces cerebral small-vessel disease,” *The Journal of clinical investigation*, vol. 124, no. 11, pp. 4877–4881, 2014.

- [9] M. M. Breteler, “Vascular involvement in cognitive decline and dementia. Epidemiologic evidence from the Rotterdam Study and the Rotterdam Scan Study.,” *Annals of the New York Academy of Sciences*, vol. 903, pp. 457–465, 2000.
- [10] E. Pagani, F. Agosta, M. a. Rocca, D. Caputo, and M. Filippi, “Voxel-based analysis derived from fractional anisotropy images of white matter volume changes with aging,” *NeuroImage*, vol. 41, no. 3, pp. 657–667, 2008.
- [11] D. H. Salat, D. N. Greve, J. L. Pacheco, B. T. Quinn, K. G. Helmer, R. L. Buckner, and B. Fischl, “Regional White Matter Volume Differences in Nondemented Aging and Alzheimer’s Disease,” *NeuroImage*, vol. 44, no. 4, pp. 1247–1258, 2009.
- [12] M. R. Benedictus, M. A. A. Binnewijzend, J. P. A. Kuijer, M. D. Steenwijk, A. Versteeg, H. Vrenken, P. Scheltens, F. Barkhof, W. M. van der Flier, and N. D. Prins, “Brain volume and white matter hyperintensities as determinants of cerebral blood flow in Alzheimer’s disease,” *Neurobiology of Aging*, vol. 35, no. 12, pp. 2665–2670, 2014.
- [13] J. M. Wardlaw, E. E. Smith, G. J. Biessels, C. Cordonnier, F. Fazekas, R. Frayne, R. I. Lindley, J. T. O’Brien, F. Barkhof, O. R. Benavente, S. E. Black, C. Brayne, M. Breteler, H. Chabriat, C. Decarli, F.-E. de Leeuw, F. Doubal, M. Duering, N. C. Fox, S. Greenberg, V. Hachinski, I. Kilimann, V. Mok, R. V. Oostenbrugge, L. Pantoni, O. Speck, B. C. M. Stephan, S. Teipel, A. Viswanathan, D. Werring, C. Chen, C. Smith, M. van Buchem, B. Norrving, P. B. Gorelick, and M. Dichgans, “Neuroimaging standards for research into small vessel disease and its contribution to ageing and neurodegeneration.,” *Lancet neurology*, vol. 12, pp. 822–38, aug 2013.
- [14] F. E. de Leeuw, J. C. de Groot, E. Achten, M. Oudkerk, L. M. Ramos, R. Heijboer, A. Hofman, J. Jolles, J. van Gijn, and M. M. Breteler, “Prevalence of cerebral white matter lesions in elderly people: a population based magnetic resonance imaging study. The Rotterdam Scan Study.,” *Journal of neurology, neurosurgery, and psychiatry*, vol. 70, no. 1, pp. 9–14, 2001.
- [15] J. Bowler, “Modern concept of vascular cognitive impairment,” *British medical bulletin*, vol. 83, no. 1, pp. 291–305, 2007.
- [16] K. Jellinger, “Alzheimer 100—highlights in the history of alzheimer research,” *Journal of neural transmission*, vol. 113, no. 11, pp. 1603–1623, 2006.
- [17] G. G. Glenner and C. W. Wong, “Alzheimer’s disease: initial report of the purification and characterization of a novel cerebrovascular amyloid protein,” *Biochemical and biophysical research communications*, vol. 120, no. 3, pp. 885–890, 1984.

- [18] J. Kang, H.-G. Lemaire, A. Unterbeck, J. M. Salbaum, C. L. Masters, K.-H. Grzeschik, G. Multhaup, K. Beyreuther, and B. Müller-Hill, “The precursor of alzheimer’s disease amyloid a4 protein resembles a cell-surface receptor,” *Nature*, vol. 325, no. 6106, pp. 733–736, 1987.
- [19] L. Bertram and R. E. Tanzi, “Thirty years of alzheimer’s disease genetics: the implications of systematic meta-analyses,” *Nature Reviews Neuroscience*, vol. 9, no. 10, pp. 768–778, 2008.
- [20] H. Braak and E. Braak, “Morphology of the human isocortex in young and aged individuals: Qualitative and quantitative findings1,” in *Histology and Histopathology of the Aging Brain*, pp. 1–15, Karger Publishers, 1988.
- [21] H. Braak and E. Braak, “Morphology of the cerebral cortex in relation to alzheimerâŽs dementia,” in *AlzheimerâŽs Disease. Epidemiology, Neuropathology, Neurochemistry, and Clinics*, pp. 85–91, Springer, 1990.
- [22] H. Braak and E. Braak, “Neuropathological stageing of Alzheimer-related changes,” *Acta Neuropathologica*, vol. 82, no. 4, pp. 239–259, 1991.
- [23] D. M. Mann, “The neuropathology of alzheimer’s disease: a review with pathogenetic, aetiological and therapeutic considerations,” *Mechanisms of ageing and development*, vol. 31, no. 3, pp. 213–255, 1985.
- [24] M. M. Esiri, Z. Nagy, M. Z. Smith, L. Barnetson, and A. D. Smith, “Cerebrovascular disease and threshold for dementia in the early stages of alzheimer’s disease,” *The Lancet*, vol. 354, no. 9182, pp. 919–920, 1999.
- [25] D. A. Snowdon, L. H. Greiner, J. A. Mortimer, K. P. Riley, P. A. Greiner, and W. R. Markesberry, “Brain infarction and the clinical expression of alzheimer disease: the nun study,” *Jama*, vol. 277, no. 10, pp. 813–817, 1997.
- [26] L. J. Launer, H. Petrovitch, G. W. Ross, W. Markesberry, and L. R. White, “Ad brain pathology: Vascular origins?: Results from the haas autopsy study,” *Neurobiology of aging*, vol. 29, no. 10, pp. 1587–1590, 2008.
- [27] J. A. Schneider, Z. Arvanitakis, W. Bang, and D. A. Bennett, “Mixed brain pathologies account for most dementia cases in community-dwelling older persons,” *Neurology*, vol. 69, no. 24, pp. 2197–2204, 2007.
- [28] J. Hardy and D. J. Selkoe, “The amyloid hypothesis of Alzheimer’s disease: progress and problems on the road to therapeutics.,” *Science (New York, N.Y.)*, vol. 297, no. 5580, pp. 353–356, 2002.
- [29] S. a. Small and K. Duff, “Linking Abeta and tau in late-onset Alzheimer’s disease: a dual pathway hypothesis.,” *Neuron*, vol. 60, pp. 534–42, nov 2008.

- [30] S. E. Arnold, B. T. Hyman, J. Flory, A. R. Damasio, G. W. V. Hoesen, and G. W. Van Hoesen, “The Topographical and Neuroanatomical Distribution of Neurofibrillary Tangles and Neuritic Plaques in the Cerebral Cortex of Patients with Alzheimer’s Disease,” *Cerebral Cortex*, vol. 1, no. 1, pp. 103–116, 1991.
- [31] B. C. Dickerson, A. Bakkour, D. H. Salat, E. Feczko, J. Pacheco, D. N. Greve, F. Grodstein, C. I. Wright, D. Blacker, H. D. Rosas, R. a. Sperling, A. Atri, J. H. Growdon, B. T. Hyman, J. C. Morris, B. Fischl, and R. L. Buckner, “The cortical signature of Alzheimer’s disease: regionally specific cortical thinning relates to symptom severity in very mild to mild AD dementia and is detectable in asymptomatic amyloid-positive individuals.,” *Cerebral cortex*, vol. 19, no. 3, pp. 497–510, 2009.
- [32] L. Regeur, “Increasing loss of brain tissue with increasing dementia: a stereological study of post-mortem brains from elderly females,” *European Journal of Neurology*, vol. 7, no. 1, pp. 47–54, 2000.
- [33] A. Brun and L. Gustafson, “Distribution of cerebral degeneration in Alzheimer’s disease,” *Archiv für Psychiatrie und Nervenkrankheiten*, vol. 33, pp. 15–33, 1976.
- [34] T. Gómez-Isla, J. L. Price, D. W. McKeel, J. C. Morris, J. H. Growdon, and B. T. Hyman, “Profound loss of layer II entorhinal cortex neurons occurs in very mild Alzheimer’s disease.,” *The Journal of neuroscience : the official journal of the Society for Neuroscience*, vol. 16, no. 14, pp. 4491–4500, 1996.
- [35] P. D. Coleman and D. G. Flood, “Neuron numbers and dendritic extent in normal aging and Alzheimer’s disease.,” *Neurobiology of aging*, vol. 8, no. 6, pp. 521–545, 1987.
- [36] S. T. DeKosky and S. W. Scheff, “Synapse loss in frontal cortex biopsies in Alzheimer’s disease: correlation with cognitive severity.,” *Annals of neurology*, vol. 27, no. 5, pp. 457–464, 1990.
- [37] S. T. DeKosky, S. W. Scheff, and S. D. Styren, “Structural correlates of cognition in dementia: quantification and assessment of synapse change.,” *Neurodegeneration : a journal for neurodegenerative disorders, neuroprotection, and neuroregeneration*, vol. 5, no. 4, pp. 417–421, 1996.
- [38] P. Coleman, H. Federoff, and R. Kurlan, “A focus on the synapse for neuroprotection in Alzheimer disease and other dementias.,” *Neurology*, vol. 63, no. 7, pp. 1155–62, 2004.
- [39] S. W. Scheff, S. T. DeKosky, and D. A. Price, “Quantitative assessment of cortical synaptic density in Alzheimer’s disease,” *Neurobiol Aging*, vol. 11, no. 1, pp. 29–37, 1990.

- [40] K. Im, J.-M. Lee, S. W. Seo, S. Hyung Kim, S. I. Kim, and D. L. Na, "Sulcal morphology changes and their relationship with cortical thickness and gyral white matter volume in mild cognitive impairment and Alzheimer's disease.," *NeuroImage*, vol. 43, no. 1, pp. 103–113, 2008.
- [41] J.-P. Coutu, A. Goldblatt, H. D. Rosas, and D. H. Salat, "White Matter Changes are Associated with Ventricular Expansion in Aging, Mild Cognitive Impairment, and Alzheimer's Disease.," *Journal of Alzheimer's disease : JAD*, vol. 49, pp. 329–342, 2015.
- [42] Y.-F. Chen, H. Wang, Y. Chu, Y.-C. Huang, and M.-Y. Su, "Regional quantification of white matter hyperintensity in normal aging, mild cognitive impairment, and Alzheimer's disease.," *Dementia and geriatric cognitive disorders*, vol. 22, pp. 177–84, jan 2006.
- [43] A. M. Brickman, F. a. Provenzano, J. Muraskin, J. J. Manly, S. Blum, Z. Apa, Y. Stern, T. R. Brown, J. a. Luchsinger, and R. Mayeux, "Regional white matter hyperintensity volume, not hippocampal atrophy, predicts incident Alzheimer disease in the community.," *Archives of neurology*, vol. 69, pp. 1621–7, dec 2012.
- [44] A. M. Brickman, L. B. Zahodne, V. A. Guzman, A. Narkhede, I. B. Meier, E. Y. Griffith, F. A. Provenzano, N. Schupf, J. J. Manly, Y. Stern, J. A. Luchsinger, and R. Mayeux, "Reconsidering harbingers of dementia: Progression of parietal lobe white matter hyperintensities predicts Alzheimer's disease incidence," *Neurobiology of Aging*, vol. 36, no. 1, pp. 27–32, 2015.
- [45] P. Scheltens, F. Barkhof, J. Valk, P. R. Algra, R. G. VAn der Hoop, J. Nauta, and E. C. Wolters, "White matter lesions on magnetic resonance imaging in clinically diagnosed Alzheimer's disease. Evidence for heterogeneity," *Brain*, vol. 115, no. 3, pp. 735–748, 1992.
- [46] P. Scheltens, F. Barkhof, D. Leys, E. C. Wolters, R. Ravid, and W. Kamphorst, "Histopathologic correlates of white matter changes on MRI in Alzheimer's disease and normal aging.," *Neurology*, vol. 45, no. 5, pp. 883–888, 1995.
- [47] F. E. De Leeuw, F. Richard, J. C. De Groot, C. M. Van Duijn, A. Hofman, J. Van Gijn, and M. M. B. Breteler, "Interaction between hypertension, apoE, and cerebral white matter lesions," *Stroke*, vol. 35, no. 5, pp. 1057–1060, 2004.
- [48] L. H. Kuller, L. Shemanski, T. Manolio, M. Haan, L. Fried, N. Bryan, G. L. Burke, R. Tracy, and R. Bhadelia, "Relationship between apoe, mri findings, and cognitive function in the cardiovascular health study," *Stroke*, vol. 29, no. 2, pp. 388–398, 1998.
- [49] D. García-Lorenzo, S. Prima, L. Collins, D. L. Arnold, C. Barillot, and S. P. Morrissey, "Multiple Sclerosis (MS) Brain segmentation combining robust Expectation Maximization (EM) and Mean Shift (MeS)," 2008.

- [50] P. Scheltens, T. Erkinjunti, D. Leys, L.-O. Wahlund, D. Inzitari, T. del Ser, F. Pasquier, F. Barkhof, R. Mäntylä, J. Bowler, *et al.*, “White matter changes on ct and mri: an overview of visual rating scales,” *European neurology*, vol. 39, no. 2, pp. 80–89, 1998.
- [51] C. R. Jack, M. A. Bernstein, N. C. Fox, P. Thompson, G. Alexander, D. Harvey, B. Borowski, P. J. Britson, J. L. Whitwell, C. Ward, A. M. Dale, J. P. Felmlee, J. L. Gunter, D. L. G. Hill, R. Killiany, N. Schuff, S. Fox-Bosetti, C. Lin, C. Studholme, C. S. DeCarli, G. Krueger, H. A. Ward, G. J. Metzger, K. T. Scott, R. Mallozzi, D. Blezek, J. Levy, J. P. Debbins, A. S. Fleisher, M. Albert, R. Green, G. Bartzokis, G. Glover, J. Mugler, and M. W. Weiner, “The Alzheimer’s Disease Neuroimaging Initiative (ADNI): MRI methods,” *Journal of Magnetic Resonance Imaging*, vol. 27, no. 4, pp. 685–691, 2008.
- [52] A. M. Dale, B. Fischl, and M. I. Sereno, “Cortical surface-based analysis. I. Segmentation and surface reconstruction.,” *NeuroImage*, vol. 9, no. 2, pp. 179–194, 1999.
- [53] A. M. Dale and M. I. Sereno, “Improved Localizadon of Cortical Activity by Combining EEG and MEG with MRI Cortical Surface Reconstruction: A Linear Approach,” *Journal of Cognitive Neuroscience*, vol. 5, no. 2, pp. 162–176, 1993.
- [54] B. Fischl and a. M. Dale, “Measuring the thickness of the human cerebral cortex from magnetic resonance images.,” *Proceedings of the National Academy of Sciences of the United States of America*, vol. 97, no. 20, pp. 11050–5, 2000.
- [55] B. Fischl, A. Liu, and A. M. Dale, “Automated manifold surgery: Constructing geometrically accurate and topologically correct models of the human cerebral cortex,” *IEEE Transactions on Medical Imaging*, vol. 20, no. 1, pp. 70–80, 2001.
- [56] B. Fischl, D. H. Salat, A. Van Der Kouwe, N. Makris, F. Segonne, B. T. Quinn, and A. M. Dale, “Sequence-independent segmentation of magnetic resonance images,” *NeuroImage*, vol. 23, no. Suppl 1, pp. S69–S84, 2004.
- [57] B. Fischl, M. I. Sereno, R. B. H. Tootell, and A. M. Dale, “High-resolution intersubject averaging and a coordinate system for the cortical surface,” *Human Brain Mapping*, vol. 8, no. 4, pp. 272–284, 1999.
- [58] X. Han, J. Jovicich, D. Salat, A. van der Kouwe, B. Quinn, S. Czanner, E. Busa, J. Pacheco, M. Albert, R. Killiany, P. Maguire, D. Rosas, N. Makris, A. Dale, B. Dickerson, and B. Fischl, “Reliability of MRI-derived measurements of human cerebral cortical thickness: The effects of field strength, scanner upgrade and manufacturer,” *NeuroImage*, vol. 32, no. 1, pp. 180–194, 2006.
- [59] J. Jovicich, S. Czanner, D. Greve, E. Haley, A. Van Der Kouwe, R. Gollub, D. Kennedy, F. Schmitt, G. Brown, J. MacFall, B. Fischl, and A. Dale, “Reliability in multi-site structural MRI studies: Effects of gradient non-linearity

correction on phantom and human data,” *NeuroImage*, vol. 30, no. 2, pp. 436–443, 2006.

- [60] J. M. Wardlaw, C. Smith, and M. Dichgans, “Mechanisms of sporadic cerebral small vessel disease: insights from neuroimaging.,” *Lancet neurology*, vol. 12, pp. 483–97, may 2013.
- [61] P. Maillard, N. Delcroix, F. Crivello, C. Dufouil, S. Gicquel, M. Joliot, N. Tzourio-Mazoyer, A. Alpérovitch, C. Tzourio, and B. Mazoyer, “An automated procedure for the assessment of white matter hyperintensities by multispectral (T1, T2, PD) MRI and an evaluation of its between-centre reproducibility based on two large community databases.,” *Neuroradiology*, vol. 50, pp. 31–42, jan 2008.
- [62] C. Schwarz, E. Fletcher, C. DeCarli, and O. Carmichael, “Fully-Automated White Matter Hyperintensity Detection With Anatomical Prior Knowledge and Without FLAIR,” *Information Processing in Medical Imaging*, vol. 21, pp. 239–251, 2009.
- [63] P. C. Mahalanobis, “On the generalised distance in statistics,” 1936.
- [64] E. C. W. van Straaten, F. Fazekas, E. Rostrup, P. Scheltens, R. Schmidt, L. Pantoni, D. Inzitari, G. Waldemar, T. Erkinjuntti, R. Mäntylä, L.-O. Wahlund, and F. Barkhof, “Impact of white matter hyperintensities scoring method on correlations with clinical data: the LADIS study.,” *Stroke; a journal of cerebral circulation*, vol. 37, pp. 836–40, mar 2006.
- [65] A. Cerasa, E. Bilotta, A. Augimeri, A. Cherubini, P. Pantano, G. Zito, P. Lanza, P. Valentino, M. C. Gioia, and A. Quattrone, “A Cellular Neural Network methodology for the automated segmentation of multiple sclerosis lesions.,” *Journal of neuroscience methods*, vol. 203, pp. 193–9, jan 2012.
- [66] J. a. Pettersen, G. Sathiyamoorthy, F.-Q. Gao, G. Szilagyi, N. K. Nadkarni, P. St George-Hyslop, E. Rogava, and S. E. Black, “Microbleed topography, leukoaraiosis, and cognition in probable Alzheimer disease from the Sunnybrook dementia study.,” *Archives of neurology*, vol. 65, pp. 790–5, jun 2008.
- [67] C. Iadecola, “The pathobiology of vascular dementia.,” *Neuron*, vol. 80, pp. 844–66, nov 2013.
- [68] V. G. Young, G. M. Halliday, and J. J. Kril, “Neuropathologic correlates of white matter hyperintensities.,” *Neurology*, vol. 71, pp. 804–11, sep 2008.
- [69] A. a. Gouw, A. Seewann, W. M. van der Flier, F. Barkhof, A. M. Rozemuller, P. Scheltens, and J. J. G. Geurts, “Heterogeneity of small vessel disease: a systematic review of MRI and histopathology correlations.,” *Journal of neurology, neurosurgery, and psychiatry*, vol. 82, pp. 126–35, feb 2011.

- [70] A. Viswanathan, “Shades of white: separating degrees of injury in the aging brain.,” *Stroke; a journal of cerebral circulation*, vol. 45, pp. 1606–7, jun 2014.
- [71] P. Maillard, E. Fletcher, S. N. Lockhart, A. E. Roach, B. Reed, D. Mungas, C. DeCarli, and O. T. Carmichael, “White Matter Hyperintensities and Their Penumbra Lie Along a Continuum of Injury in the Aging Brain.,” *Stroke; a journal of cerebral circulation*, vol. 45, pp. 1721–1726, jun 2014.
- [72] D. García-Lorenzo, S. Francis, S. Narayanan, D. L. Arnold, and D. L. Collins, “Review of automatic segmentation methods of multiple sclerosis white matter lesions on conventional magnetic resonance imaging.,” *Medical image analysis*, vol. 17, pp. 1–18, jan 2013.
- [73] D. Mortazavi, A. Z. Kouzani, and H. Soltanian-Zadeh, “Segmentation of multiple sclerosis lesions in MR images: a review,” *Neuroradiology*, vol. 54, pp. 299–320, apr 2012.
- [74] P. Kapeller, R. Barber, R. Vermeulen, H. Ader, P. Scheltens, W. Freidl, O. Almkvist, M. Moretti, T. del Ser, P. Vaghfeldt, C. Enzinger, F. Barkhof, D. Inzitari, T. Erkinjuntti, R. Schmidt, and F. Fazekas, “Visual Rating of Age-Related White Matter Changes on Magnetic Resonance Imaging: Scale Comparison, Interrater Agreement, and Correlations With Quantitative Measurements,” *Stroke*, vol. 34, pp. 441–445, jan 2003.
- [75] F. Fazekas, J. B. Chawluk, and a. Alavi, “MR signal abnormalities at 1.5 T in Alzheimer’s dementia and normal aging,” *American Journal of Neuroradiology*, vol. 8, no. 3, pp. 421–426, 1987.
- [76] P. Scheltens, F. Barkhof, D. Leys, J. P. Pruvost, J. J. Nauta, P. Vermersch, M. Steinling, and J. Valk, “A semiquantitative rating scale for the assessment of signal hyperintensities on magnetic resonance imaging.,” *Journal of the neurological sciences*, vol. 114, no. 1, pp. 7–12, 1993.
- [77] E. R. Lindemer, D. H. Salat, E. E. Smith, K. Nguyen, B. Fischl, and D. N. Greve, “White matter signal abnormality quality differentiates mild cognitive impairment that converts to Alzheimer’s disease from nonconverters,” *Neurobiology of Aging*, vol. 36, no. 9, pp. 2447–57, 2015.
- [78] G. B. Frisoni, S. Galluzzi, L. Pantoni, and M. Filippi, “The effect of white matter lesions on cognition in the elderly - small but detectable,” *Nat Clin Pract Neurol*, vol. 3, no. 11, pp. 620–627, 2007.
- [79] A. M. Brickman, J. Muraskin, and M. E. Zimmerman, “Structural neuroimaging in Alzheimer’s disease: do white matter hyperintensities matter?,” *Dialogues in Clinical Neuroscience*, vol. 11, no. 2, pp. 181–190, 2009.
- [80] A. M. Brickman, A. Zahra, J. Muraskin, J. Steffener, C. M. Holland, C. Habeck, A. Borogovac, M. a. Ramos, T. R. Brown, I. Asllani, and Y. Stern, “Reduction

in cerebral blood flow in areas appearing as white matter hyperintensities on magnetic resonance imaging.,” *Psychiatry research*, vol. 172, pp. 117–20, may 2009.

- [81] C. DeCarli, J. Massaro, D. Harvey, J. Hald, M. Tullberg, R. Au, A. Beiser, R. D'Agostino, and P. A. Wolf, “Measures of brain morphology and infarction in the framingham heart study: Establishing what is normal,” *Neurobiology of Aging*, vol. 26, no. 4, pp. 491–510, 2005.
- [82] M. Yoshita, E. Fletcher, D. Harvey, M. Ortega, O. Martinez, D. M. Mungas, B. R. Reed, and C. S. DeCarli, “Extent and distribution of white matter hyperintensities in normal aging, MCI, and AD,” *Neurology*, vol. 67, no. 12, pp. 2192–2198, 2006.
- [83] J. C. de Groot, F. E. de Leeuw, M. Oudkerk, a. Hofman, J. Jolles, and M. M. Breteler, “Cerebral white matter lesions and subjective cognitive dysfunction: the Rotterdam Scan Study.,” *Neurology*, vol. 56, no. 11, pp. 1539–1545, 2001.
- [84] J. C. de Groot, F. E. de Leeuw, M. Oudkerk, J. Van Gijn, A. Hofman, J. Jolles, and M. M. B. Breteler, “Periventricular cerebral white matter lesions predict rate of cognitive decline,” *Annals of Neurology*, vol. 52, no. 3, pp. 335–341, 2002.
- [85] C. Dufouil, A. de Kersaint-Gilly, V. Besancon, C. Levy, E. Auffray, L. Brunnerneau, A. Alperovitch, and C. Tzourio, “Longitudinal study of blood pressure and white matter hyperintensities: The EVA MRI Cohort,” *Neurology*, vol. 56, no. 7, pp. 921–926, 2001.
- [86] W. T. Longstreth Jr., “Brain abnormalities in the elderly: frequency and predictors in the United States (the Cardiovascular Health Study). Cardiovascular Health Study Collaborative Research Group,” *J.Neural Transm.Suppl*, vol. 53, no. 0303-6995 (Print), pp. 9–16, 1998.
- [87] R. D. Zimmerman, C. A. Fleming, B. C. Lee, L. A. Saint-Louis, and M. D. Deck, “Periventricular hyperintensity as seen by magnetic resonance: prevalence and significance.,” *AJR. American journal of roentgenology*, vol. 146, no. 3, pp. 443–450, 1986.
- [88] A. Spilt, R. Goekoop, R. G. J. Westendorp, G. J. Blauw, A. J. M. de Craen, and M. A. van Buchem, “Not all age-related white matter hyperintensities are the same: a magnetization transfer imaging study.,” *AJNR. American journal of neuroradiology*, vol. 27, no. 9, pp. 1964–1968, 2006.
- [89] J. C. Augustinack, K. E. Huber, G. M. Postelnicu, S. Kakunoori, R. Wang, A. J. W. Van Der Kouwe, L. L. Wald, T. D. Stein, M. P. Frosch, and B. Fischl, “Entorhinal verrucae geometry is coincident and correlates with Alzheimer’s lesions: A combined neuropathology and high-resolution ex vivo MRI analysis,” *Acta Neuropathologica*, vol. 123, no. 1, pp. 85–96, 2012.

- [90] D. Erten-Lyons, R. Woltjer, J. Kaye, N. Mattek, H. H. Dodge, S. Green, H. Tran, D. B. Howieson, K. Wild, and L. C. Silbert, “Neuropathologic basis of white matter hyperintensity accumulation with advanced age.,” *Neurology*, vol. 81, pp. 977–83, sep 2013.
- [91] R. Schmidt, F. Fazekas, P. Kapeller, H. Schmidt, and H. P. Hartung, “MRI white matter hyperintensities: three-year follow-up of the Austrian Stroke Prevention Study.,” *Neurology*, vol. 53, no. 1, pp. 132–139, 1999.
- [92] H. Damasio, “A computed tomographic guide to the identification of cerebral vascular territories.,” *Archives of neurology*, vol. 40, no. 3, pp. 138–142, 1983.
- [93] D. Haines, *Neuroanatomy: An Atlas of Structures, Sections, and Systems*. Baltimore: Urban and Schwarzenberg, 2 ed., 1995.
- [94] Y. Chen, D. A. Wolk, J. S. Reddin, M. Korczykowski, P. M. Martinez, E. S. Musiek, A. B. Newberg, P. Julin, S. E. Arnold, J. H. Greenberg, and J. A. Detre, “Voxel-level comparison of arterial spin-labeled perfusion MRI and FDG-PET in Alzheimer disease,” *Neurology*, vol. 77, no. 22, pp. 1977–1985, 2011.
- [95] J. J. Chen, H. D. Rosas, and D. H. Salat, “The Relationship between Cortical Blood Flow and Sub-Cortical White-Matter Health across the Adult Age Span,” *PLoS ONE*, vol. 8, no. 2, p. e56733, 2013.
- [96] J. C. van Swieten, J. H. van den Hout, B. A. van Ketel, A. Hijdra, J. H. Wokke, and J. van Gijn, “Periventricular lesions in the white matter on magnetic resonance imaging in the elderly. A morphometric correlation with arteriolosclerosis and dilated perivascular spaces.,” *Brain : a journal of neurology*, vol. 114, no. 2, pp. 761–774, 1991.
- [97] L. Pantoni and J. H. Garcia, “Pathogenesis of leukoaraiosis: a review.,” *Stroke; a journal of cerebral circulation*, vol. 28, no. 3, pp. 652–659, 1997.
- [98] H. G. Birnbaum, A. G. White, M. Schiller, T. Waldman, J. J. M. Cleveland, B. Setnik, G. Pixton, C. L. C. Roland, B. Setnik, G. Pixton, and C. L. C. Roland, “Societal Costs of Opioid Abuse, Dependence and Misuse in The United States,” *Value in Health*, vol. 13, no. 3, p. A111, 2010.
- [99] D. M. Moody, C. R. Thore, J. a. Anstrom, V. R. Challa, C. D. Langefeld, and W. R. Brown, “Quantification of afferent vessels shows reduced brain vascular density in subjects with leukoaraiosis.,” *Radiology*, vol. 233, no. 3, pp. 883–890, 2004.
- [100] H. Wolf, G. M. Ecke, S. Bettin, J. Dietrich, and H. J. Gertz, “Do white matter changes contribute to the subsequent development of dementia in patients with mild cognitive impairment? A longitudinal study.,” *International journal of geriatric psychiatry*, vol. 15, pp. 803–12, sep 2000.

- [101] E. E. Smith, S. Egorova, D. Blacker, R. J. Killiany, A. Muzikansky, B. C. Dickerson, R. E. Tanzi, M. S. Albert, S. M. Greenberg, and C. R. G. Guttmann, “Magnetic resonance imaging white matter hyperintensities and brain volume in the prediction of mild cognitive impairment and dementia.,” *Archives of neurology*, vol. 65, pp. 94–100, jan 2008.
- [102] G. Tosto, M. E. Zimmerman, O. T. Carmichael, and A. M. Brickman, “Predicting aggressive decline in mild cognitive impairment: the importance of white matter hyperintensities.,” *JAMA neurology*, vol. 71, no. 7, pp. 872–7, 2014.
- [103] M. Reuter, N. J. Schmansky, H. D. Rosas, and B. Fischl, “Within-subject template estimation for unbiased longitudinal image analysis,” *NeuroImage*, vol. 61, no. 4, pp. 1402–1418, 2012.
- [104] D. Sorenson, “MATLAB, version 8.2 0.701,” 2013.
- [105] R. Barber, P. Scheltens, A. Ghokar, C. Ballard, I. McKeith, P. Ince, R. Perry, and J. O’Brien, “White matter lesions on magnetic resonance imaging in dementia with Lewy bodies, Alzheimer’s disease, vascular dementia, and normal aging,” *Journal of Neurology, Neurosurgery & Psychiatry*, vol. 67, no. 1, pp. 66–72, 1999.
- [106] N. D. Prins, E. J. van Dijk, T. den Heijer, S. E. Vermeer, P. J. Koudstaal, M. Oudkerk, A. Hofman, and M. M. B. Breteler, “Cerebral white matter lesions and the risk of dementia.,” *Archives of neurology*, vol. 61, pp. 1531–4, oct 2004.
- [107] K. Matsubayashi, K. Shimada, A. Kawamoto, and T. Ozawa, “Incidental brain lesions on magnetic resonance imaging and neurobehavioral functions in the apparently healthy elderly.,” *Stroke; a journal of cerebral circulation*, vol. 23, pp. 175–180, 1992.
- [108] C. H. Kawas, R. C. Kim, J. A. Sonnen, S. S. Bullain, and T. Trieu, “Multiple pathologies are common and related to dementia in the oldest-old,” *Neurology*, vol. 85, pp. 535–542, 2015.
- [109] J. B. Toledo, S. E. Arnold, K. Raible, J. Brettschneider, S. X. Xie, M. Grossman, S. E. Monsell, W. A. Kukull, and J. Q. Trojanowski, “Contribution of cerebrovascular disease in autopsy confirmed neurodegenerative disease cases in the National Alzheimer’s Coordinating Centre.,” *Brain : a journal of neurology*, vol. 136, no. Pt 9, pp. 2697–706, 2013.
- [110] C. Genovese and L. Wasserman, “Operating characteristics and extensions of the false discovery rate procedure,” *Journal of the Royal Statistical Society. Series B: Statistical Methodology*, vol. 64, no. 3, pp. 499–517, 2002.
- [111] D. M. Moody, M. a. Bell, and V. R. Challa, “Features of the cerebral vascular pattern that predict vulnerability to perfusion or oxygenation deficiency: An anatomic study,” *American Journal of Neuroradiology*, vol. 11, no. 3, pp. 431–439, 1990.

- [112] P. Maillard, O. Carmichael, D. Harvey, E. Fletcher, B. Reed, D. Mungas, and C. DeCarli, “FLAIR and diffusion MRI signals are independent predictors of white matter hyperintensities,” *American Journal of Neuroradiology*, vol. 34, no. 1, pp. 54–61, 2013.
- [113] B. C. Dickerson, I. Goncharova, M. P. Sullivan, C. Forchetti, R. S. Wilson, D. A. Bennett, L. A. Beckett, and L. DeToledo-Morrell, “MRI-derived entorhinal and hippocampal atrophy in incipient and very mild Alzheimer’s disease,” *Neurobiology of Aging*, vol. 22, pp. 747–754, 2001.
- [114] F. Shi, B. Liu, Y. Zhou, C. Yu, and T. Jiang, “Hippocampal volume and asymmetry in mild cognitive impairment and Alzheimer’s disease: Meta-analyses of MRI studies,” *Hippocampus*, vol. 19, no. 11, pp. 1055–1064, 2009.
- [115] L. a. van de Pol, F. Verhey, G. B. Frisoni, M. Tsolaki, P. Papapostolou, F. Nobili, L.-O. Wahlund, L. Minthon, L. Frölich, H. Hampel, H. Soininen, D. L. Knol, F. Barkhof, P. Scheltens, and P. J. Visser, “White matter hyperintensities and medial temporal lobe atrophy in clinical subtypes of mild cognitive impairment: the DESCRIPA study.,” *Journal of neurology, neurosurgery, and psychiatry*, vol. 80, no. 10, pp. 1069–1074, 2009.
- [116] A. Caroli, C. Testa, C. Geroldi, F. Nobili, U. P. Guerra, M. Bonetti, and G. B. Frisoni, “Brain perfusion correlates of medial temporal lobe atrophy and white matter hyperintensities in mild cognitive impairment,” *Journal of Neurology*, vol. 254, no. 8, pp. 1000–1008, 2007.
- [117] C. R. Jack, D. S. Knopman, W. J. Jagust, R. C. Petersen, M. W. Weiner, P. S. Aisen, L. M. Shaw, P. Vemuri, H. J. Wiste, S. D. Weigand, T. G. Lesnick, V. S. Pankratz, M. C. Donohue, and J. Q. Trojanowski, “Tracking pathophysiological processes in Alzheimer’s disease: An updated hypothetical model of dynamic biomarkers,” *The Lancet Neurology*, vol. 12, no. 2, pp. 207–216, 2013.
- [118] A. Convit, M. J. De Leon, C. Tarshish, S. De Santi, W. Tsui, H. Rusinek, and A. George, “Specific hippocampal volume reductions in individuals at risk for Alzheimer’s disease,” *Neurobiol Aging*, vol. 18, no. 2, pp. 131–138, 1997.
- [119] K. M. Gosche, J. A. Mortimer, C. D. Smith, W. R. Markesberry, and D. A. Snowdon, “Hippocampal volume as an index of Alzheimer neuropathology: findings from the Nun Study.,” *Neurology*, vol. 58, no. 10, pp. 1476–1482, 2002.
- [120] C. R. Jack, R. C. Petersen, Y. C. Xu, P. C. O’Brien, G. E. Smith, R. J. Ivnik, B. F. Boeve, S. C. Waring, E. G. Tangalos, and E. Kokmen, “Prediction of AD with MRI-based hippocampal volume in mild cognitive impairment.,” *Neurology*, vol. 52, no. 7, pp. 1397–1403, 1999.
- [121] N. Schuff, N. Woerner, L. Boreta, T. Kornfield, L. M. Shaw, J. Q. Trojanowski, P. M. Thompson, C. R. Jack, and M. W. Weiner, “MRI of hippocampal volume

- loss in early Alzheimer's disease in relation to ApoE genotype and biomarkers.,” *Brain*, vol. 132, no. 4, pp. 1067–1077, 2009.
- [122] E. Canu, G. B. Frisoni, F. Agosta, M. Pievani, M. Bonetti, and M. Filippi, “Early and late onset Alzheimer's disease patients have distinct patterns of white matter damage.,” *Neurobiology of aging*, vol. 33, pp. 1023–33, jun 2012.
 - [123] M. Pievani, F. Agosta, E. Pagani, E. Canu, S. Sala, M. Absinta, C. Geroldi, R. Ganzola, G. B. Frisoni, and M. Filippi, “Assessment of white matter tract damage in mild cognitive impairment and Alzheimer's disease.,” *Human brain mapping*, vol. 31, pp. 1862–75, dec 2010.
 - [124] J. L. Tanabe, D. Amend, N. Schuff, V. DiSclafani, F. Ezekiel, D. Norman, G. Fein, and M. W. Weiner, “Tissue segmentation of the brain in Alzheimer disease.,” *AJNR. American journal of neuroradiology*, vol. 18, pp. 115–23, jan 1997.
 - [125] S. Xie, J. X. Xiao, G. L. Gong, Y. F. Zang, Y. H. Wang, H. K. Wu, and X. X. Jiang, “Voxel-based detection of white matter abnormalities in mild Alzheimer disease.,” *Neurology*, vol. 66, pp. 1845–9, jun 2006.
 - [126] M. M. Swanberg, R. E. Tractenberg, R. Mohs, L. J. Thal, and J. L. Cummings, “Executive dysfunction in Alzheimer disease.,” *Archives of neurology*, vol. 61, no. 4, pp. 556–60, 2004.
 - [127] G. M. Peavy, D. P. Salmon, S. D. Edland, S. Tam, L. A. Hansen, E. Masliah, D. Galasko, and J. M. Hamilton, “Neuropsychiatric features of frontal lobe dysfunction in autopsy-confirmed patients with lewy bodies and "pure" alzheimer disease,” *American Journal of Geriatric Psychiatry*, vol. 21, no. 6, pp. 509–519, 2013.
 - [128] M. Tullberg, E. Fletcher, C. DeCarli, D. Mungas, B. R. Reed, D. J. Harvey, M. W. Weiner, H. C. Chui, and W. J. Jagust, “White matter lesions impair frontal lobe function regardless of their location.,” *Neurology*, vol. 63, no. 2, pp. 246–253, 2004.
 - [129] C. Ballatore, V. M.-Y. Lee, and J. Q. Trojanowski, “Tau-mediated neurodegeneration in alzheimer's disease and related disorders,” *Nature Reviews Neuroscience*, vol. 8, no. 9, pp. 663–672, 2007.
 - [130] H. Arai, M. Terajima, M. Miura, S. Higuchi, T. Muramatsu, N. Machida, H. Seiki, S. Takase, C. M. Clark, V. M.-Y. Lee, *et al.*, “Tau in cerebrospinal fluid: a potential diagnostic marker in alzheimer's disease,” *Annals of neurology*, vol. 38, no. 4, pp. 649–652, 1995.
 - [131] C. M. Clark, S. Xie, J. Chittams, D. Ewbank, E. Peskind, D. Galasko, J. C. Morris, D. W. McKeel, M. Farlow, and S. L. Weitlauf, “Cerebrospinal Fluid Tau and Beta- Amyloid,” *Arch Neurol*, vol. 60, pp. 1696–1702, 2003.

- [132] J. Hertze, S. Palmqvist, L. Minthon, and O. Hansson, “Tau pathology and parietal white matter lesions have independent but synergistic effects on early development of Alzheimer’s disease,” *Dement Geriatr*, vol. 3, no. 1, pp. 113–122, 2013.
- [133] T. A. Pascoal, M. Dadar, S. Manitsirikul, J. C. Breitner, D. L. Collins, J. Poirier, A. Labonté, and P. Rosa-Neto, “Association between apolipoprotein a-i levels and white matter hyperintensities depends on CSF tau levels in a high-risk cohort of aging cognitively normal persons: The prevent-alzheimer’s disease study,” *Alzheimer’s & Dementia*, vol. 11, no. 7, p. P103, 2015.
- [134] K. E. McAleese, M. Firbank, M. Dey, L. Walker, M. Johnson, S. McParland, J. T. O’Brien, and J. Attems, “Cortical hyperphosphorylated tau load is a predictor for white matter lesions in Alzheimer’s disease,” *Alzheimer’s & Dementia*, vol. 11, no. 7, pp. P562–P563, 2015.
- [135] B. B. Bendlin, C. M. Carlsson, S. C. Johnson, H. Zetterberg, K. Blennow, A. a. Willette, O. C. Okonkwo, A. Sodhi, M. L. Ries, A. C. Birdsill, A. L. Alexander, H. a. Rowley, L. Puglielli, S. Asthana, and M. a. Sager, “CSF T-Tau/A β 42 Predicts White Matter Microstructure in Healthy Adults at Risk for Alzheimer’s Disease,” *PLoS ONE*, vol. 7, no. 6, p. e37720, 2012.
- [136] K. E. McAleese, M. Dey, M. Firbank, S. McParland, J. T. O’Brien, and J. Attems, “the Role of Cortical Hyperphosphorylated Tau Pathology in the Pathogenesis of White Matter Lesions in Alzheimer’S Disease,” *Alzheimer’s & Dementia*, vol. 10, no. 4, pp. P428–P429, 2014.
- [137] F. Provenzano, J. Muraskin, G. Tosto, A. Narkhede, B. T. Wasserman, E. Y. Griffith, V. a. Guzman, I. B. Meier, M. E. Zimmerman, and A. M. Brickman, “White matter hyperintensities and cerebral amyloidosis: necessary and sufficient for clinical expression of Alzheimer disease?,” *JAMA neurology*, vol. 70, pp. 455–61, apr 2013.
- [138] T. Grimmer, M. Faust, F. Auer, P. Alexopoulos, H. F??rstl, G. Henriksen, R. Perneczky, C. Sorg, B. H. Yousefi, A. Drzezga, and A. Kurz, “White matter hyperintensities predict amyloid increase in Alzheimer’s disease,” *Neurobiology of Aging*, vol. 33, no. 12, pp. 2766–2773, 2012.
- [139] M. Maruyama, T. Matsui, H. Tanji, M. Nemoto, N. Tomita, M. Ootsuki, H. Arai, and H. Sasaki, “Cerebrospinal Fluid Tau Protein and Periventricular White Matter Lesions in Patients with Mild Cognitive Impairment: Implications for 2 Major Pathways,” *Archives of Neurology*. 61 (5) (pp 716-720),, vol. 61, no. May 2004, p. May, 2004.
- [140] L. C. a. Rutten-Jacobs, F.-E. de Leeuw, L. Geurts-van Bon, M. C. Gordinou de Gouberville, A. N. Schepens-Franke, P. J. Dederen, W. G. M. Spliet, P. Wesseling, and A. J. Kiliaan, “White Matter Lesions Are Not Related to β -Amyloid

Deposition in an Autopsy-Based Study.,” *Current gerontology and geriatrics research*, vol. 2011, p. 826862, jan 2011.

- [141] D. Zhang, Y. Wang, L. Zhou, H. Yuan, D. Shen, A. D. N. Initiative, *et al.*, “Multimodal classification of alzheimer’s disease and mild cognitive impairment,” *Neuroimage*, vol. 55, no. 3, pp. 856–867, 2011.
- [142] R. Cuingnet, E. Gerardin, J. Tessieras, G. Auzias, S. Lehéricy, M.-O. Habert, M. Chupin, H. Benali, O. Colliot, A. D. N. Initiative, *et al.*, “Automatic classification of patients with alzheimer’s disease from structural mri: a comparison of ten methods using the adni database,” *neuroimage*, vol. 56, no. 2, pp. 766–781, 2011.
- [143] S. Klöppel, C. M. Stonnington, C. Chu, B. Draganski, R. I. Scahill, J. D. Rohrer, N. C. Fox, C. R. Jack, J. Ashburner, and R. S. Frackowiak, “Automatic classification of mr scans in alzheimer’s disease,” *Brain*, vol. 131, no. 3, pp. 681–689, 2008.
- [144] C. Davatzikos, P. Bhatt, L. M. Shaw, K. N. Batmanghelich, and J. Q. Trojanowski, “Prediction of mci to ad conversion, via mri, csf biomarkers, and pattern classification,” *Neurobiology of aging*, vol. 32, no. 12, pp. 2322–e19, 2011.
- [145] E. Westman, J.-S. Muehlboeck, and A. Simmons, “Combining mri and csf measures for classification of alzheimer’s disease and prediction of mild cognitive impairment conversion,” *Neuroimage*, vol. 62, no. 1, pp. 229–238, 2012.
- [146] M. Ewers, C. Walsh, J. Q. Trojanowski, L. M. Shaw, R. C. Petersen, C. R. Jack, H. H. Feldman, A. L. Bokde, G. E. Alexander, P. Scheltens, *et al.*, “Prediction of conversion from mild cognitive impairment to alzheimer’s disease dementia based upon biomarkers and neuropsychological test performance,” *Neurobiology of aging*, vol. 33, no. 7, pp. 1203–1214, 2012.
- [147] L. M. Shaw, H. Vanderstichele, M. Knapik-Czajka, C. M. Clark, P. S. Aisen, R. C. Petersen, K. Blennow, H. Soares, A. Simon, P. Lewczuk, R. Dean, E. Siemers, W. Potter, V. M. Lee, J. Q. Trojanowski, and I. Adni, “Cerebrospinal Fluid Biomarker Signature in Alzheimer’s Disease Neuroimaging Initiative Subjects,” *Annals of neurology*, vol. 65, pp. 403–413, 2009.
- [148] N. Andreasen, E. Vanmechelen, A. Van de Voorde, P. Davidsson, C. Hesse, S. Tarvonen, I. Räihä, L. Sourander, B. Winblad, and K. Blennow, “Cerebrospinal fluid tau protein as a biochemical marker for alzheimer’s disease: a community based follow up study,” *Journal of Neurology, Neurosurgery & Psychiatry*, vol. 64, no. 3, pp. 298–305, 1998.
- [149] N. Schoonenboom, Y. Pijnenburg, C. Mulder, S. Rosso, E.-J. Van Elk, G. Van Kamp, J. Van Swieten, and P. Scheltens, “Amyloid β (1–42) and phosphorylated tau in csf as markers for early-onset alzheimer disease,” *Neurology*, vol. 62, no. 9, pp. 1580–1584, 2004.

- [150] N. Andreasen, L. Minthon, P. Davidsson, E. Vanmechelen, H. Vanderstichele, B. Winblad, and K. Blennow, “Evaluation of csf-tau and csf-a β 42 as diagnostic markers for alzheimer disease in clinical practice,” *Archives of neurology*, vol. 58, no. 3, pp. 373–379, 2001.
- [151] L. R. White, S. D. Edland, L. S. Hemmy, K. S. Montine, C. Zarow, J. A. Sonnen, J. H. Uyehara-Lock, R. P. Gelber, G. W. Ross, H. Petrovitch, *et al.*, “Neuropathologic comorbidity and cognitive impairment in the nun and honolulu-asia aging studies,” *Neurology*, vol. 86, no. 11, pp. 1000–1008, 2016.
- [152] L. E. Gibbons, A. C. Carle, R. S. Mackin, D. Harvey, S. Mukherjee, P. Insel, S. M. Curtis, D. Mungas, and P. K. Crane, “A composite score for executive functioning, validated in Alzheimer’s Disease Neuroimaging Initiative (ADNI) participants with baseline mild cognitive impairment,” *Brain Imaging and Behavior*, vol. 6, no. 4, pp. 517–527, 2012.
- [153] P. K. Crane, A. Carle, L. E. Gibbons, P. Insel, R. S. Mackin, A. Gross, R. N. Jones, S. Mukherjee, S. M. Curtis, D. Harvey, M. Weiner, and D. Mungas, “Development and assessment of a composite score for memory in the Alzheimer’s Disease Neuroimaging Initiative (ADNI),” *Brain Imaging and Behavior*, vol. 6, no. 4, pp. 502–516, 2012.
- [154] W. W. Barker, C. A. Luis, A. Kashuba, M. Luis, D. G. Harwood, D. Loewenstein, C. Waters, P. Jimison, E. Shepherd, S. Sevush, *et al.*, “Relative frequencies of alzheimer disease, lewy body, vascular and frontotemporal dementia, and hippocampal sclerosis in the state of florida brain bank,” *Alzheimer Disease & Associated Disorders*, vol. 16, no. 4, pp. 203–212, 2002.
- [155] X. Zhu, A. K. Raina, G. Perry, and M. A. Smith, “Alzheimer’s disease: the two-hit hypothesis,” *The Lancet Neurology*, vol. 3, no. 4, pp. 219–226, 2004.
- [156] E. E. Smith, D. H. Salat, J. Jeng, C. R. McCreary, B. Fischl, J. D. Schmabmann, B. C. Dickerson, A. Viswanathan, M. S. Albert, D. Blacker, and S. M. Greenberg, “Correlations between MRI white matter lesion location and executive function and episodic memory,” *Neurology*, vol. 76, no. 17, pp. 1492–1499, 2011.
- [157] Y. S. Shim, D.-W. Yang, C. M. Roe, M. A. Coats, T. L. Benzinger, C. Xiong, J. E. Galvin, N. J. Cairns, and J. C. Morris, “Pathological correlates of white matter hyperintensities on magnetic resonance imaging.,” *Dementia and geriatric cognitive disorders*, vol. 39, no. 1-2, pp. 92–104, 2015.
- [158] H. Braak, K. Del Tredici, U. Rüb, R. A. de Vos, E. N. J. Steur, and E. Braak, “Staging of brain pathology related to sporadic parkinsonâŽs disease,” *Neurobiology of aging*, vol. 24, no. 2, pp. 197–211, 2003.

- [159] B. Zlokovic, “Neurovascular pathways to neurodegeneration in Alzheimer’s disease and other disorders,” *Nature Reviews Neuroscience*, vol. 12, no. 12, pp. 723–738, 2014.
- [160] M. O’Sullivan, D. J. Lythgoe, a. C. Pereira, P. E. Summers, J. M. Jarosz, S. C. R. Williams, and H. S. Markus, “Patterns of cerebral blood flow reduction in patients with ischemic leukoaraiosis.,” *Neurology*, vol. 59, no. 3, pp. 321–326, 2002.
- [161] B. C. Bowen, W. W. Barker, D. A. Loewenstein, J. Sheldon, and R. Duara, “MR signal abnormalities in memory disorder and dementia.,” *AJR. American journal of roentgenology*, vol. 11, no. 2, pp. 283–290, 1990.
- [162] J. L. Tanabe, F. Ezekiel, W. J. Jagust, B. R. Reed, D. Norman, N. Schuff, M. W. Weiner, H. Chui, and G. Fein, “Magnetization transfer ratio of white matter hyperintensities in subcortical ischemic vascular dementia.,” *AJNR. American journal of neuroradiology*, vol. 20, pp. 839–44, may 1999.
- [163] K. E. Mcaleese, M. Firbank, D. Hunter, L. Sun, R. Hall, J. W. Neal, D. M. A. Mann, M. Esiri, K. A. Jellinger, J. T. O’Brien, and J. Attems, “Magnetic resonance imaging of fixed post mortem brains reliably reflects subcortical vascular pathology of frontal, parietal and occipital white matter,” *Neuropathology and Applied Neurobiology*, vol. 39, no. 5, pp. 485–497, 2013.
- [164] M. A. Erickson and W. A. Banks, “Blood-brain barrier dysfunction as a cause and consequence of Alzheimer’s disease.,” *Journal of cerebral blood flow and metabolism : official journal of the International Society of Cerebral Blood Flow and Metabolism*, vol. 33, no. 10, pp. 1500–13, 2013.
- [165] R. Barker, E. L. Ashby, D. Wellington, V. M. Barrow, J. C. Palmer, P. G. Kehoe, M. M. Esiri, and S. Love, “Pathophysiology of white matter perfusion in Alzheimer’s disease and vascular dementia.,” *Brain*, p. awu040, mar 2014.
- [166] C. Iadecola, “The overlap between neurodegenerative and vascular factors in the pathogenesis of dementia.,” *Acta neuropathologica*, vol. 120, no. 3, pp. 287–96, 2010.
- [167] Y. H. Huang, W. W. Zhang, L. Lin, J. Feng, X. X. Zhao, W. H. Guo, and W. Wei, “Could changes in arterioles impede the perivascular drainage of interstitial fluid from the cerebral white matter in leukoaraiosis?,” *Neuropathology and Applied Neurobiology*, vol. 36, no. 3, pp. 237–247, 2010.
- [168] L. Pantoni, “Cerebral small vessel disease: from pathogenesis and clinical characteristics to therapeutic challenges.,” *Lancet neurology*, vol. 9, pp. 689–701, jul 2010.
- [169] R. Topakian, T. R. Barrick, F. a. Howe, and H. S. Markus, “Blood-brain barrier permeability is increased in normal-appearing white matter in patients with

- lacunar stroke and leucoaraiosis.,” *Journal of neurology, neurosurgery, and psychiatry*, vol. 81, pp. 192–197, 2010.
- [170] M. E. Gurol, M. C. Irizarry, E. E. Smith, S. Raju, R. Diaz-Arrastia, T. Bottiglieri, J. Rosand, J. H. Growdon, and S. M. Greenberg, “Plasma beta-amyloid and white matter lesions in AD, MCI, and cerebral amyloid angiopathy.,” *Neurology*, vol. 66, pp. 23–9, jan 2006.
 - [171] H. Huang, X. Fan, M. Weiner, K. Martin-Cook, G. Xiao, J. Davis, M. Devous, R. Rosenberg, and R. Diaz-Arrastia, “Distinctive disruption patterns of white matter tracts in Alzheimer’s disease with full diffusion tensor characterization.,” *Neurobiology of aging*, vol. 33, pp. 2029–45, sep 2012.
 - [172] G. Bartzokis, D. Sultzer, P. H. Lu, K. H. Nuechterlein, J. Mintz, and J. L. Cummings, “Heterogeneous age-related breakdown of white matter structural integrity: Implications for cortical "disconnection" in aging and Alzheimer’s disease,” *Neurobiology of Aging*, vol. 25, no. 7, pp. 843–851, 2004.
 - [173] B. Fischl, D. H. Salat, E. Busa, M. Albert, M. Dieterich, C. Haselgrove, A. van der Kouwe, R. Killiany, D. Kennedy, S. Klaveness, A. Montillo, N. Makris, B. Rosen, and A. M. Dale, “Whole brain segmentation: automated labeling of neuroanatomical structures in the human brain.,” *Neuron*, vol. 33, pp. 341–55, jan 2002.